May 2019

Anomalous Effect of Spinning Conditions on the Mechanical and Transport Properties of Mesophase Pitch-Based Carbon Fibers

Victor Bermudez
Clemson University, victorbersa@gmail.com

ANOMALOUS EFFECT OF SPINNING CONDITIONS ON THE MECHANICAL AND TRANSPORT PROPERTIES OF MESOPHASE PITCH-BASED CARBON FIBERS

A Dissertation
Presented to
the Graduate School of
Clemson University

In Partial Fulfillment
of the Requirements for the Degree
Doctor of Philosophy
Chemical Engineering

---

by
Victor Bermudez, M.Sc.
May 2019

Accepted by:
Dr. Amod A. Ogale, Committee Chair
Dr. Mark E. Roberts
Dr. Igor Luzinov
Dr. David P. Anderson

ABSTRACT

Mesophase pitch, a nematic liquid crystal composed of disc-like polyaromatic hydrocarbons, has significant potential as an inexpensive and high-carbon-yielding precursor for structural carbon fibers. Before such potential is realized, the strength of mesophase pitch-based carbon fibers (MPCFs) must be enhanced while retaining their superior modulus and electrical/thermal conductivities. In MPCFs, lattice-related properties are favored by the three-dimensional graphitic development that originates from the preferential order that the liquid crystal molecules achieve during fiber formation. Carbon fibers derived from polyacrylonitrile (PAN), a long-chain polymer, do not possess graphitic microstructure; it is referred to as "turbostratic" carbon. Nevertheless, PAN-based carbon fibers constitute over 90% of global carbon fiber market, because of their higher tensile and compressive strengths (relative to those of MPCFs) that originate from less-perfectly formed carbon structure coupled with less aligned texture that prevents crack propagation. In MPCFs, it is believed that the large graphitic regions are also defect sensitive, and the tensile strength is lowered because it is a defect-limited property.

Previous studies have demonstrated that fiber spinning/process conditions play an important role in the development of carbon fiber microstructure, which in turn determines the strength of the carbon fiber. MPCF processing consists of three main steps, namely melt spinning of mesophase pitch where fiber is formed, oxidative stabilization where fiber is rendered infusible, and high temperature treatment where carbon layer and crystallinity get developed. Studies on the relationships between fiber microstructure and carbon fiber properties have focused on fiber formation because it is in this step that the microstructure

starts to develop. The melt spinning step consists of three main operations: melting of pitch, extrusion of molten pitch through spinnerets, and drawdown of filaments. Most discoveries relating the formation of fiber microstructure to MPCF properties have emphasized on processing conditions during the melting/extrusion steps, while the drawing step has not been investigated systematically. Therefore, the primary goal of this dissertation was to study how the microstructure and properties of MPCFs were influenced by changes in drawdown ratio (DDR). The specific objectives were to investigate the effects of DDR on (i) carbon fiber microstructure, (ii) fiber mechanical properties, and (iii) fiber transport properties.

To accomplish these goals, precursor pitch fibers were melt-spun from a synthetic, naphthalene-based mesophase pitch using multiple sets of ultrafine diameter spinnerets with a range of capillary diameters of 50-150 μm. Pitch fibers were oxidatively stabilized in air (220-240 °C), and carbonized at 2100 °C under helium atmosphere. As a result, carbon fiber samples with average diameters in the range 8-16 μm were obtained, with drawdown ratios ranging from about 10 to 200.

The microstructure of carbon fibers was studied by scanning electron microscopy (SEM), Raman spectroscopy and wide-angle x-ray diffraction (WAXD). SEM of the cross-section of fibers revealed a line-origin radial type of transverse microstructure across samples, which meant that transverse microstructure would not constitute a confounding variable in further analysis. Raman spectroscopy revealed that decreasing DDR led to an enhancement of crystallite coherence length along the fiber axis. The coherence length increased from ~ 60 nm for DDR of 190 to ~ 85 nm for DDR of 15, while at the same time

reducing the defect density of carbon layer planes. WAXD revealed a 2θ peak position of ~ 26.0° for (002) planes indicating d_{002} spacing of 0.342 nm and L_c stacking thickness of approximately 20 nm, generally consistent with prior results on mesophase pitch-based carbon fibers produced at 2100 °C. However, significant differences in crystalline features resulting from different DDRs could not be detected, likely due to instrumental limitations.

Tensile properties of carbon fibers were measured by single filament tensile testing. Between samples of equivalent fiber diameter and heat treatment temperature yet contrasting DDR, tensile strength was favored by decreasing DDR. Tensile strength was found to increase from 1.4 ± 0.2 GPa for DDR ~ 190 to 2.3 ± 0.3 GPa for DDR ~ 15, for carbon fibers with nominal diameter of 8 μm. Limited samples were tested by the tension-recoil testing to estimate compressive strength. The compressive strength displayed no measurable change, and remained about 800 MPa as the DDR was reduced from 190 to 15. The behavior of tensile strength with DDR is somewhat anomalous with that observed for carbon fibers derived from PAN for which a higher DDR is known to enhance tensile strength, via the improvement of molecular orientation along fiber axis caused by more pronounced drawing. Weibull analysis revealed that for samples of comparable fiber diameter, the Weibull modulus increases with low DDR, which means that the distribution of tensile strength is narrower.

The electrical conductivity of single carbon fibers was experimentally measured, and the thermal conductivity was estimated using the Issi-Lavin electrical/thermal conductivity correlation. Limited measurements of thermal diffusivity of carbon fiber/polymer matrix composites were conducted using a laser/light flash analysis (LFA)

technique. For the experimental carbon fibers the electrical resistivity was measured at ~ 6 μΩ·m and the estimated thermal conductivity at ~ 200 W/m·K. These measurements confirm that the conductivity of these MPCFs were a whole order of magnitude better than those of PAN-based fibers. However, no significant difference could be detected in the electrical or thermal conductivity as a function of the different DDRs. This is generally consistent with x-ray results that indicated no significant changes in graphitic crystallinity. In summary, while ***decreasing*** drawdown ratio used during pitch fiber spinning did not deteriorate electrical/thermal conductivity, the tensile strength was observed to increase with decreasing DDR.

ACKNOWLEDGMENTS

I would like to express my gratitude to the following people and organizations, whose support was fundamental for the successful completion of this dissertation.

The Fulbright Student Program and the Administrative Department of Science, Technology and Innovation in Colombia (COLCIENCIAS), for believing and investing in my vision.

Dr. Amod Ogale for his direction throughout the entire duration of my doctorate program, and for giving me the opportunity to expand my professional range.

Dr. David Anderson, Dr. Igor Luzinov and Dr. Mark Roberts, for their constructive evaluation of this work. Dr. Kris Kitchens, Dr. Sapna Sarupria and Dr. Mark Thies, for their suggestions towards improving the original research proposal. Kim Ivey, for her help with differential scanning calorimetry, and Dr. Jessica Larsen, for her advice on statistical analysis.

All past and present members of Dr. Ogale's research group, for sharing their knowledge and skills. I would like to thank Sagar Kanhere and Özgün Özdemir for their friendship, kindness and generosity.

Finally, I would like to thank Bill Coburn, Roshell Hicks, Terri McAllister, Joy Rodatz and Diana Stamey and for their generous support and for creating a welcoming and friendly environment at Earle Hall.

TABLE OF CONTENTS

Table of Contents (Continued)

Page

LIST OF TABLES

List of Tables (Continued)

Page

LIST OF FIGURES

List of Figures (Continued)

Page

List of Figures (Continued)

Page

CHAPTER 1

INTRODUCTION

1.1 Carbon fiber generalities

Carbon fibers (CFs) are defined as fibers with a carbon content of at least 92% w/w [1]. Possessing tensile strengths over 6 GPa and specific gravity of only about 1.8, these carbon materials are ideal reinforcements for structural applications that require an extremely high strength-to-weight ratio such as aerospace and race/sports cars. Components of fighter aircrafts have been made of carbon fiber-epoxy resin composites for several decades, and in more recent years, airliners such as Boeing 787 and Airbus 350 XWB use carbon fiber reinforced polymer (CFRP) composites on their fuselages and wings amounting to almost 50 wt% of the aircraft weight. The use of carbon fiber composite monocoque has become ubiquitous in racing cars since its introduction in Formula One in 1981, followed by its introduction in sports cars in 1990. Currently, CFRPs are used in numerous components of high-end road cars to reduce weight and improve fuel efficiency [2,3].

Apart from their high strength and low density, carbon fibers are also valued for other characteristics that permit their use in other applications: high tensile modulus and stiffness for robotic arms and printer rolls, high dimensional stability for aircraft brakes, high electrical conductivity for electromagnetic interference shielding, and high corrosion

and thermal resistance for chemical and nuclear industries. However, there is not a single type of carbon fiber that exhibits all the properties listed above.

All carbon fibers are processed from hydrocarbon-type precursors because carbon in its elemental form does not melt or dissolve in any solvent. Therefore, to produce carbon fibers, it is necessary to start with a precursor material that is processable either as a melt or as a solution. The precursors must possess (i) spinnability to be turned into thin filaments, (ii) adequate reactivity to be stabilized, and (ii) sufficient carbon yield after thermal treatment in the range 1000-3000 °C. These requirements have limited the commercial production of carbon fibers to three types of precursors: rayon, polyacrylonitrile (PAN), and pitch.

The first carbon fibers to be commercially produced in continuous form were based in rayon precursor, in the early 1960s by Union Carbide [4]. Because of their low thermal conductivity and excellent heat resistance, such rayon-based carbon fibers are still used in heat shields and exit cone applications where the temperature exceeds 1000 °C. However, the limited strength and environmental issues of producing rayon have limited further development of rayon-based carbon fibers [5].

Carbon fibers based on PAN precursor started commercial production in the mid-1960s and they were further developed through the next three decades to become the leading type of carbon fiber, with an estimated 90% share of the global market. Due to their outstanding mechanical strength, PAN-based carbon fibers are used almost exclusively for high-performance structural composites [6]. PAN dissolved in a solvent (e.g., dimethyl

sulfoxide) is wet-spun into precursor fibers that, after thermo-oxidative stabilization at 200-300 °C, are carbonized at 1000-1500 °C to provide a carbon yield of about 45 wt%. Thus, over 55% of precursor mass is lost during carbonization as reaction products that include hydrogen cyanide and carbon monoxide.

Pitch precursors for carbon fiber processing, comprising isotropic and anisotropic mesophase pitches, were studied as early as 1963. By 1970, the first pitch-based carbon fibers were commercially available. Their lower tensile and compressive strengths, when compared to those of PAN-based carbon fibers, excludes their use in structural composites. Carbon fibers based on pitch precursors have an estimated 8% share in the carbon fiber market. Some of these isotropic pitch-based carbon fibers (IPCFs) are used as felts for furnace insulation, whereas applications requiring thermal conductivity and electromagnetic interference shielding use mesophase pitch-based carbon fibers (MPCFs). Such specialized applications of MPCFs are possible due to the high electrical and thermal conductivities that this type of carbon fibers can attain, which are not achievable in PAN-based carbon fibers. In addition, when considering that mesophase pitch can be derived from inexpensive residues of petroleum and coal tar refining [7], with a higher carbon yield in carbon fiber processing (~ 75%) when compared to PAN [1], it is generally recognized that mesophase pitch has significant potential as a low-cost precursor for high-performance carbon fibers. Therefore, the emphasis of the research presented in this dissertation is on mesophase pitch-based carbon fibers.

1.2 Mesophase pitch precursors

As noted above, pitch precursors can be classified as isotropic or anisotropic. Carbon fibers derived from isotropic pitch are categorized as general-performance carbon fibers (GPCFs) and they possess low or no preferred molecular orientation, whereas the ones derived from anisotropic pitch are classified as high-performance carbon fibers (HPCFs) with high degrees of molecular orientation [8]. The anisotropy of pitches originates from the disc-like architecture of a certain category of pitch molecules that results in layering of such discotic molecules, which leads to nematic liquid crystalline behavior. Such pitches are also known as "mesophase pitches" to identify its state as being somewhere between liquid and crystalline solid because these materials possess orientational order, but not positional order. A schematic of the layering arrangement of mesophase pitch molecules is shown in Figure 1 (a).

Brooks and Taylor (1965) are credited as the first to observe the formation of spheres of mesophase-or liquid crystal-from an isotropic pitch upon thermal treatment [9]. Their discovery was complemented by White et al. (1967) [10], who reported that the mesophase domains could be subjected to deformation by flow, which remained after high temperature treatment. In the early 1970s, Singer et al. used those previous studies to demonstrate that a mesophase pitch could be melt spun into fibers that, in turn, could be oxidized and carbonized to obtain carbon fibers of high modulus and high thermal conductivity. This route was used by Union Carbide for mesophase pitch-based carbon fiber production [11].

1.2.1 Sources of mesophase pitch

Pitch is a mixture of polycyclic aromatic hydrocarbons (PAHs) with alkyl side-chains and heterocyclic compounds; a typical chemical structure of a mesophase pitch molecule is shown in Figure 1 (b). Although pitch exists in natural deposits in a few regions of the world, isotropic pitch for GPCF production is mostly obtained from the refining of crude oil (petroleum pitch) or from the pyrolysis of coal (coal tar pitch). In addition, anisotropic pitch can also be synthesized from aromatic hydrocarbons such as naphthalene [12].

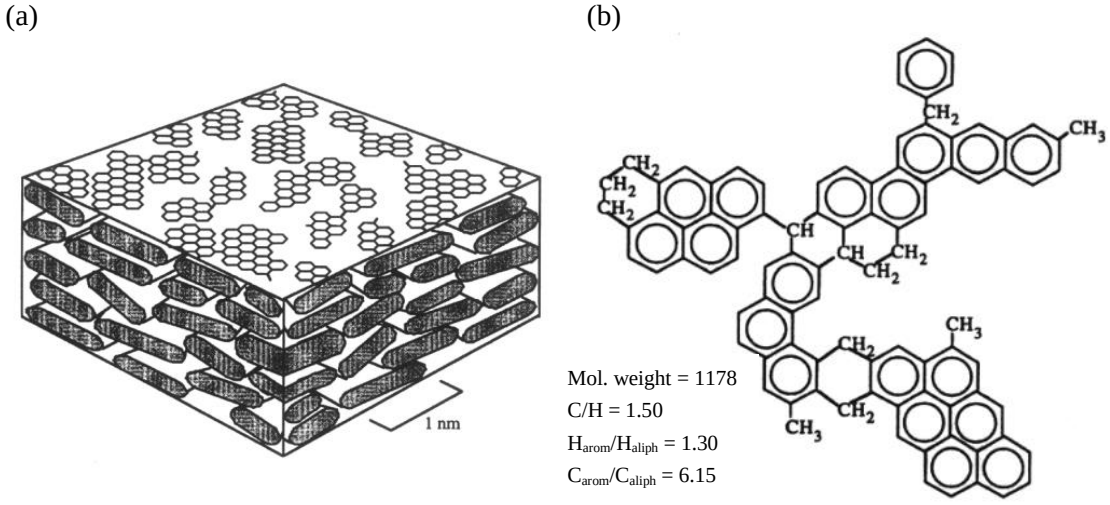

Figure 1. (a) Stacking arrangement of mesophase pitch molecules; (b) typical polycyclic aromatic hydrocarbon in mesophase pitch [13].

Regardless of the raw material, a pitch precursor for either isotropic or anisotropic pitch-based carbon fibers must provide narrow molecular weight distribution, low volatile content, adequate viscosity at the spinning temperature, low concentration of inorganic

impurities, and high carbon yield [14]. In addition, the softening point of the pitch must be appropriate to balance between a good spinning performance (favored by a low softening point) and a short stabilization step (favored by a high softening point). Hence, raw pitches, either petroleum- or coal tar-based, require an adjustment by separation and/or chemical reaction to achieve the desired properties.

Petroleum pitch can be obtained from by-products of petroleum distillation such as catalytic cracking bottoms, pyrolysis fuel oil and catalytic slurry oil [7,15]. The production of pitch from these materials consists of one of the following methods or their combinations: (1) further heat treatment to increase molecular weight; (2) air blowing at about 250 °C; (3) steam stripping and vacuum to remove the more volatile components; and (4) distillation. Physical and chemical properties of the resulting pitch are dependent on the process conditions used in any of the four methods above, e.g. higher temperatures and longer times typically lead to a more aromatic and more anisotropic pitch [16].

Coal tar pitch is defined as the residue, involatile at 450 °C, from the distillation of coal tars, which are produced by the high temperature (> 1000 °C) pyrolysis of coal [17]. The molecular structure of coal tar pitches usually consists of an aromatic core with only a few methyl groups attached. In that sense, coal tar pitch is more aromatic and has a smaller degree of substitution than does petroleum pitch. This makes coal tar pitches more thermally stable than natural pitches because bubbling, caused by the separation of alkyl chains commonly present in natural pitches, is not extensive [18]. However, much greater fractions of PAHs make coal tar pitches less attractive than petroleum-derived pitches,

since the increased thermal stability given by the greater aromaticity results in inferior chemical reactivity which is needed in the stabilization step.

Starting from a purified petroleum or coal tar pitch, isotropic pitch is prepared by thermal condensation (> 350 °C), when dehydrogenation and cross-linking occur resulting in molecular weight and softening point increases. Anisotropic pitch can then be produced from such isotropic pitches by several methods that essentially aim to form larger molecules which further aggregate into liquid crystalline phase with nematic order [4]. Most methods involve two stages, (1) removal of low molecular weight species by either heating, solvent extraction, vacuum distillation or inert gas sparging; and (2) heat treatment of high molecular weight species in the range 300-500 °C to promote polymerization and condensation reactions [19]. Figure 2 shows the evolution from isotropic to anisotropic pitch under light microscopy.

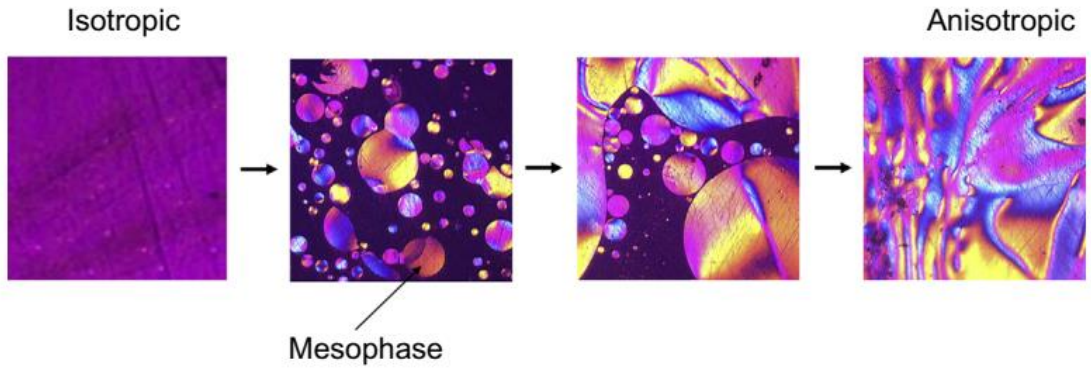

Figure 2. Formation of mesophase pitch from isotropic pitch on heating in the range from 350 to 450 °C [19].

Depending on the source of the crude oil or coal, petroleum residues and coal tars have not only a wide range of chemical structures, but also have a highly variable content of these species. This makes it difficult to control the structure of the isotropic or anisotropic pitch to get the desired balance between low softening point and high stabilization reactivity. With the aim of obtaining a more controlled precursor of higher purity, Mochida et al. (1988) [20] developed a synthetic pitch from aromatic hydrocarbons, such as naphthalene and anthracene, using HF/BF_3 as a catalyst. The process consisted of catalytic polymerization in the range 220-260°C under autogenous pressure for 4 hours. The catalyst, unreacted monomer and volatiles were distilled out of the reaction product by heating to 340 °C under nitrogen flow to obtain 100% anisotropic pitch. In 1991, Mitsubishi Gas Chemical Company began production of naphthalene-derived mesophase pitch using HF/BF_3 in a commercial-base facility, and labeled it AR-resin. Figure 3 shows a simplified flow diagram of the Mitsubishi process for AR-resin production. Such mesophase pitch was used in the production of HPCF and anodic materials for Li-ion batteries [21].

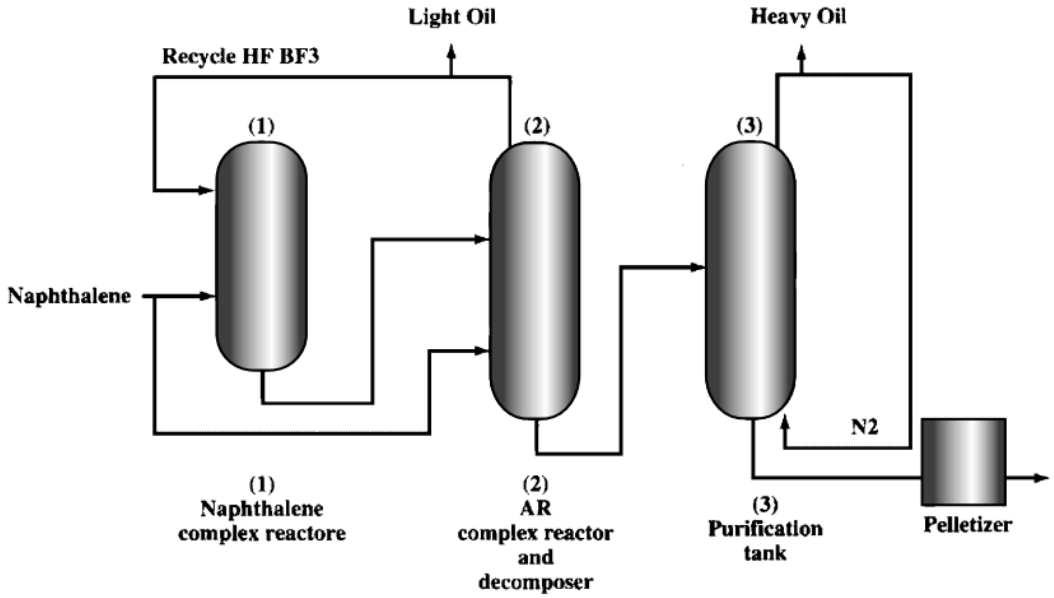

Figure 3. Simplified flow diagram of the industrial preparation of AR-resin using HF/BF_3 [21].

1.2.2 Rheology of mesophase pitch

The rheological behavior of a mesophase pitch during spinning depends on the temperature, the shear rates experienced in the vicinity and within the spinneret capillaries, and the chemical composition of the material. Molten mesophase pitches behave as shear-thinning at low shear rates (~ 0.1 to 10 s^{-1}) and become Newtonian at higher shear rates (~ 100 to 1000 s^{-1}), which is the type of behavior required for stable spinning of fibers [18]. For a synthetic AR-type mesophase pitch, Kundu found the transition from shear-thinning to Newtonian to occur at ~ 3 s^{-1} and the consolidation of such behavior in the range 200-10000 s^{-1} [22].

Because mesophase pitch is not a true crystalline form, it does not display a solid-to-liquid phase transition upon heating, and does not have a true melting point. It gradually softens or becomes less viscous as temperature increases. Various grades of mesophase pitch typically soften and flow at temperatures in the range 250-350 °C. Compared to that of common melt-spinnable polymers, temperature dependence of viscosity is extreme in mesophase pitches, hence there is a very narrow temperature window in which viscosity is adequate for spinning [23]. Spinning below such window results in high viscosities and brittle fracture during drawdown, whereas spinning above the window leads to low viscosities and capillary breakup; both cases lead to filament breakage [24]. This makes the melt spinning of mesophase pitch very difficult when compared to polymers. Because of the strong dependence of viscosity on temperature, the shear stress experienced by the material in the spinneret capillary, where mesophase molecules orient, is also affected by the spinning temperature.

1.3 Mesophase pitch-based carbon fibers

1.3.1 Processing

The processing of MPCFs (Figure 4) consists of three main steps, namely (i) melt spinning where the mesophase pitch is melted and extruded into filaments, (ii) stabilization where the extruded filaments are oxidatively thermoset, and (iii) and carbonization/graphitization where carbon is concentrated and crystallinity is developed in

the fiber. All commercial MPCFs are produced by the steps above. Post-treatment of carbon fibers includes surface treatment to promote adhesion to the polymer matrix, and sizing to protect the fibers from abrasion.

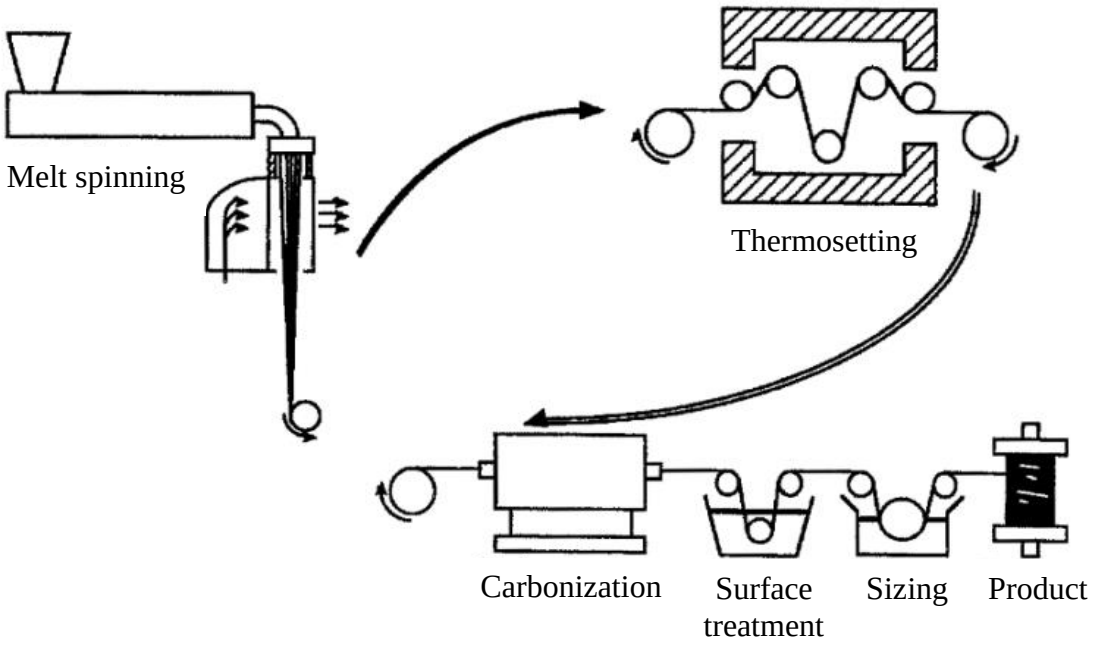

Figure 4. MPCF processing. A continuous extruder is used to melt and form fibers, which are stabilized by thermosetting in air and carbonized to concentrate carbon. Surface treatment and sizing ready the carbon fibers for interaction with a polymer matrix [13].

Melt spinning is a process that involves three steps, namely melting of the material, extrusion of the molten material through a spinneret, and drawing of the extrudate to form filaments. Because a mesophase pitch softens over a range of temperatures rather than at a defined temperature, the spinning of mesophase pitches is typically performed ~ 30 °C above the softening point. The mesophase pitch precursor is typically melted in an extruder

and pumped into a spin pack, which contains a filter and a spinneret with a series of capillaries (0.2-0.05 mm in diameter) where extrudates are formed. The filter prevents particles and impurities from blocking the spinneret capillaries. A metering pump may be placed before the spin pack to provide a constant volumetric flow. The molten extrudates are drawn down by take-up rolls and quenched by surrounding air to form thin mesophase pitch fibers of approximately 12–30 μm in diameter.

Stabilization converts the thermoplastic precursor fibers to a thermoset material that is able to keep its microstructure and shape during the carbonization step [18]. Oxygen reacts with the fiber to cross-link the pitch molecules while ketones, aldehydes and carboxylic acids form as reaction products. Along with chemical reaction, the stabilization process also involves mass transport as oxygen must diffuse to the fiber surface and within the fiber, and reaction products must diffuse in the opposite direction. Since the rate of oxidative thermosetting is a function of temperature, stabilization of as-spun fibers is performed at the highest possible temperature, although safely below the softening point of the precursor mesophase pitch to avoid fiber sticking (typically 30-100 °C below).

The high temperature treatment processes, carbonization and graphitization, can be carried on separate equipment or in a single furnace. Carbonization typically covers the temperature range 900-1800 °C, wherein most non-carbon elements are removed in the form of gases such as water, carbon dioxide, carbon monoxide, methane and hydrogen. Heating rate must be controlled to avoid the disruption of the fiber by the rapid release of those chemical species. During graphitization, which takes place in the range 1800-3500 °C, mesophase domains evolve into three-dimensional crystalline structures that

approximate those of graphite. Both carbonization and graphitization are carried on under an inert atmosphere, usually nitrogen, argon or helium.

1.3.2 Structure

The basic structural unit (BSU) of carbon fibers is often considered to be a stack of carbon layers that create coherent domains [25]. They usually exist in turbostratic form where the interlayer distance is 0.344 nm and the layers are not planar (Figure 5, right), although a graphitic structure with a characteristic interplanar spacing of 0.3354 nm is present in some MPCFs (Figure 5, left), particularly the ones heat-treated at high temperatures, ≥ 3000 °C.

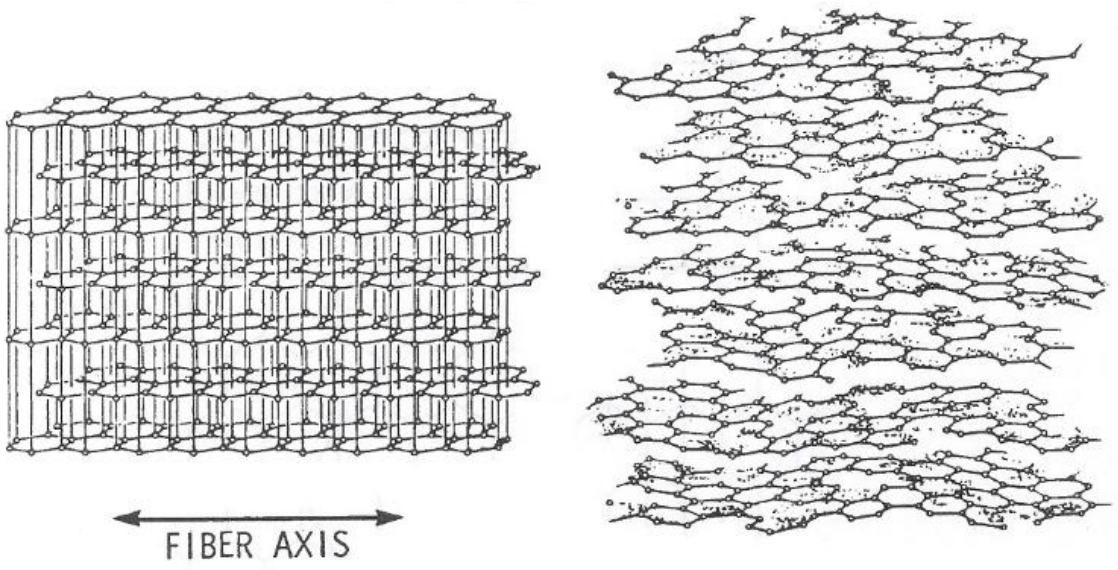

Figure 5. Crystal structure of graphite crystal (left) and turbostratic carbon (right) [26].

These fundamental structural units are originated in the fiber formation process. They can split, fold, twist and join other units to form larger domains, which in turn can experience the same dislocations and interactions. Thus, the spinning process creates microdomains which are elongated along the fiber axis, and are connected to other microdomains by regions of pores or dislocations [27]. These microdomains interact with each other to create meso and macrodomains, which form the transverse and longitudinal microtextures found in MPCFs. Such microtextures represent the existence of a very long range, statistical orientation of the macrodomains. The various types of transverse microtextures depend on the precursor and the process conditions in melt spinning (Figure 6).

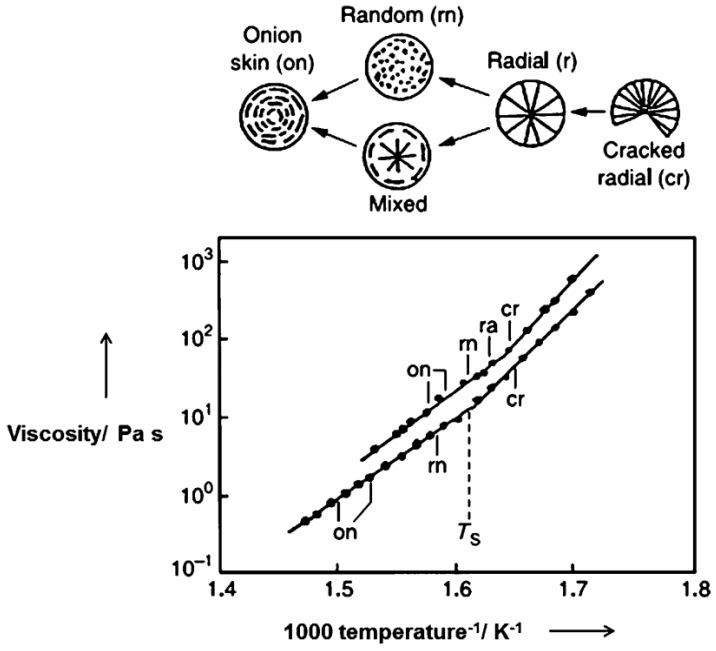

Figure 6. Change in transverse microtexture with melt spinning temperature for two types of pitch [28].

Although micro, meso and macrodomains are created during spinning, the subsequent stabilization, and particularly the high temperature treatment, refine the fiber microstructure by removing heteroatoms, increasing density and bringing domains closer. Planar layers of crystalline carbon start to appear at temperatures exceeding 2000 °C. Analysis of longitudinal sections of fiber by scanning tunneling microscopy (STM) has evidenced that the atomic structure of pitch precursor carbon fibers resembles the hexagonal structure of graphite [29].

Figure 7 shows a schematic representation of a carbon crystallite within a carbon fiber. These crystallites are typically described by four values: $L_{a\parallel}$ (persistence length, parallel to the fiber axis), $L_{a\perp}$ (persistence length, perpendicular to the fiber axis), L_c (graphene layer stack height) and d_{002} (spacing between graphene layers). These dimensions can be measured by x-ray diffraction, Raman spectroscopy, transmission electron microscopy (TEM) and STM.

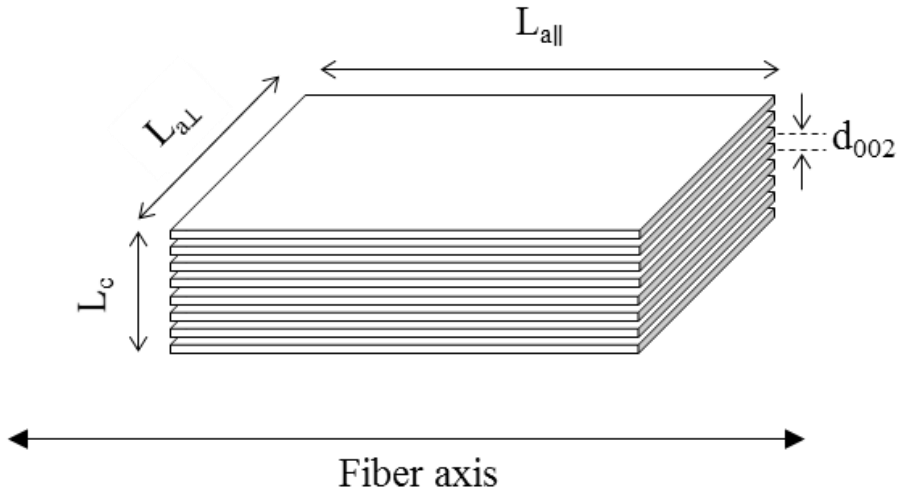

Figure 7. Schematic representation of a carbon crystallite inside a carbon fiber. Adapted from [1].

A recent model for high modulus MPCFs has proposed as structural unit a series of longitudinally arranged, lamellar stacks of carbon layers of average length $L_{a\parallel}$, separated by defective regions of approximate constant length δ as seen in Figure 8 (a). Defective regions consist of disordered grain boundaries that may include 5/7 membered rings, vacancies, distorted hexagon rings and octagon rings, as exemplified in Figure 8 (b) [30].

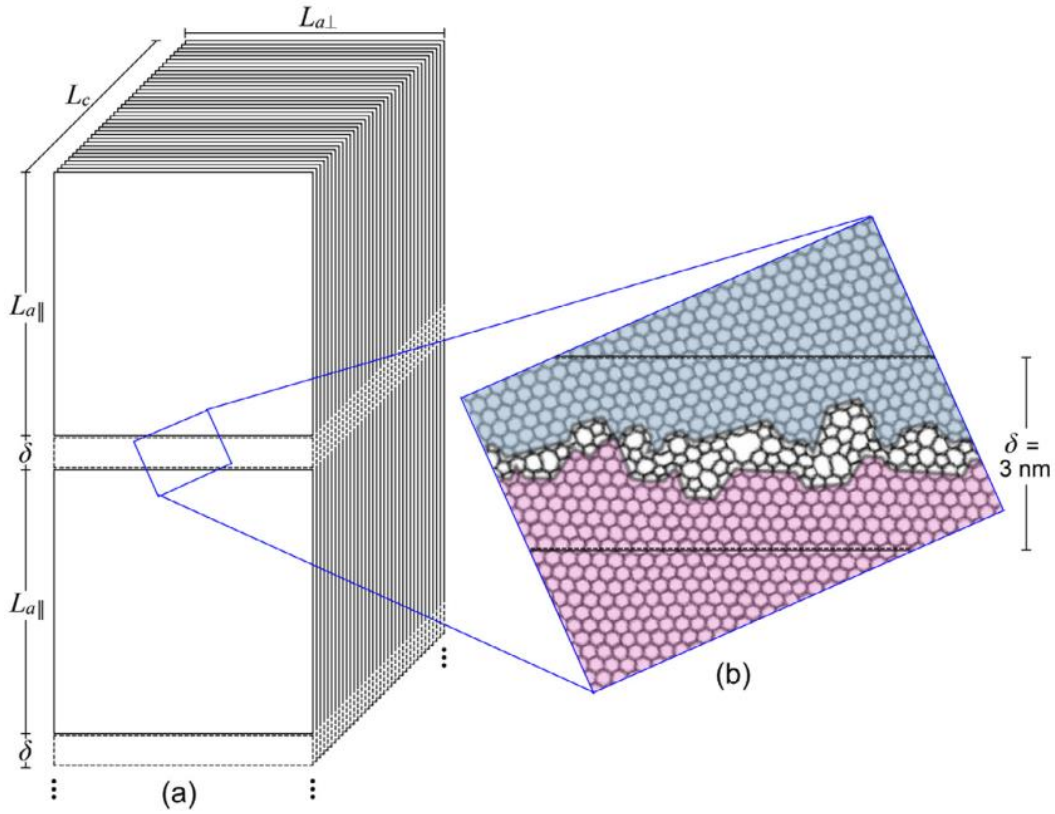

Figure 8. (a) Proposed model for structural unit of MPCFs; (b) suggested type of defective region [30].

1.3.3 Properties

Carbon fibers derived from mesophase pitch exhibit a wide range of physical and mechanical properties due to the wide range of microstructure that develops in such carbon fibers. For MPCFs, the tensile modulus and electrical conductivity are exceedingly large, whereas transverse properties and compressive strength are poor due to the high degree of molecular orientation present in the graphene planes along the fiber axis. In contrast, a lack of crystalline structure and absence of any major molecular alignment leads to quite low mechanical properties in IPCFs.

For any given temperature of heat treatment, the density of MPCFs is greater than that of IPCFs due to the tight layer packing resulting from the orientation of the anisotropic pitch. Density of both IPCFs and MPCFs increases with increasing heat treatment temperature (HTT), although the dependence is much stronger for the latter group. The density of mesophase pitch-based carbon fibers increases from about 1800 $kg \cdot m^{-3}$ for a HTT of 1000 °C to about 2200 $kg \cdot m^{-3}$ for a HTT of 3000 °C. As the graphene layers become more graphitic with increasing temperature, the overall packing is improved and the density is increased. Such rearrangement of graphene layers takes place at a much smaller scale in IPCFs, hence the slight increase in density (from 1600 to 1700 $kg \cdot m^{-3}$) with increasing temperature (1000 to 2500 °C) [18].

While it is relatively easy to measure the coefficient of thermal expansion (CTE) in the axial direction, the measurement in the transverse direction is more difficult because of the smaller dimensions. However, some measurements of CTE in the transverse direction

have been made on carbon fiber composites using scanning electron microscopy (SEM) and laser diffraction. Figure 9 presents the CTE along the fiber axis of two pitch precursor carbon fibers and two PAN-based carbon fibers as a function of temperature. The axial CTE of T300 PAN-based carbon fiber is positive for all the temperature range, and up to 5 times greater than the axial CTE of the pitch-based carbon fibers, particularly at the highest temperatures. In contrast, for the pitch-based carbon fibers, the axial CTE is negative for a large range of temperature, and it only becomes positive near 1000 °C. A negative CTE along the fiber axis, coupled with a high axial modulus, allows the preparation of composites with virtually zero thermal expansion by controlling the fiber orientation in the composite. The axial shrinkage that carbon fibers experiment near room temperature is caused by the bending of the graphene layers. The CTE in the transverse direction is always positive with temperature.

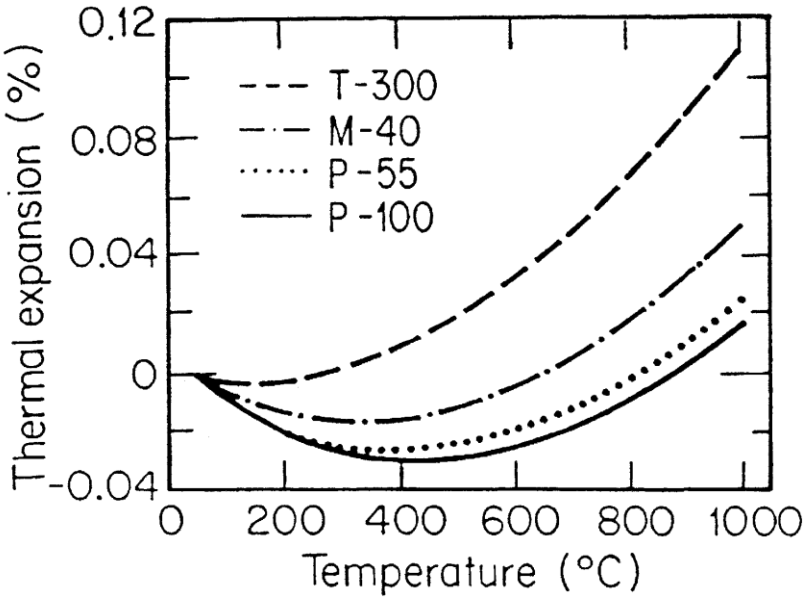

Figure 9. Thermal expansion as a function of temperature for two PAN-based carbon fibers (T-300 and M-40) and two MPCFs (P-55 and P-100) [18].

Strength (tensile and compressive) and modulus (axial and transversal) are the most relevant mechanical properties of mesophase pitch precursor carbon fibers. Although it is known that the properties of carbon fibers are determined by the structure of the fibers, these two mechanical properties are a function of different structural characteristics of MPCFs. While strength is controlled by the density of defects and the occurrence of microbuckling, modulus is a strong function of the degree of orientation of the graphene layers with respect to the fiber axis, i.e., modulus is a lattice-related property. Table 1 presents the mechanical properties of commercially available MPCFs and other reinforcing fibers for comparison.

Table 1. Mechanical properties of reinforcing fibers [31].

Classification	Type	Tensile strength, GPa	Tensile modulus, GPa	Density, g/cm^3
MPCF	P25	1.38	159	1.90
	P75	2.10	517	2.00
	P100	2.41	758	2.16
	K1100	3.10	966	2.20
PAN-based CF	T300	3.75	231	1.76
	T1000	6.37	294	1.80
Cellulose-based CF	RG 10	0.82	41	1.4
Aramid fiber	Kevlar 49	2.76	120	1.45
Glass	E glass	3.4	73	2.60
Metal fiber	A663 steel, hot rolled	0.40	207	7.86

MPCFs can have an exceptionally high thermal conductivity, since their highly graphitic, axially aligned structure closely recreates the basal plane of graphite, the material with the highest room temperature axial thermal conductivity, about 2000 W/m·K [6] . Direct measurements of thermal conductivity of single filaments are difficult to perform.

Since there is a strong correlation between thermal and electrical conductivities in carbon fibers, electrical resistivity (reciprocal of electrical conductivity) measurements of single carbon fiber filaments are made instead, and the thermal conductivity is estimated from the Lavin et al. correlation [32]:

$$\kappa = 440000/(\rho+258) - 295 \quad (1)$$

where ρ is the electrical resistivity expressed in $\mu\Omega\cdot$cm and κ is the thermal conductivity expressed in W/m·K.

The electrical conductivity of carbon fibers increases with heat treatment temperature due to the increase of degree of graphitization. Rayon-based and isotropic pitch-based carbon fibers show a relatively small increase in electrical conductivity in the range from 1000 to 3000 °C because no significant increase in graphitic crystallinity occurs due to the inherent chemical structure of the precursor not conducive to graphitization. Electrical conductivity of PAN-based carbon fibers increases very rapidly between 1000 and 1500 °C, remains virtually constant between 1500 and 2500 °C, and increases again between 2500 and 3000 °C. MPCFs experience a rapid and continuous increase in electrical conductivity in the range from 1000 to 2000 °C, with a more gradual increase upon heating to 3000 °C. For a given heat treatment temperature, the electrical conductivity of mesophase pitch based carbon fibers is greater than that of PAN-based carbon fibers. MPCFs have a higher electrical conductivity than IPCFs and rayon-based carbon fibers, in some cases by one order of magnitude [5]. Table 2 presents the mechanical properties of commercially available MPCFs and other materials for comparison.

Table 2. Electrical and thermal properties of reinforcing fibers and other materials [33,34].

Classification	Type	Electrical resistivity, μΩ·m	Thermal conductivity, W/m·K
MPCF	P25	12.1	36
	P100	4.6	321
	K1100	1.1-1.3	900-1000
PAN-based CF	T300	18.0	14
Metals	Copper	0.02	398
	Stainless steel	0.5	15.9

1.4 Objectives

Carbon fibers from mesophase pitch precursor are a reinforcement material with particular capabilities due to their superior tensile modulus, electrical and thermal conductivities and CTE. They can achieve those properties due to their highly crystalline microstructure. However, it is their lower strength, along with their higher cost, what limits their expansion into more carbon fiber market niches. Therefore, the enhancing of tensile and compressive strengths is of great importance for both current and upcoming applications of MPCFs, since low compressive strength limits the handling characteristics of the fibers in present-day composite production, and low tensile strengths prohibit future use as structural reinforcement. As explained above, the mechanical and transport properties of carbon fibers are strongly influenced by their microstructure, which in turn is largely defined in the fiber formation step – high temperature treatment refines the microstructure created in spinning. Thus, the control of spinning conditions is key to microstructure development and carbon fiber property enhancement.

Therefore, the objectives of the research presented in this dissertation were to

(1) Investigate the effect of spinning conditions on the microstructure of mesophase pitch-based carbon fibers;

(2) Determine the effect of microstructure on carbon fiber mechanical properties; and

(3) Assess the effect of process-induced microstructure on electrical/thermal conductivity of carbon fibers.

The rest of this dissertation is organized as follows: Chapter 2 describes the materials and methods used to process mesophase pitch-based carbon fibers for the current research. The analytical techniques used to characterize the fiber microstructure are also covered, and the differences are discussed for carbon fibers derived from different spinning conditions. Chapter 3 presents the tensile and compressive properties of resulting carbon fibers discussed in Chapter 2. Also, it relates the differences in mechanical properties to the differences in fiber microstructure observed in Chapter 2, for carbon fibers of different spinning conditions.

Chapter 4 presents experimental techniques and results on the transport properties of the mesophase pitch-based carbon fibers discussed in the two previous chapters. The electrical and thermal conductivity is interrelated with different spinning conditions. Finally, Chapter 5 summarizes the conclusions of the work presented in Chapters 2, 3 and 4, and provides recommendations for future work.

CHAPTER 2

EFFECT OF MESOPHASE DRAWDOWN RATIO ON CARBON FIBER MICROSTRUCTURE

2.1 Introduction

Carbon fibers derived from mesophase pitch (MP) achieve outstanding tensile modulus and thermal conductivity, exceeding 500 GPa and 200 W/m·K, respectively, due to their highly crystalline microstructure. The preferential order that the nematic, liquid crystal molecules of mesophase pitch can achieve during precursor fiber formation results in interlayer spacing of the order of 0.34 nm which is approximate to that of perfect graphite [35]. Due to their excellent thermal and electrical conductivities, mesophase pitch-based carbon fibers are used in specialized thermal management and electromagnetic interference shielding applications [19]. Such exceptional properties of MPCFs cannot be achieved in carbon fibers based on polyacrylonitrile (PAN). However, MPCFs lag behind PAN-based carbon fibers in terms of mechanical strength [13]. Consequently, PAN-based carbon fibers are preferred for structural applications, including medium to large-scale use in aerospace and automotive applications, while the applications of MPCFs represent smaller markets [6]. For this reason, PAN-based carbon fibers have a 90% share of the worldwide carbon fiber market, valued in USD 2 billion in 2015, while MPCFs share about 8% of the market [33].

Mesophase pitch can be obtained from low-cost precursors derived from inexpensive residues of petroleum and coal tar refining. Also, a high carbon yield of 75 wt% is obtained from mesophase pitch as compared to only ~ 45 wt% for PAN precursors [1]. Furthermore, the production of PAN and the oxidative stabilization and carbonization of PAN-based carbon fibers release toxic gases such as HCN. In contrast, the heat treatment of pitch produces primarily CO_2 [16]. Considering the above factors, mesophase pitch has significant potential as a low-cost precursor for high-performance carbon fibers.

The potential of MP precursor carbon fibers lies in improving their strength, while maintaining their superior electrical and thermal conductivities. Previous studies have successfully explored different approaches to enhancing strength by focusing on the chemistry and rheology of the liquid crystalline pitch [36], the oxidative stabilization conditions of the as-spun pitch fibers [37] and the high temperature treatment conditions of the oxidized pitch fibers [38]. Improving the melt spinning conditions can potentially lead to further enhancements because it is during this step that the fiber microstructure develops, which is retained in carbon fibers and largely determines the properties of the resulting carbon fibers [39].

Melt spinning is a process that involves three main steps, namely melting of the pitch, extrusion of the molten pitch through a spinneret, and drawing of the extrudate to form filaments. For carbon fibers from discotic mesophase pitch, the vast majority of studies on the relationships between melt spinning conditions, fiber microstructure and carbon fiber properties have investigated variables involving the melting and extrusion steps. Among the most important findings of such studies are the important roles spinning

temperature [28], pre-spinneret flow deformation [40], spinneret geometry [39] and spinneret capillary shear rates [41] play in the evolution of a transverse microtexture in MPCFs, and the existence of a correlation between transverse microtexture and carbon fiber properties [5,42]. Also, modeling and simulation studies on flow of nematic liquid crystals through capillaries have focused on the development of textures in the transverse direction [43,44]. However, the effect of drawdown of mesophase pitch extrudate on the microstructure and properties of resulting MPCFs has not been systematically investigated.

Drawdown occurs in multiple steps of the processing of polymer and PAN fibers, and the relationship between drawing and fiber microstructure has been reported extensively in the literature, with numerous studies establishing that the degree of crystalline orientation of PAN fibers improves with increasing DDR, which in turns leads to enhanced carbon fiber properties [45,46]. However, this approach has not been systematically investigated for MPCFs, since mesophase pitch is a nematic liquid crystal consisting of discotic molecules only about a few nanometers in length, in contrast to long-chain PAN molecules that are tens of nm long in extended state [1]. Thus, this part of the dissertation will focus on evaluating the effect of drawdown ratio (DDR) on the microstructure of mesophase pitch-based carbon fibers. The presented experimental results can stimulate future modeling and simulation studies on the development of longitudinal textures in MPCFs, to complement the ones on transverse textures mentioned above.

2.2 Experimental

2.2.1 Materials

The material used in this study as precursor for fiber processing was ARMP, a synthetic pitch with 100% mesophase content, produced by Mitsubishi Gas Chemical Company through catalytic synthesis of naphthalene. The use of a synthetic MP is preferred in technical studies because of the uniformity in properties as compared to petroleum pitches [18]. However, the overall molecular architecture, disc-like polyaromatic hydrocarbons, is similar in both ARMP mesophase pitch and petroleum-based mesophase pitches. In addition, the ARMP mesophase pitch has a softening point generally similar to that several petroleum-based mesophase pitches, about 270-290 °C. Also, ARMP and petroleum-derived MPs have comparable viscosity, 10-30 Pa·s, at typical spinning conditions [47,48].

The softening point of the pitch ARMP was measured following the ASTM D3104 standard test method using a Mettler Toledo FP90. At a heating rate of 10 °C/min, the softening point was measured at 281 ± 17 °C. Note that mesophase pitch does not display a true melting phenomenon. However, the softening point is a useful empirical property because fiber spinning is typically conducted at temperatures about 30 °C above the softening point. Table 3 summarizes typical properties of the AR grade mesophase pitch used throughout this study .

Table 3. Typical properties of AR grade mesophase pitch [49]

Appearance, visual	Black Pellet
Bulk Density (g/cm^3)	>0.65
Specific Gravity (25 °C)	1.23
Specific Heat (cal/g·°C)	0.65
Softening point (°C)	275～295
Mesophase content, wt%	100
Hydrogen / Carbon (atom/atom)	0.58～0.64
Flash Point (°C)	>300
Ash (ppm)	<20

2.2.2 Processing

Melt spinning

Throughout this study, precursor fibers were obtained using a batch unit (Alex James and Associates, Greenville, SC) operating at a constant volumetric flow rate. The batch process used about 30 g of the crushed pitch that was degasified in vacuum for one day prior to spinning. The precursor was charged to a steel barrel with appropriate spinneret attached at the bottom. The barrel was purged with nitrogen for a minimum of 12 hours before spinning, and during the entire duration of the spinning run to prevent the oxidation and crosslinking of the pitch. Note that pitch possesses residual reactivity that is utilized during subsequent oxidative stabilization process, i.e., after pitch fibers have been melt-spun.

A heating jacket set to 300 °C accomplished the melting of the material, and a positive displacement accomplished the extrusion of the molten material. Pressure drops in the spinneret capillary varied in the range 300-2300 psi across the spinning runs. The

extrusion linear speeds ranged between 0.5 and 7.0 m/min. The drawing of the extruded fibers used a 4 inches-diameter roll spinning at linear speeds controlled between 25 and 700 m/min. Natural convection air cooling was used for the solidification of the precursor fibers down the spinning line, which had a constant length of 2 feet (distance between spinneret and roll).

Four custom-designed spinnerets were used, each one with an individual set of ultrafine capillary diameter, capillary length and number of holes, as presented in Table 4. The rationale behind this varied choice of spinnerets is to obtain fibers of equivalent diameter with contrasting drawdown ratios, in order to assess the effect of DDR on carbon fiber properties while leveling the effect of diameter.

Table 4. Characteristics of spinnerets.

Capillary diameter, μm	Capillary length, μm	Number of holes
50	250	18
75	370	18
100	200	12
150	300	12 or 40

A filter was placed above the spinneret to prevent the blocking of the spinneret capillaries by any impurities in the mesophase pitch. The spinnerets with 50 and 75 μm capillary diameters used multilayer sintered metal filters with a mesh size as small as 14 μm, while the spinnerets with 100 and 150 μm of capillary diameters used multilayer stainless steel wire cloth filters with a mesh size as small as 44 μm.

DDR was calculated from the as-spun fiber diameter (d_L) and the spinneret capillary diameter (d_0) as

$$DDR = (d_0/d_L)^2 \quad (2)$$

The apparent shear rate at the wall of the spinneret capillary, $\gamma|_{app}$, was calculated as

$$\gamma|_{app} = \frac{4Q}{\pi R^3} \quad (3)$$

where R is the spinneret capillary radius and Q is the flow through a single spinneret capillary. The above equation gives the true shear rate at the wall of a capillary for a Newtonian fluid, and hence, in the case of a non-Newtonian fluid, it gives the *apparent* shear rate at the wall of a capillary. For a non-Newtonian fluid, the true shear rate at the wall of a capillary, $\gamma|_w$, is given by the Weissenberg-Rabinowitsch correction [50,51]:

$$\gamma|_w = \gamma|_{app}\left(\frac{3}{4}+\frac{1}{4}\frac{d\ln Q}{d\ln \tau_w}\right) \quad (4)$$

where τ_w is the shear stress at the capillary wall. In the case of power law fluids, for example, the derivative in equation 4 is equal to 1/n, thus the Weissenberg-Rabinowitsch equation can be expressed as [50,51]:

$$\gamma|_w = \gamma|_{app}\left(\frac{3n+1}{4n}\right) = \frac{4Q}{\pi R^3}\left(\frac{3n+1}{4n}\right) \quad (5)$$

As discussed in section 1.2.2. and seen in Figure 10, it has been shown in previous studies (e.g., Kundu [22]) that AR-type mesophase pitch displays a fairly flat viscosity profile at intermediate to high shear rates over a range of temperatures (280–297 °C) typically used for melt spinning. In the present work, shear rates under 10000 s^{-1} were encountered at spinning temperatures exceeding 300 °C, so the Newtonian assumption was reasonable.

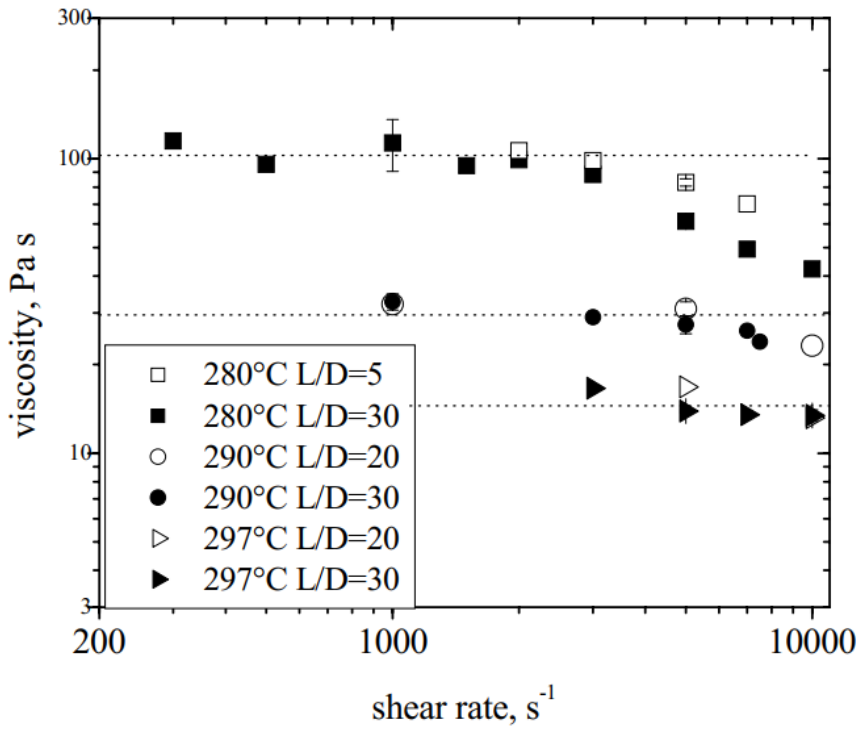

Figure 10. Apparent viscosity of mesophase pitch as a function of shear rates. Dotted lines represent the trend [22]

Stabilization

As-spun fibers were oxidatively stabilized in a forced convection, atmospheric oven. The fibers in the bundles were carefully separated to reduce the packing density and thus lessen the external diffusion limitations to mass transfer. The stabilization was realized over the temperature range 220-240 °C for a period of time in the range 30-75 hours to achieve an average mass gain of 12%. A heating rate ~ 3 °C/min was used to heat the oven from room temperature to the final stabilization temperature. The extent of the cross-linking was also verified by a heat test in which the stabilized fibers were put in contact with a soldering iron at ~ 400 °C. Any observed distortion of the fibers indicated an insufficient stabilization, while a lack of deformation signified an adequate stabilization.

High temperature treatment

Three high temperature furnaces were used to carbonize and graphitize the oxidized fibers (Astro 1000, Astro 1100 and HP50, Thermal Technology LLC). The furnaces were vacuumed three times and purged with helium before starting the heating. Each sample was encased in a box made of Grafoil® (flexible graphite). To obtain samples to study the effect of DDR on carbon fiber microstructure, the heat treatment program below was followed:

- Room temperature to 400 °C at a rate of ~ 20 °C/min
- 400 to 1000 °C at a rate of 3 °C/min
- 1000 to 2100 °C at a rate of 15 °C/min

The heat treatment program above translates into an average heating rate of ~ 8 °C/min. The final HTT was held for a minimum of 30 min to ensure a complete conversion from pitch to graphitic carbon, after which the furnace was water-cooled to room temperature at a rate of 35 °C/min.

The effect of heating rate on crystallite coherence length was studied for constant spinning conditions, stabilization program, and heat treatment temperature. For this purpose, subsets of a limited number of oxidized fiber samples underwent two heat treatment programs to 2400 °C, one at an average heating rate of ~ 8 °C/min as described above, and another that consisted of heating from room temperature at a rate of ~ 60 °C/min, holding the final HTT for 60 minutes and cooling to room temperature at a rate of 30 °C/min.

2.2.3 Fiber characterization

Measurement of fiber diameter

As-spun fiber diameter and carbon fiber diameter were measured by either laser diffraction, or by light microscopy on an Olympus BX60 microscope with a 50x objective and using Image-Pro plus software for image processing. A minimum of 20 specimens per sample were used to report diameter as average with a 95% level of confidence from a t-statistic.

The measurement of fiber diameter by the laser diffraction technique is explained as follows, adapted from Perry et al. [52]. The laser diffraction pattern of an infinitely thin

sheet of width d is the same as that of a slit of the same width. It consists of a series of maxima and minima on both sides of a central maximum. The separation δ_s between the first corresponding pair of minima is given by

$$\delta_s = \frac{2\lambda \cdot s}{d} \tag{6}$$

where λ is the laser wavelength and s is the distance between the screen and the lath. Assuming that a fiber diffracts as a slit, i.e. the slit approximation, its diameter can be derived from equation 6. In the present work, the following parameters were used in equation 6:

$\lambda = 632.8$ nm

$s = 556.26$ mm

The experimental arrangement using the above parameters is highly desired for the accurate measurement of diameter of thin fibers ($\leq$ 7 μm), unlike some automated machines. That is because the laser diffraction pattern created by thin fibers has a $\delta_s \geq 10$ cm. The values of fiber diameter obtained from the laser diffraction technique compared well with the ones obtained by light microscopy, as displayed in Figure 11.

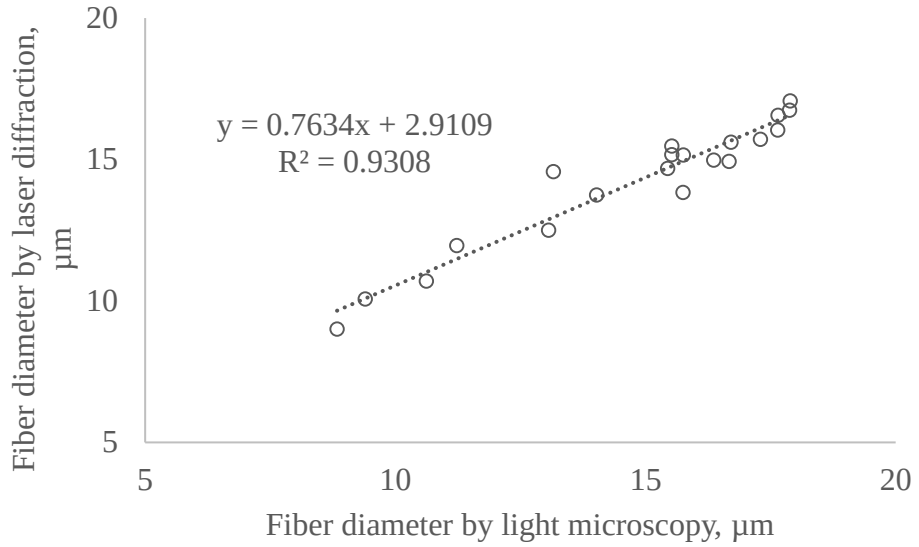

Figure 11. Carbon fiber diameter measured by laser diffraction vs. measured by light microscopy.

Analysis of microtexture by scanning electron microscopy

Transverse and longitudinal textures of carbon fibers were examined by scanning electron microscopy (SEM) of the exposed cross-sections, using a Hitachi S4800 at accelerating voltages in the range 3.0-15.0 kV. Fiber samples were cut to ~ 5 mm length and placed parallel to the electron beam for observation of the exposed cross-section. The longitudinal surface was observed by cutting fiber samples to ~ 15 mm length and placing them perpendicularly to the electron beam. ImageJ image processing software was used to measure microstructural features from the SEM micrographs.

Analysis of microstructure by Raman spectroscopy

Microstructural features of carbon fibers, namely crystallite size (L_a) and point-like defect density (L_D), were quantified by Raman spectroscopy of the fiber surface. The instrument used was a Renishaw Ramascope spectrometer with the following specifications:

- Laser wavelength: 785 nm
- Laser power: 25 mW
- Magnification: 50x
- Laser spot size: ~ 2 μm
- Exposure time: 10 s
- Temperature: 300 K

Previous studies on graphitic materials have indicated that the ratio of the integrated intensities (areas) of bands D and G (expressed as A_D/A_G) is inversely proportional to the crystallite coherence length, L_a [53,54]. Cançado et al. [55] developed a general relationship to determine L_a of graphitic systems for any excitation laser energy in the visible range,

$$L_a = \left(2.4\times10^{-10}\right)\lambda_l^4 \left(A_D/A_G\right)^{-1} \quad (7)$$

where λ_l is the laser line wavelength in nanometers. In addition, studies on graphene samples by Cançado et al. [56] revealed that the ratio of intensities between the D and G bands (expressed as I_D/I_G) strongly depends on the laser wavelength, for a given point-like

defect density. Based on their finding, they also developed a correlation for the determination of the distance between point-like defects (L_D) in graphene by Raman spectroscopy for any excitation wavelength in the visible spectrum,

$$L_D^2(\mathrm{nm}^2)=(1.8\pm0.5)\times10^{-9}\lambda_l^4(I_D/I_G)^{-1} \quad (8)$$

Wire 3.4 curve fitting software was utilized to compute the intensities and integrated intensities of the Raman bands. Values of L_a and L_D are reported as average with a standard error.

Analysis of microstructure by wide-angle x-ray diffraction

Carbon fiber bundles were analyzed by wide-angle x-ray diffraction (WAXD) in a Bruker D8 Venture diffractometer with a copper Incoatec Microfocus Source IμS, with a wavelength of 0.15406 nm, and operated at 50 kV and 1 mA. The bundles, ~ 20 mm long x ~ 0.1 mm thick, were prepared by impregnating the fibers with a bonding agent such as acrylate glue or a sizing solution of nonionic polypropylene, and carefully aligning the fibers within the bundle. The diffraction pattern was captured by a Photon 100 CMOS detector after an exposure time of 90 seconds. Each sample was tested by duplicate. APEX3 software was used for instrument control and data processing, including the integration of the diffraction pattern to generate a diffractogram of integrated intensity vs. diffraction angle 2θ.

The interplanar spacing (spacing between graphene layers in carbon crystallite) was calculated from Bragg's law:

$$d_{002} = \frac{\lambda}{2 \sin \theta} \tag{9}$$

Where d_{002} is the interplanar spacing, λ is the x-ray wavelength and θ is the diffraction angle corresponding to the (002) planes, in radians. In crystalline carbon, such planes typically display a 2θ peak in the range 25.9-26.6° [57].

2.3 Results and discussion

2.3.1 Fiber processing

Table 5 presents the spinning conditions used to produce as-spun fiber samples A-H, and the resulting drawdown ratios (DDR). The range of values for $\gamma|_{app}$ in the capillary are generally consistent with those observed by other authors for the spinning of mesophase pitch [58].

Table 5. Spinning conditions of ARMP precursor fiber samples.

Sample	Capillary diameter d_0, μm	Capillary wall shear rate $\gamma\|_{app}$, 10^3 s^{-1}	Pitch fiber drawdown ratio (DDR)
A	150	2	117 ± 28
B	75	7	17 ± 3
C	100	4	58 ± 10
D	75	7	32 ± 3
E	75	2	44 ± 5
F	50	9	19 ± 3
G	150	2	189 ± 29
H	50	9	14 ± 2
J	75	3	43 ± 5

For a spinneret with a fixed capillary diameter d_0, a constant as-spun fiber diameter (d_L) results from a specific value of DDR. Therefore, precursor fibers of equivalent final as-spun diameter but different DDRs have to be obtained from different spinnerets, as explained earlier in section 2.2.2.

Also, since the batch unit operates at constant volumetric flow rate, and hence the volumetric flow rate through a spinneret capillary Q is also constant, the apparent shear rate at the wall of the spinneret capillary $\gamma|_{app}$ varies only with the capillary diameter, according to equation 3. Thus, using spinnerets with a relatively large number of holes scales down Q so that extrusion from the finest capillary diameters, in order to obtain low DDRs, would not be constrained by an excessively high $\gamma|_{app}$ [19].

As-spun fiber samples were converted to carbon fibers according to the procedure described in section 2.2.2, with an average carbon yield of about 70-75 wt% in the carbonization/graphitization process. After oxidative stabilization, samples A through H

were heat-treated to 2100 °C using Astro 1000 furnace, which has been recently refurbished and readily available.

To study the effect of heating rate on crystallite coherence length, limited samples were also heat-treated to 2400 °C using Astro 1100 furnace because this furnace is more difficult and expensive to operate. Two heating rates, a low heating rate of ~ 8 °C/min and a high heating rate of ~ 60 °C/min, were used. For the remainder of this work, samples heat-treated to 2100 °C will be labeled with the suffix "21". The ones heat-treated to 2400 °C using a heating rate of 8 °C/min will be labeled with the suffix "24", and the ones heat-treated to 2400 °C using a heating rate of 60 °C/min will be labeled with the suffix "24H".

Table 6 presents the average fiber diameter of the corresponding carbon fiber samples. Overall, carbon fiber diameter (d_{cf}) varied in the range 8-16 µm, with the lower end of the range being consistent with the fiber diameters reported for most commercially available MPCFs [31]. While carbon fiber diameters of samples D24 and E24 are similar to those of their counterparts D21 and E21, d_{cf} of sample B24 is significantly larger than that of its counterpart B21. The differences in carbon fiber diameter between sample B21, and samples B24/B24H, likely arose from some variability in as-spun diameters arising from the use of a batch spinning process (versus more stable but more expensive continuous spinning).

Table 6. Average diameter of carbon fiber samples heat-treated to 2100 and 2400 °C.

Precursor sample	Carbon fiber sample	HTT	Rate, °C/min	d_{cf}, µm
A	A21	2100	8	13.6 ± 0.7
B	B21	2100	8	12.1 ± 0.5
	B24	2400	8	15.5 ± 0.8
	B24H	2400	60	14.8 ± 0.7
C	C21	2100	8	10.6 ± 0.6
D	D21	2100	8	10.6 ± 0.3
	D24	2400	8	10.7 ± 0.1
	D24H	2400	60	10.7 ± 0.3
E	E21	2100	8	9.1 ± 0.2
	E24	2400	8	8.8 ± 0.3
	E24H	2400	60	9.0 ± 0.3
F	F21	2100	8	9.0 ± 0.5
G	G21	2100	8	8.3 ± 0.4
H	H21	2100	8	8.5 ± 0.4
J	J24	2400	8	8.0 ± 0.4
	J24H	2400	60	9.3 ± 0.4

2.3.2 Scanning electron microscopy

Figure 12 shows the SEM micrographs of longitudinal surfaces of representative specimens from carbon fiber samples heat-treated to 2100 °C. All samples exhibit definite fibrils running parallel to the fiber axis, similar to prior results reported for MPCFs [59,60]. Nominal fibril thickness was measured for each sample, varying in the range 70-220 µm as specified in the caption for Figure 12.

When samples are paired according to equivalent fiber diameter, viz. A21-B21, C21-D21, E21-F21 and G21-H21, it can be seen that the samples of low DDR of each pair present thicker fibrils with clearer contours than those of their high-DDR counterparts. The nominal thickness of fibrils for samples of high DDR was measured in the range 70-125

nm, while that for samples of low DDR was measured in the range 160-220 nm. The widening of fibrils with increasing HTT has been previously reported by Korai et al. [60], who measured a fibril thickness of 100 nm for mesophase pitch-based carbon fibers heat-treated to 1500 °C. However, this is the first time textural development has been identified as a function of DDR used during pitch fiber spinning. A possible reason is that a higher DDR translates into a more rapid quenching of the filament down the spinning line (for constant cooling air temperature and velocity), which in turn inhibits the stacking of the liquid crystal molecules [19]. Figure 13 presents the overall plot of fibril thickness vs. DDR, showing a moderate inverse relationship (Pearson coefficient = -0.705 with p-value = 0.051).

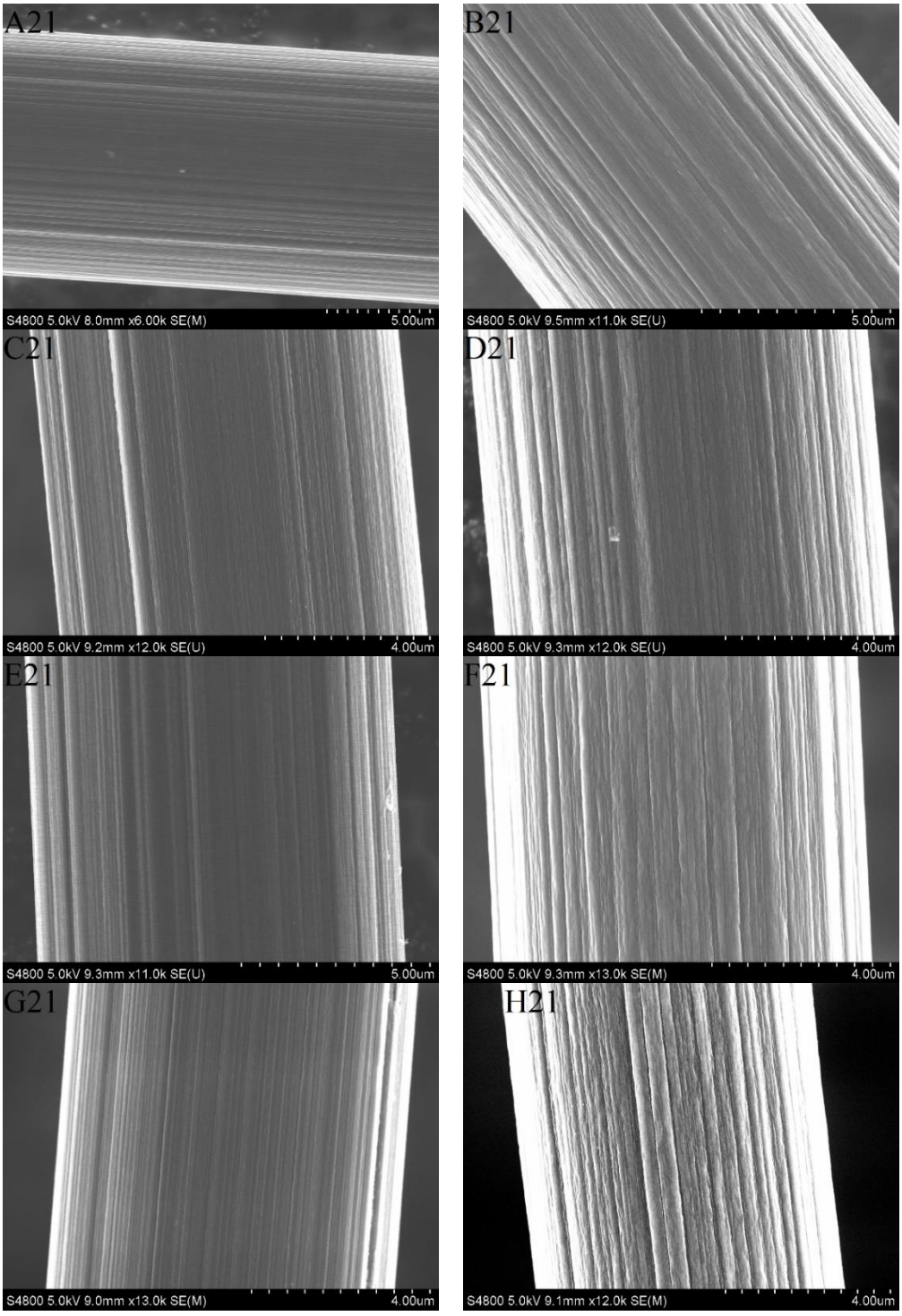

Figure 12. SEM of longitudinal surface of carbon fiber samples heat-treated to 2100 °C. Approximate fibril thickness of each sample as follows: A21, 125 nm; B21, 220 nm; C21, 80 nm; D21, 170 nm; E21, 100 nm; F21, 160 nm; G21, 70 nm; H21, 180 nm.

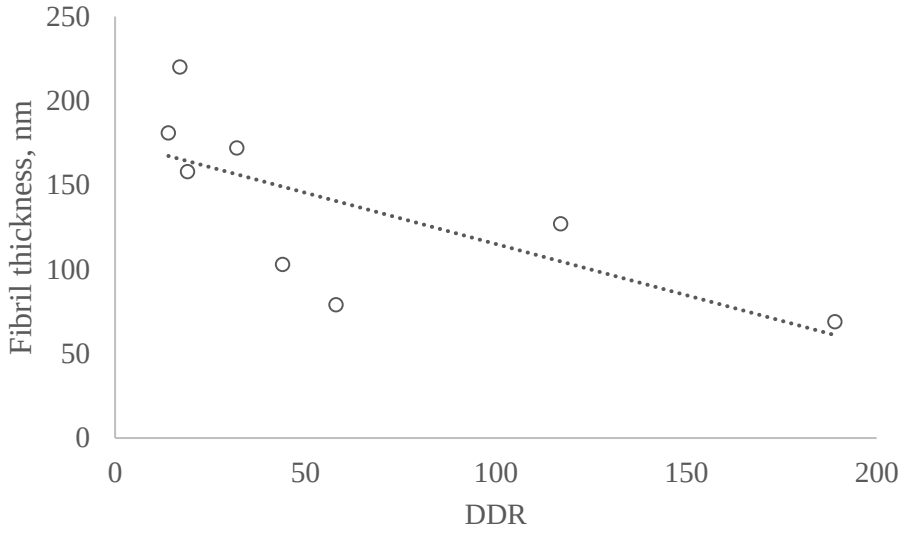

Figure 13. Fibril thickness vs. DDR for experimental carbon fiber samples heat-treated to 2100 °C.

Figure 14 presents the scanning electron microscopy (SEM) micrographs of cross-sections of representative specimens from carbon fiber samples A-H heat-treated to 2100 °C. The cross-sections of samples A21 through H21 show a radial-type layer plane texture, consistent with that typically reported in the literature for MPCFs [13,19,33]. Sample A21 appears slightly different, but the Pac-Man split is actually a consequence of radial texture. The split can occurs in fiber diameters larger than 10 μm to relieve the hoop direction stress generated during graphitization. Therefore, for the purpose of the current study, the transverse microstructure is radial in all of the samples and does not constitute a confounding variable with regards to mechanical properties that will be discussed later in Chapter 3.

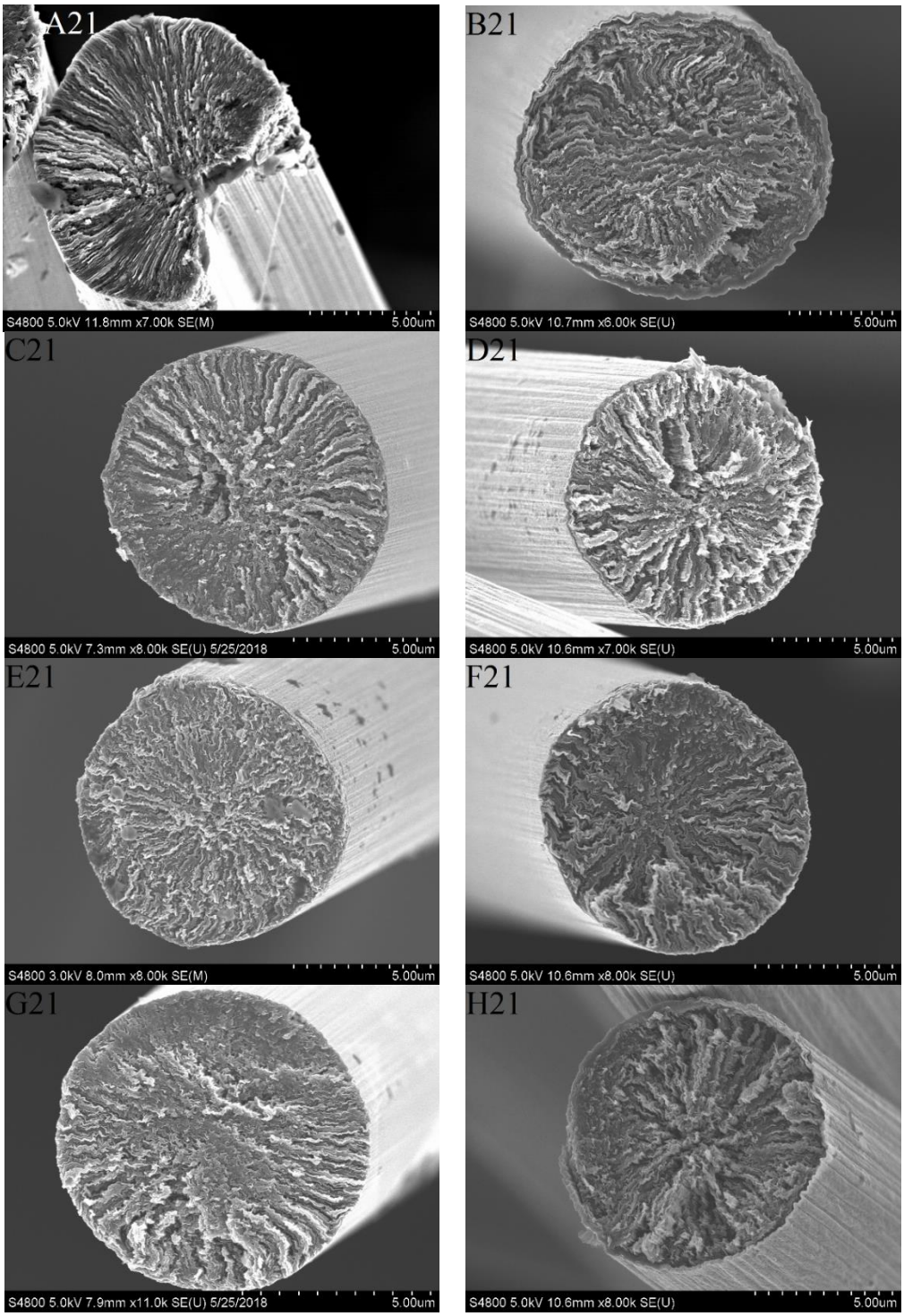

Figure 14. SEM of cross-section of experimental carbon fiber samples heat-treated to 2100 °C. Apparent capillary wall shear rate (x 10^3 s^{-1}) and DDR of each sample are as follows: A21, 2 and 117 ± 28; B21, 7 and 17 ± 3; C21, 4 and 58 ± 10; D21, 7 and 32 ± 3; E21, 2 and 44 ± 5; F21, 9 and 19 ± 3; G21, 2 and 189 ± 29; H21, 9 and 14 ± 2.

Further, it is noted that it is not possible to obtain much thicker fibers than type A-B; the starting as-spun fibers were as thick as ~ 19 μm, which represents a practical limit in terms of oxidative stabilization. If sufficient oxygen does not diffuse to the center of the fibers and the pitch does not get adequately cross-linked in the middle, partial melting can occur during the carbonization step, leading ultimately to gross defects/holes. If sub-par stabilization occurs in the middle, partial relaxation/reordering of textural orientation can take place in the middle, which can lead to slightly different texture in the fiber core. Also, as noted earlier, even when oxidative stabilization is adequate, the relatively large diameter fibers experience a large hoop direction shrinkage during graphitization (as layer coalesce during graphitic layer formation) [61], which leads to the classical Pac-Man splitting.

2.3.3 Raman spectroscopy

Figure 15 displays Raman spectra of carbon fiber samples heat-treated to 2100 °C arranged as four pairs with four nominal diameters; each pair consists of low and high DDR. All spectra show the **D** and **G** bands characteristic of carbon materials, at around 1350 and 1580 cm^{-1}, respectively. **D'** and **G'** bands also appear at around 1620 and 2650 cm^{-1} [55]. For all pairs, the sample of low DDR has a more intense **G** band, which is representative of graphitic ordering, relative to a broader **D** band, which is related to disordered carbon [1]. This translates into a greater crystallite coherence length and fewer point-like defects, according to equations 7 and 8.

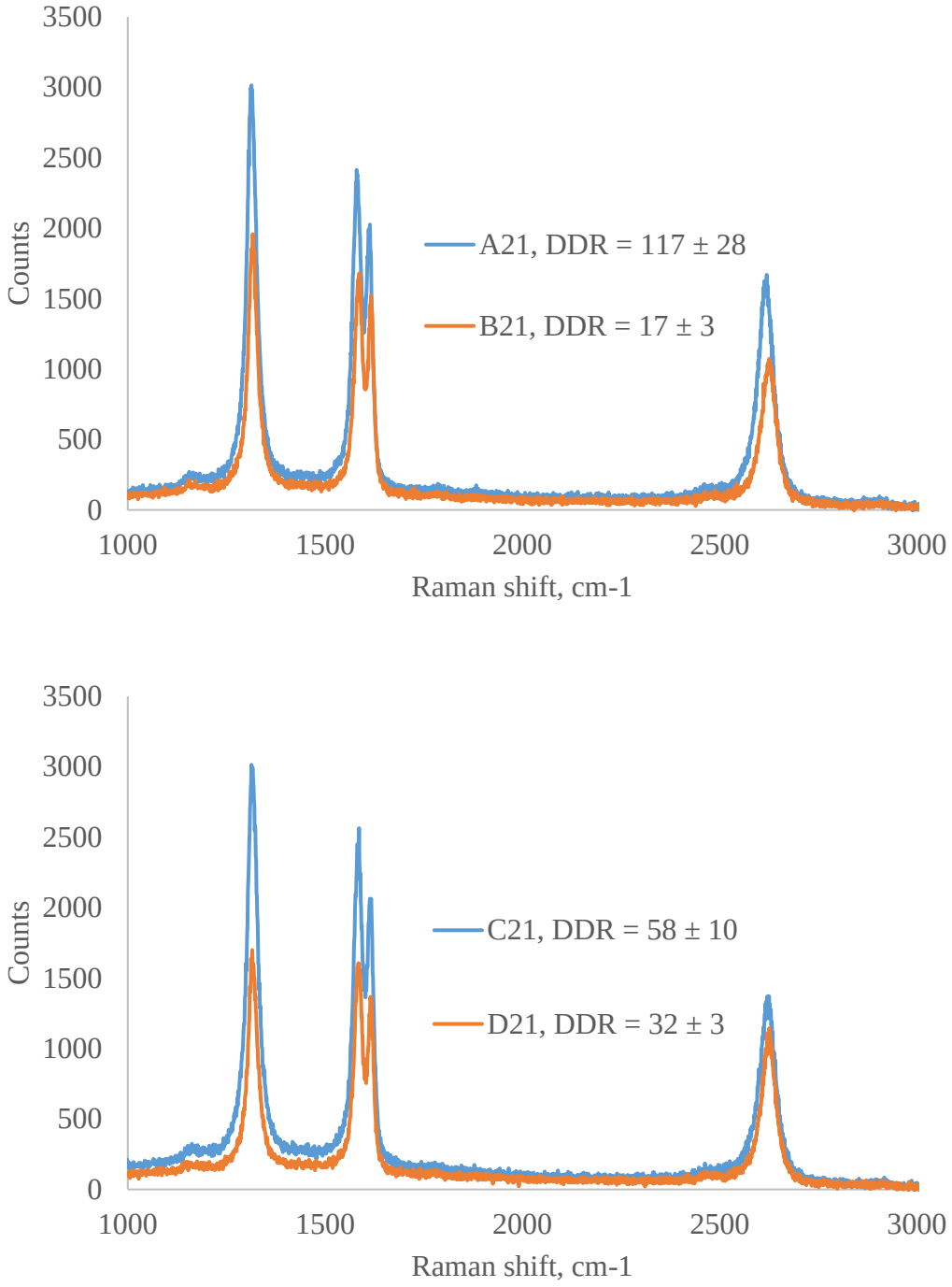

Figure 15. Raman spectra of carbon fiber samples heat-treated to 2100 °C.

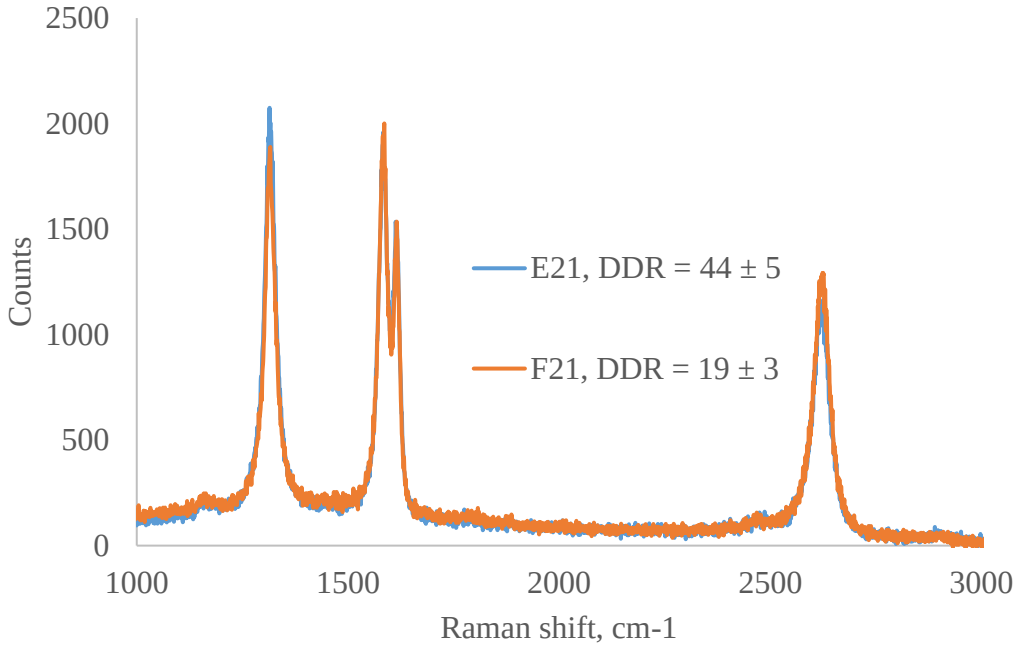

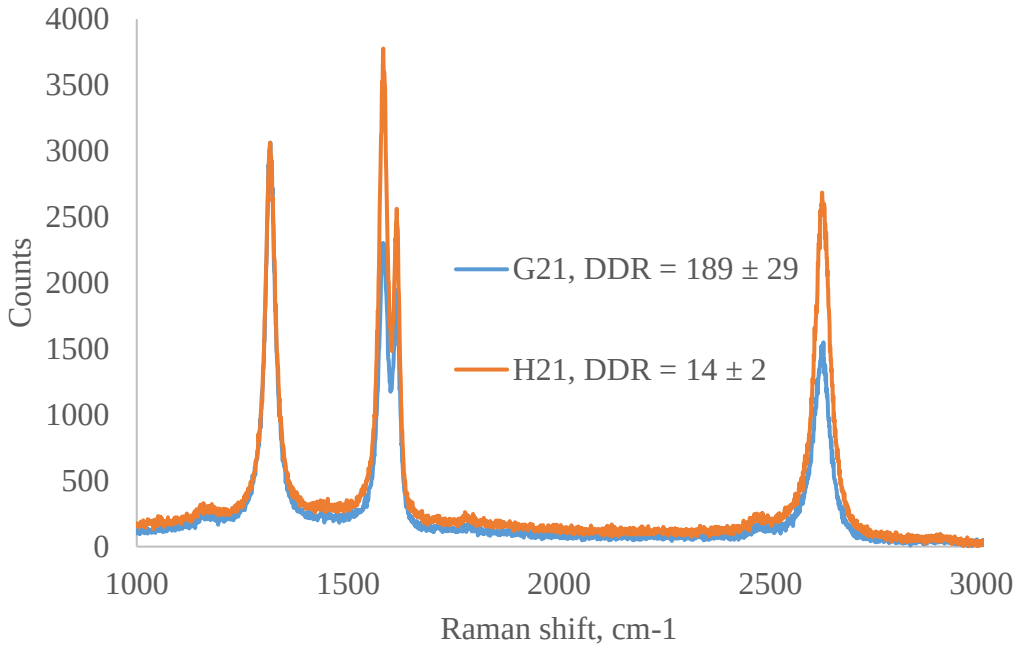

Figure 15 (continued). Raman spectra of carbon fiber samples heat-treated to 2100 °C.

Table 7 presents A_D/A_G, I_D/I_G, L_a and L_D of experimental carbon fiber samples heat-treated to 2100 °C. Average L_a and L_D across samples were ~ 71 nm and ~ 25 nm, respectively. K1100 carbon fibers were used as a control sample and displayed L_a = 160 ± 5 nm and L_D = 49 ± 2 nm; by comparison, L_a measured by x-ray diffraction has been reported around 120 nm for K1100 carbon fibers [58].

Table 7. Raman spectroscopy results for experimental carbon fiber samples heat-treated to 2100 °C.

Sample	A_D/A_G	I_D/I_G	L_a, nm	L_D, nm	DDR
A21	1.42 ± 0.05	1.23 ± 0.05	64 ± 2	24 ± 1	117 ± 28
B21	1.29 ± 0.02	1.09 ± 0.03	71 ± 1	25 ± 1	17 ± 3
C21	1.40 ± 0.04	1.15 ± 0.03	65 ± 2	24 ± 1	58 ± 10
D21	1.25 ± 0.02	1.06 ± 0.01	73 ± 1	25 ± 1	32 ± 3
E21	1.28 ± 0.02	1.06 ± 0.01	71 ± 1	25 ± 1	44 ± 5
F21	1.21 ± 0.02	1.00 ± 0.02	75 ± 1	26 ± 1	19 ± 3
G21	1.58 ± 0.02	1.34 ± 0.02	58 ± 1	23 ± 1	189 ± 29
H21	1.07 ± 0.02	0.86 ± 0.02	85 ± 2	28 ± 1	14 ± 2

The plot of L_a as a function of DDR for samples A21 through H21 is presented in Figure 16. An inverse relationship is evident (a negative correlation coefficient = -0.830 with p-value = 0.011). These results systematically document the novel effect of drawdown on the crystallite coherence length of MPCFs.

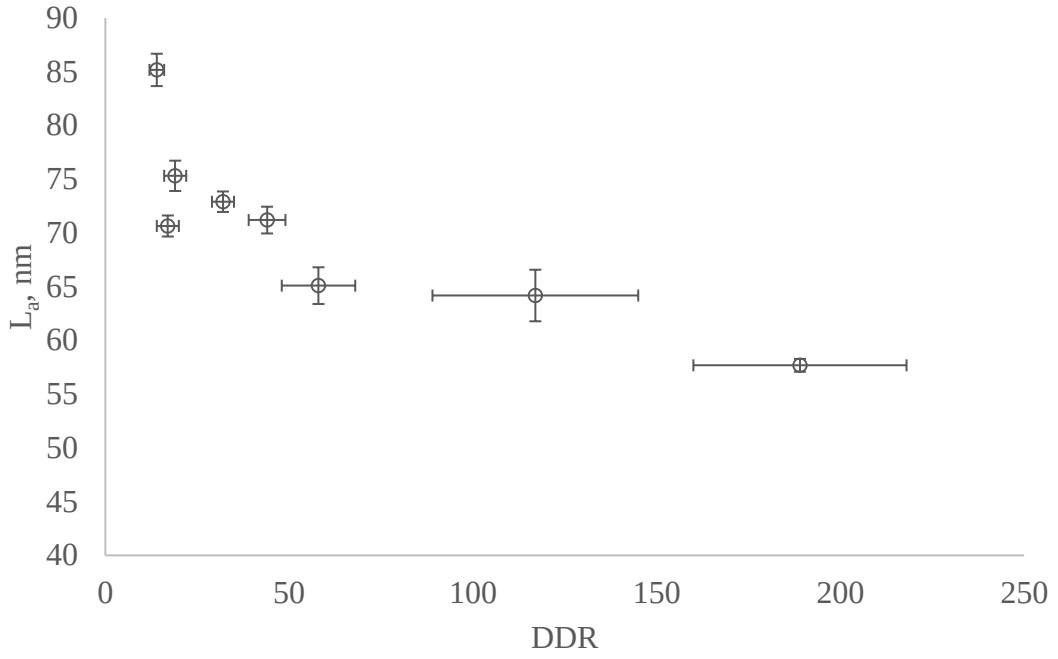

Figure 16. Crystallite coherence length (L_a) vs. drawdown ratio (DDR) for experimental carbon fiber samples heat-treated to 2100 °C.

Finally, Table 8 presents the crystallite coherence length of limited carbon fiber samples heat-treated to 2400 °C at two heating rates: ~ 8 and ~ 60 °C/min, as described in section 2.2.2. Four pairs of carbon fiber samples were compared (B24-B24H, D24-D24H, E24-E24H, and J24-J24H); the samples in each pair were derived from the same as-spun sample and hence they had the same spinning conditions. In all pairs, the sample of high heating rate has a larger crystallite coherence length L_a. This phenomenon can be related to the findings of Rogers et al. [62], who studied the graphitization of a high-sulfur mesophase pitch-based fiber and reported a less severe fiber damage during the sulfur removal period (1600-2000 °C) with high heating rates (≥ 60 °C/min).

Table 8. Crystallite coherence length of experimental carbon fiber samples heat-treated to 2400 °C at two heating rates.

Sample	Rate, °C/min	L_a, nm
B24	8	120 ± 6
B24H	60	166 ± 10
D24	8	113 ± 5
D24H	60	132 ± 6
E24	8	96 ± 3
E24H	60	130 ± 5
J24	8	98 ± 2
J24H	60	123 ± 3

2.3.4 WAXD

Figure 17 displays the diffraction patterns for experimental sample C21 as compared with commercial K1100, a highly-graphitic MPCF sample. The diffraction produced by the (002) planes of the carbon crystallites, preferentially oriented along fiber direction, is represented by an arc. As expected, K1100 has a more intense (002) arc, because of the higher graphitic content/orientation as a consequence of extremely high graphitization temperature, likely exceeding 3000 °C. This extreme treatment also makes such fibers quite expensive, with some reports citing a price of over $ 1000/lb.

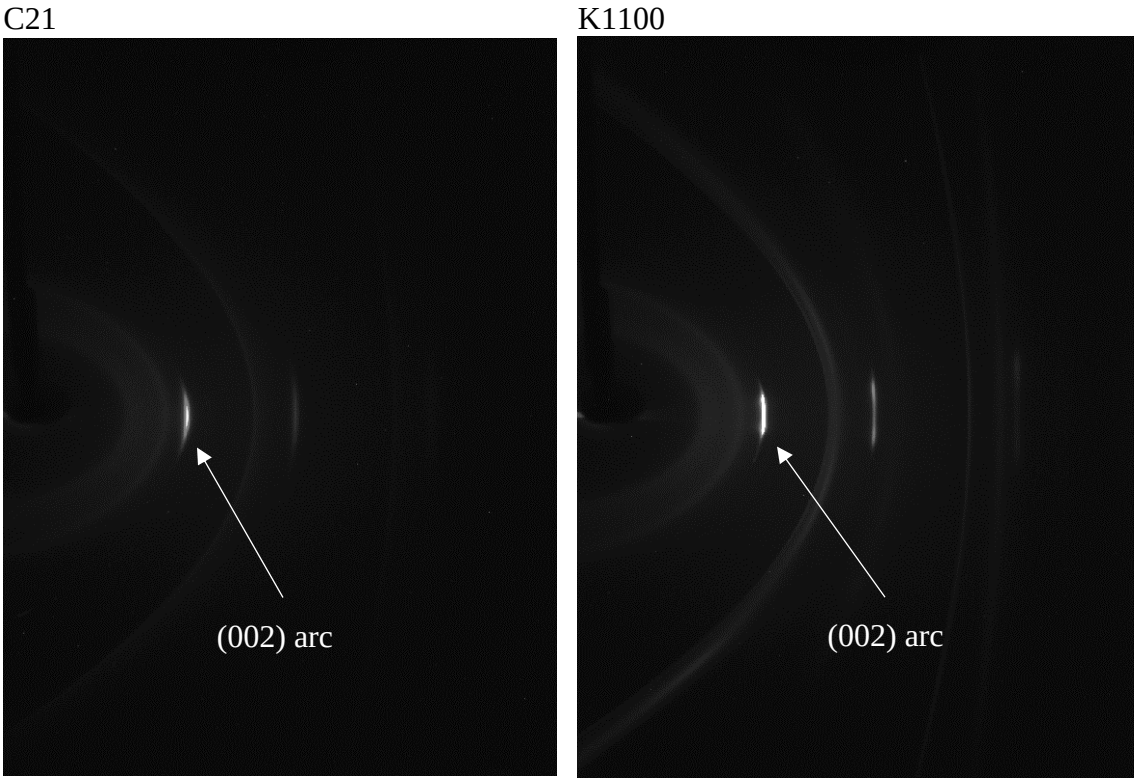

Figure 17. WAXD patterns of samples C21 and K1100, showing the higher intensity of the arc in sample K1100.

Figure 18 presents representative integrated azimuthal profiles over 2θ angle of experimental carbon fiber samples heat-treated to 2100 °C, along with the one for K1100 carbon fibers. The diffractogram for K1100 carbon fibers shows a narrower peak for the (002) plane, with the peak position slightly more than 26.5°, i.e., shifted to the right with respect to those of the experimental carbon fiber samples and consistent with a more graphitic sample. Peaks for experimental samples were all clustered close to 26.0°, with very little difference (≤ 0.05°) within the pairs of samples of comparable diameter. The

values of 2θ angle translated into values of d_{002} in the range 0.342-0.343 nm. A previous study on AR-pitch based carbon fibers heat-treated to 2100 °C calculated a slightly smaller value of d_{002}, about 0.341 nm [63]. For the control sample K1100, d_{002} was calculated as 0.3376 nm, and consistent with a value of 0.337 nm reported in a previous study by Alway-Cooper et al. [58]. Based on the full width at half maximum height, the stacking height, L_c, was estimated at 20 nm, and consistent with that reported in prior literature studies [18]. Overall, no significant differences in crystallinity were detected between the experimental carbon fibers tested, i.e., specific effect of DDR on overall crystalline development could not be precisely determined using the available x-ray diffractometer, which was designed for single crystal diffraction, not carbon fiber diffraction.

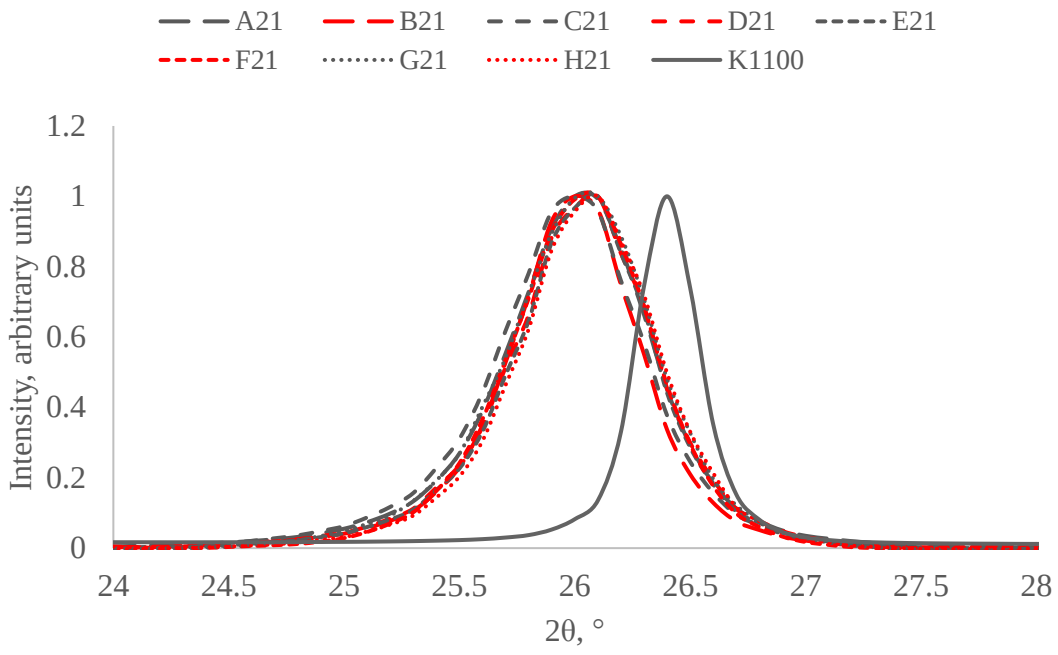

Figure 18. WAXD diffractograms of experimental carbon fiber samples heat-treated to 2100 °C, and K1100 carbon fibers.

2.4 Conclusions

This chapter presented microstructural differences for carbon fibers derived from pitch precursors fibers from different spinning drawdown ratios yet equivalent fiber diameters and heat treatment conditions. For a similar radial transverse texture, obtained for all carbon fiber samples, the effects of DDR on longitudinal microstructure and mechanical/transport properties were reported. Pac-Man splitting was present in the thicker fibers (~ 14 μm), which is caused by circumferential shrinkage during high temperature treatment. This study has also found evidence for the effect of DDR on the surface longitudinal microstructure: with decreasing DDR, thicker fibrils were observed along the fiber axis. Raman spectroscopy revealed that a decreasing DDR led to a larger crystallite size L_a, but reduced point defect density. For carbon fibers of ~ 8 μm diameter and a HTT of 2100 °C, L_a increased from 58 ± 1 to 85 ± 2 nm, for a drop in DDR from 189 ± 29 to 14 ± 2. The values of interplanar spacing d_{002}, obtained from WAXD, are consistent with those reported in the literature for carbon fibers derived from the same type of pitch and heat-treated to the same temperature. However, significant differences in crystallinity between the experimental carbon fiber samples could not be detected due to instrumental limitation. Future studies using different x-ray diffraction instrumentation are recommended for further clarification.

CHAPTER 3

EFFECT OF MESOPHASE DRAWDOWN RATIO ON CARBON FIBER MECHANICAL PROPERTIES

3.1 Introduction

As mentioned in the previous chapters, carbon fibers derived from mesophase pitch have inferior mechanical properties when compared to carbon fibers derived from polyacrylonitrile. More specifically, their mechanical strength, both tensile and compressive, are below the levels achieved for PAN-based carbon fibers. The tensile modulus of mesophase pitch-based carbon fibers, however, can reach the highest values among all carbon fiber types. This difference in ranking between two categories of mechanical properties, strength and modulus, speaks of the different mechanisms by which they are governed. Tensile strength is a defect-limited property, that is, it depends on the density of critical defects in the fiber structure, rather than on the overall perfection of the crystalline structure. It is susceptible to surface flaws, internal particulates, voids and misoriented crystalline regions [18]. On the other hand, tensile modulus is a lattice-dependent property, that is, it is strongly defined by the level of refinement of the graphitic structure. Therefore, tensile modulus is not as sensitive to critical defects as tensile strength is.

Since mesophase pitch-based carbon fibers exhibit a low tensile strength relative to their tensile modulus (as compared with PAN-based counterparts), their strain-to-failure values are also low. The opposite is true for PAN-based carbon fibers. Therefore, MPCFs

are more difficult to handle than PAN-based carbon fibers, which in turns discourages the use of MPCFS in the manufacture of composites. Thus, exhibiting superior tensile modulus is not sufficient condition for MPCFs to be extensively used in structural composites. For this reason, only such specialized applications in which deformation is strictly unwanted and rigidity is critical constitute a niche for MPCFs, due to their remarkable tensile modulus, and also their low, negative values of CTE (~ -1 x 10^{-6} K^{-1}). Some of these applications include aerospace and industrial products such as components of Unmanned Aerial Vehicles (UAVs), and wind turbine blades [64,65]. However, when considerable loads are involved, PAN-based carbon fibers are favored for use in structural composites.

With the aim of improving the mechanical strength of MPCFs, previous studies have found relationships between fiber processing conditions and carbon fiber tensile strength, with the fiber microstructure as an intermediate between the two, as discussed in Chapter 2. Lower spinning temperatures and no stirring before extrusion lead to radial transverse microstructure, which in turn is related to lower tensile strengths than those of non-radial microstructures [5]. Carbon fibers spun with stirring show non-radial microstructures, are less graphitizable, and have higher tensile strength [40]. These are examples of process conditions during pitch extrusion influencing the microstructure and the properties of the resulting MPCFs.

Regarding process conditions during drawing, it is a fact that, for a constant spinneret capillary diameter, a higher take-up speed leads to smaller as-spun diameters, according to the conservation of mass under steady state, which leads to finer carbon fibers. Also, it has been reported that smaller carbon fiber diameters are directly related to higher

tensile strengths because of a smaller probability of occurrence of a critical defect in the fiber cross-section. Therefore, higher take-up speeds have been indirectly linked to higher tensile strengths, because of the finer-diameter fibers thus produced. However, a higher take-up speed is not the only criterion for producing thinner fibers; capillary diameter is yet another factor as the use of a smaller capillary diameter can produce thinner fibers by using a smaller take-up speed. Thus, the drawdown ratio, which involves both the spinneret capillary diameter and the as-spun diameter as seen in equation 2, constitutes a more comprehensive variable to study the effects of spinning drawing on the mechanical strength of MPCFs.

Since mesophase pitch consists of discotic molecules, in contrast to long-chain polymers, the effects of a more severe drawing are not completely understood as they are in PAN fiber processing, as mentioned in Chapter 2. Therefore, the primary goal of this chapter is to report on the effect of drawdown ratio on mechanical properties of MPCFs, more specifically tensile and compressive strengths. The analysis of experimental data will be carried out across carbon fiber samples of equivalent fiber diameter and heat treatment conditions, to avoid confounding variables.

3.2 Experimental

3.2.1 Materials and processing

The materials and processing methods used in this part of the study were the same described in Chapter 2. Carbon fiber samples heat-treated to 2100 °C, using a low heating

rate of ~ 8 C°/min, were used to study the effect of drawdown ratio on mechanical properties. To verify the effect of heating rate on tensile properties, subsets of some carbon fiber samples were heat-treated to 2400 °C via two heating rates, ~ 8 and ~ 60 °C/min. The subsets that experienced the two heat treatment programs came from as-spun samples B, D, E and J in Table 5.

3.2.2 Fiber characterization

Analysis of tensile properties

Tensile properties of carbon fibers, namely tensile strength (σ_t), tensile modulus (E) and strain-to-failure (ε), were measured by single filament testing using the ASTM D3379-75 standard test method as a reference. The method consisted of the following steps: (i) separating a filament from the fiber bundle; (ii) mounting it on the centerline of a slotted cardboard tab; (iii) applying epoxy resin on the filament at each edge of the slot to bond the filament to the tab, allowing a minimum of 12 hours for the epoxy resin to cure at room temperature; (iv) aligning the tab with the pneumatic grips of a testing machine and gripping it; (v) burning away the sides of the tab with a soldering iron; and (vi) stressing the filament to failure at a constant strain rate. Specially care must be taken to align the fiber to the centerline of tab and to align the tab with the pneumatic grips of the testing machine, so that the filament experiences only tensile stress while being pulled apart by the machine. Otherwise, the filament could experience shear stress and the results would

not represent the tensile properties of the specimen. Figure 19 shows the typical mounting method for a single filament specimen.

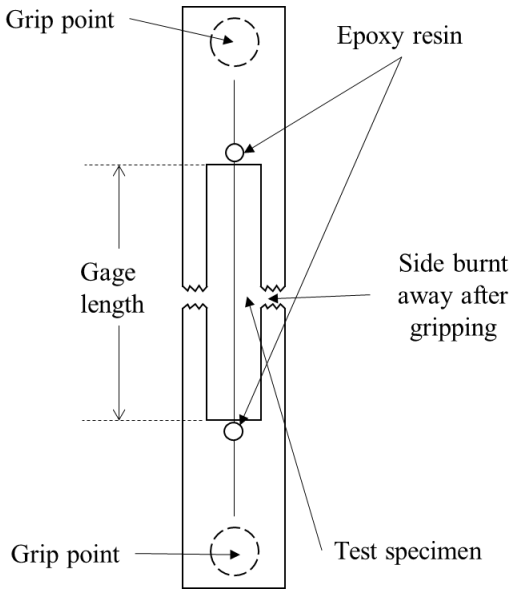

Figure 19. Representation of fiber mounting method for tensile testing (adapted from [66]).

The tests were performed in a MTI Phoenix machine equipped with a load cell of 500 g, using a constant crosshead velocity of 0.5 mm/min. Prior to tensile testing, fiber diameter of each specimen was measured by the laser diffraction technique described in section 2.2.3. The load cell of the machine measured the force required to elongate the specimen, and the tensile stress was calculated as

$$\sigma = \frac{F}{A} = \frac{F}{\pi(d_{cf})^2/4} \tag{10}$$

where F is the force, d_{cf} is the carbon fiber diameter, and σ is the tensile stress. This calculation of the tensile stress used the assumption of circularity for the cross-section of

the specimen being tested. In the present work, such assumption was verified by SEM of the cross-section of the carbon fiber samples (Figure 14), which shows circular cross-section in all samples. Values of tensile strength and tensile modulus were reported as average with a 95% level of confidence from a t-statistic.

System compliance was determined using tensile data from 25, 35 and 40 mm gage lengths, and a gage length of 25 mm was subsequently used for all testing. This determination was carried out to eliminate then effect of end-tab slippage during tensile test. The method of system compliance measurement is detailed as follows.

The elongation of sample is given by

$$\Delta L = \frac{L \cdot \varepsilon}{100\%} \tag{11}$$

where ΔL is the sample elongation (mm), L is the gage length (mm), and ε is the strain-to-failure obtained from tensile test (%).

Assuming a circular cross-section, the cross-sectional area of sample is given by

$$A = \frac{\pi \cdot d^2}{4} \tag{12}$$

where A is the fiber cross-sectional area (mm^2), and d is the fiber diameter (mm).

The indicated compliance is given by

$$C = \frac{\Delta L}{F} \tag{13}$$

where C is the indicated compliance (mm/N), ΔL is the sample elongation (mm), and F is the force or load at tensile failure (N).

For a given sample, several specimens are tensile-tested using a minimum of three gage lengths. After calculating C and A for each specimen of each gage length, a plot of C vs. L/A is created. The resulting curve is linearly fitted and the slope obtained is the inverse of the compliance-corrected tensile modulus.

Analysis of compressive properties

Compressive strength of carbon fibers was measured by the tensile recoil technique developed by Allen [67] for polymeric high-performance fibers. This technique is based on the recoil forces that act on the broken ends of a fiber right after tensile failure. Such recoil forces cause serious damage to a fiber when the magnitude of the compressive stresses that originate during snap-back are greater than the compressive strength of the fiber. Therefore, the tensile recoil technique applies only when the compressive strength is smaller than the tensile strength of a given fiber.

The sample preparation for compressive testing of carbon fibers was the same as that described above for tensile testing, involving the separation of a single filament from the bundle and bonding of the filament to the centerline of a cardboard tab. The tests were performed in the same MTI Phoenix machine used for tensile testing, using. a gage length of 25 mm. Carbon fiber diameter was measured by light microscopy or laser diffraction prior to testing.

After the tab was gripped to the testing machine and the sides of the tab were burned away, the filament was stressed at a constant strain rate to a stress level safely below its expected tensile strength, rather than being stressed to failure. In the practice, this was accomplished by using the HOLD function on the MTI Phoenix software, which allows the user to stop the crosshead movement at any moment.

After the crosshead was stopped at a desired stress level, it was normal for the stress to decay slightly because the motor/internal mechanism of the testing machine led to bounce-back. To slow down the decay of the tension, a constant crosshead velocity of 0.2 mm/min was used when the filament was being stressed, instead of the 0.5 mm/min used for tensile testing. Once the stress decreased to a desired level, the filament was split by a high-voltage electric arc (10000 V, 23 mA, 240 VA) causing the recoil of the two halves. The electric arc formed between two metal electrodes that had been brought within 5 mm of each side of the filament. The stress at which the filament had been subjected to right before the strike of the electric arc manifested into compressive stress upon recoil. Each half of the filament would either survive the recoil or fail under it, which was visually determined right after the arc strike.

Survival is represented by the fact that the compressive stress applied is smaller than the compressive strength of the fiber, whereas failure means that the compressive strength of the fiber has been exceeded by the compressive stress wave. A survival (1) or failure (0) grade was recorded for each half of the filament of each specimen tested, thus generating a binary response data. A survival grade was given when the half of the filament appeared intact, maintaining most of its length, while a failure grade was given when the

half was totally snapped, or most of its length was absent. The analysis of the outcome of the tensile recoil test was assisted by a camera that recorded the strike of the electric arc splitting the filament. The ability to play the videos in slow motion helped determine the survival or failure of a filament half.

3.3 Results and discussion

3.3.1 Tensile testing

Table 9 presents tensile testing properties (tensile strength σ_t, tensile modulus E and strain-to-failure ε) of experimental carbon fiber samples heat-treated to 2100 °C, along with their corresponding spinning conditions. The samples have been grouped as pairs with similar fiber diameters (A21-B21, C21-D21, etc.) with group G21-H21 having the smallest diameter.

Table 9. Tensile properties and spinning conditions of experimental carbon fiber samples heat-treated to 2100 °C.

Sample	d_{cf}, μm	σ_t, GPa	*E*, GPa	ε, %	$\gamma\|_{app}$, 10^3 s^{-1}	DDR
A21	13.6 ± 0.7	1.34 ± 0.24	413 ± 37	0.32 ± 0.05	2	117 ± 28
B21	12.1 ± 0.5	1.92 ± 0.20	514 ± 13	0.37 ± 0.04	7	17 ± 3
C21	10.6 ± 0.6	1.48 ± 0.26	427 ± 42	0.35 ± 0.06	4	58 ± 10
D21	10.6 ± 0.3	1.84 ± 0.18	541 ± 16	0.34 ± 0.03	7	32 ± 3
E21	9.1 ± 0.2	1.48 ± 0.30	394 ± 34	0.38 ± 0.07	2	44 ± 5
F21	9.0 ± 0.5	2.16 ± 0.19	514 ± 24	0.42 ± 0.04	9	19 ± 3
G21	8.3 ± 0.4	1.42 ± 0.19	470 ± 22	0.30 ± 0.04	2	189 ± 29
H21	8.5 ± 0.4	2.31 ± 0.28	515 ± 30	0.45 ± 0.05	9	14 ± 2

For all four pairs (having different diameters), the sample of low DDR has a higher tensile strength (statistical significant at p = 0.05). For instance, sample B produced at a lower DDR of 17 (vs 117 for A) led to a higher tensile strength. This is in spite of the fact that sample B was produced from the smaller capillary diameter that led to a higher shear rate. Previous studies have reported that increased shear rate leads to reduced tensile properties in MPCFs [19]. Results presented in Table 9 indicate that a low DDR results in a significantly higher tensile strength for carbon fibers generated from similar spinning temperature, stabilization conditions and HTT, and with similar diameter, despite the expected detrimental effect of a greater $\gamma|_{app}$ on the tensile strength.

While specific DDR values have not been reported in literature studies, mechanical properties of carbon fiber samples were generally consistent with literature values for MPCFs [31]. Average carbon fiber diameter, tensile strength and tensile modulus are ~ 10 μm, 1.7 GPa and 480 GPa across samples heat-treated to 2100 °C.

As discussed in Chapter 2, for samples of comparable fiber diameter and heat treatment temperature, the sample of low DDR displayed a larger crystallite coherence length (L_a) and distance between defects (L_D). For a given fiber length, a longer average crystallite size would translate into a smaller size of the defective inter-crystalline regions (assuming the structural model presented in Figure 8 (a) is applicable) and would result in enhanced tensile strength because strength is a defect-dominated property.

The tensile modulus values for the carbon fiber samples heat treated to 2100 °C varied in the overall range 400-550 GPa, without compliance correction. These values are

about 50% greater than those reported for most commercial PAN-based carbon fibers [31]. The compliance-corrected modulus for sample D21 was measured at 578 GPa. The plot of indicated compliance, C, vs gage length by cross-sectional area, L/A, for sample D21 is presented in Appendix A1. The modulus value is consistent with compliance-corrected values of ~ 600 GPa also reported for petroleum-based carbon fibers of HTT 2100 °C by Edie et al. [68].

Since tensile modulus is a lattice-dominated property, larger crystallite size could have a favorable effect on the tensile modulus. However, other crystallite features (*Z*, G, etc.) also have an effect on tensile modulus [69]. As explained in Chapter 2, the differences in these variables as a function of DDR could not be determined from WAXD because of instrumental limitation. Therefore, there is not sufficient evidence to establish a link between spinning DDR and tensile modulus. Also, it is noted that the tensile moduli reported in Table 9 are apparent values (not compliance-corrected), so a detailed statistical analysis was not conducted.

To study the relationship between tensile strength and carbon fiber diameter, a Weibull analysis was conducted. This type of analysis is recommended for brittle materials such as carbon fibers, for which strength is size-dependent. The Weibull model likens the behavior of the material to a chain wherein rupture under stress is controlled by the weakest link. That weakest link in a fiber usually is represented by a critical internal defect; if the weakest link reaches its fracture limit, the entire fiber breaks [70]. The probability of finding a critical internal defect increases with the size of the fiber, therefore the strength decreases with increasing length or diameter of the fiber [71]. In the present work, the gage

length for tensile is fixed, and the dependence of tensile strength on carbon fiber diameter is studied.

The two-parameter Weibull function is defined as

$$P = 1-\exp[-(\sigma/\sigma_o)^m] \quad (14)$$

where P is the probability of failure of the fiber, σ is the tensile strength of the fiber, and the parameters σ_o and *m* are the characteristic Weibull strength and the Weibull modulus, respectively. The Weibull modulus is a measure of the variability of the distribution, with a smaller *m* representing a broader distribution of fracture strength and a greater *m* representing a narrower distribution. Ductile metals are known to have a Weibull modulus approaching 100 indicating a narrowly distributed strength. Typical values of Weibull modulus for different reinforcing fibers are presented in Table 10.

Table 10. Weibull modulus of reinforcing fibers.

Type of fiber	Weibull modulus	Reference
Carbon	5-6	[72]
Glass	10-12	
Jute	2.7	
PE	10.0-15.2	[73]
PBO (Zylon)	7.4-7.8	
PPTA (Kevlar)	8.2-11.8	

Equation 14 can be rewritten as

$$\ln\{\ln[1/(1-P)]\} = m\ln\sigma - m\ln\sigma_o \quad (15)$$

If the Weibull treatment is valid for the material, experimental data plotted as $\ln\{\ln[1/(1-P)]\}$ vs $\ln\sigma$ gives a straight line, and the values of m and σ_o can be obtained from a least squares regression. The values of P were determined from the following estimator, which has been shown to lead to less biased m values for sample sizes smaller than 50 [74]:

$$P_i = (i-0.5)/N \tag{16}$$

where P_i is the probability of failure for the i^{th} strength and N is the sample size.

A commercial PAN-based carbon fiber, T300, was used as a control sample to verify the validity of the Weibull model in carbon fibers, wherein tensile strength is a defect-limited property. This commercial carbon fiber was used as a control sample because it represents a standard in tensile strength within the carbon fiber market, considering that, in general, PAN-based carbon fiber possess higher tensile strength than mesophase pitch-based carbon fibers, as mentioned before. Figure 20 presents the Weibull plot for T300, obtained from tensile testing data performed on 60 specimens following the same methodology described in section 3.2.2, showing a good coefficient of determination for the linear fit. The Weibull parameters were calculated as $m = 5.6$ and $\sigma_o = 2.5$ GPa. The value of the Weibull modulus is relatively consistent with a previous study on T300 that reported a value of $m = 7.0$, using a gage of length of 25 mm as well [75].

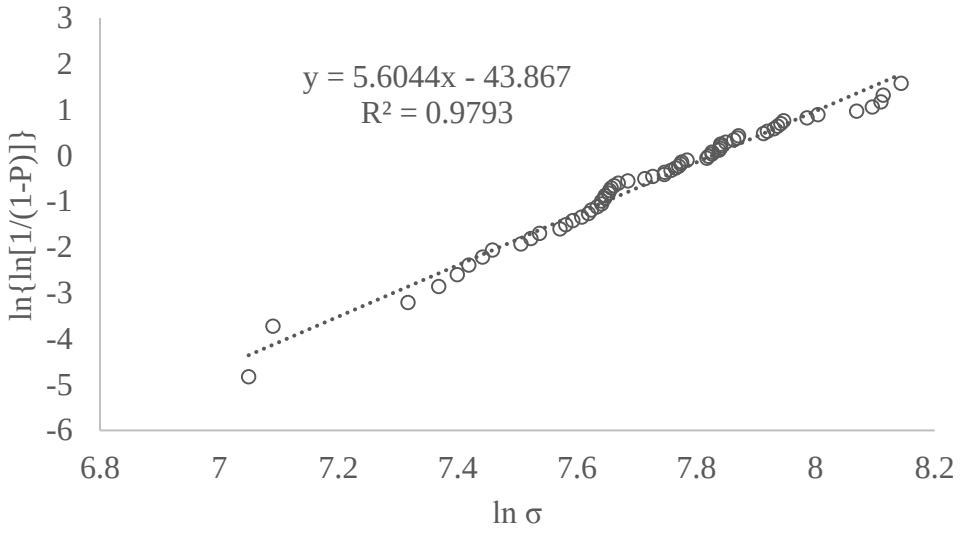

Figure 20. Weibull plot for T300, PAN-based carbon fiber.

The Weibull plots for samples A21 through H21 are presented in Figure 21. The Weibull parameters are calculated from the slope and the intercept of the regression equation. All regressions yielded reasonably good coefficients of determination R^2 (> 0.80).

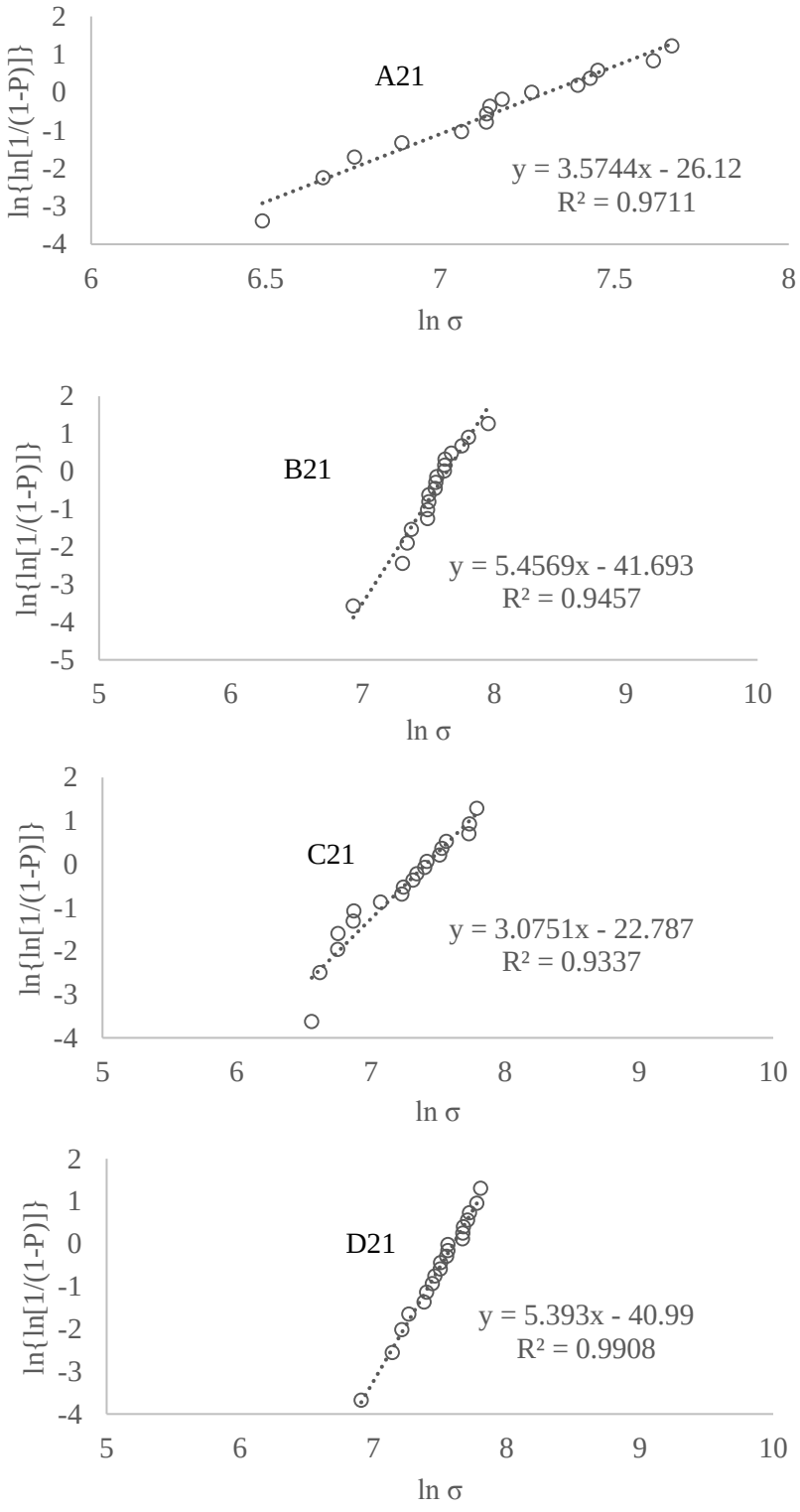

Figure 21. Weibull plots for experimental carbon fiber samples heat-treated to 2100 °C.

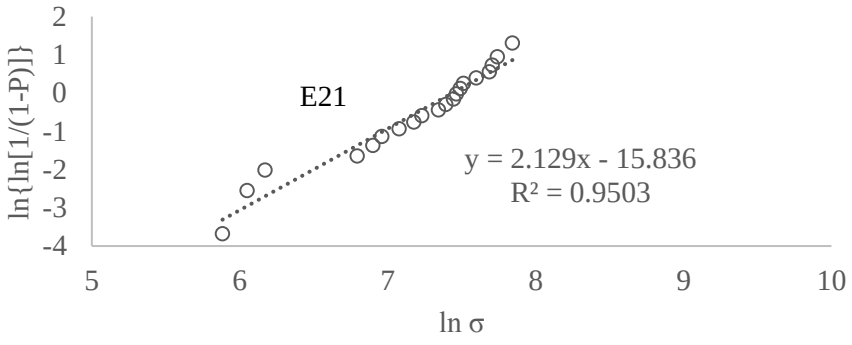

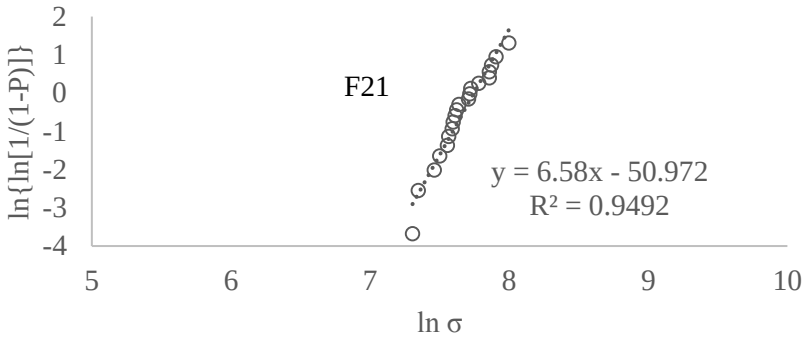

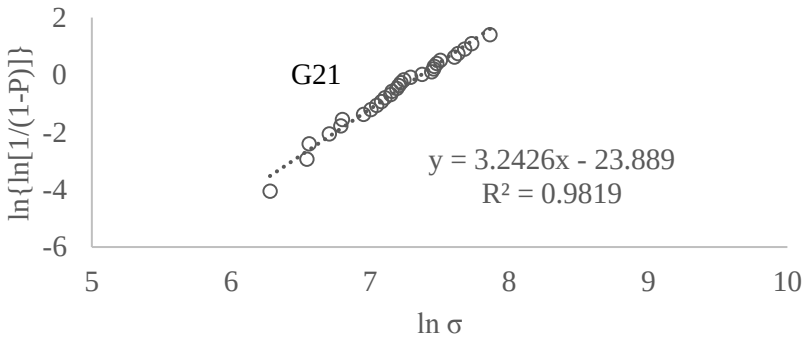

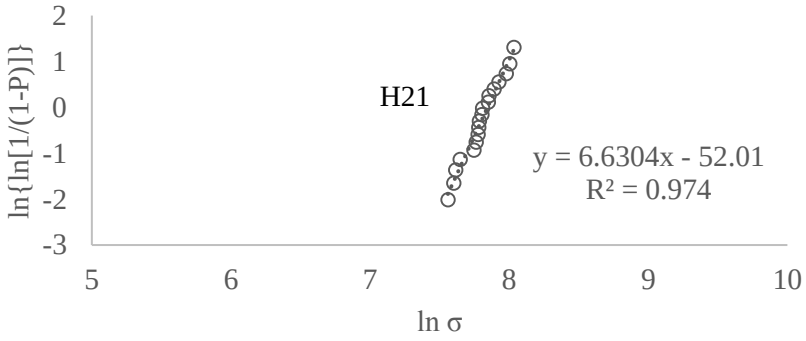

Figure 21 (continued). Weibull plots for experimental carbon fiber samples heat-treated to 2100 °C.

Table 11 presents the Weibull parameters of experimental carbon fiber samples heat-treated to 2100 °C, and the plot of σ_o vs d_{cf} is presented in Figure 22, grouped by level of DDR (high and low). An inverse relationship (i.e., negative correlation) is present for both levels, being stronger for the samples of low DDR (Pearson coefficient = -0.641 with p-value = 0.359 for high DDR samples and Pearson coefficient = -0.802 with p-value = 0.198 for low DDR samples), which is in accordance with previous studies on the relationship between tensile strength and fiber diameter [76].

Table 11. Weibull parameters for the experimental carbon fiber samples heat-treated to 2100 °C.

Sample	*m*	σ_o, GPa
A21	3.6	1.5
B21	5.5	2.1
C21	3.1	1.7
D21	5.4	2.0
E21	2.1	1.7
F21	6.6	2.3
G21	3.2	1.6
H21	6.6	2.6

The values of Weibull modulus ranged from 2.1 to 6.6 across all samples. These values are consistent with the range of 5-6 reported in the literature for the Weibull modulus of carbon fibers (Table 10). It should be noted that the Weibull modulus for samples with low DDR was greater than that of the samples with high DDR, i.e., the distribution of tensile strength in the sample of low DDR is slightly narrower.

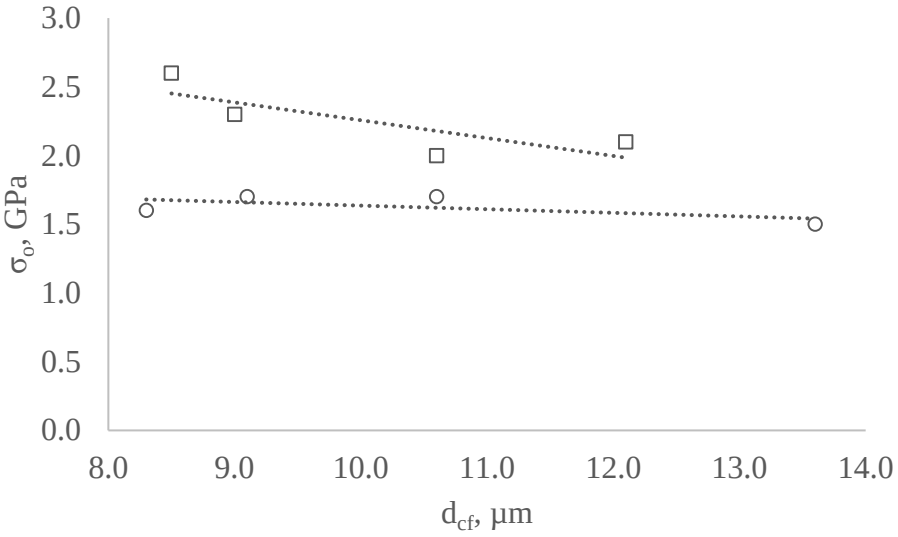

Figure 22. Weibull characteristic strength vs. carbon fiber diameter for experimental carbon fiber samples heat-treated to 2100 °C.

Finally, Table 12 presents the tensile properties of limited number of carbon fiber samples heat-treated to 2400 °C at two heating rates: ~ 8 and ~ 60 °C/min. The samples in each pair were derived from the same as-spun sample and hence they had the same spinning conditions. Results show that the samples produced from high heating rate have a lower tensile strength. Also, the sample of low heating rate has a lower tensile modulus. The behavior of the tensile strength is consistent with previous studies on MPCFs [62] and PAN-based carbon fibers [77,78], which showed that increasing the heating rate is detrimental to tensile strength because of the voids created in the fiber structure by the removal of non-carbon elements. On the other hand, the behavior observed for the tensile modulus has been previously reported for petroleum-derived, mesophase pitch-based carbon fibers of high sulfur content [79], for which a high heating rate favors a reduced

misorientation of the graphite basal planes, which in turn improves lattice-dependent properties such as tensile modulus.

Table 12. Tensile properties of experimental carbon fiber samples heat-treated to 2400 °C at two heating rates.

Sample pair	Rate, °C/min	d_{cf}, μm	σ_t, GPa	*E*, GPa
B24	8	15.5 ± 0.8	1.44 ± 0.25	432 ± 57
B24H	60	14.8 ± 0.7	1.39 ± 0.16	384 ± 45
D24	8	10.7 ± 0.1	1.92 ± 0.18	467 ± 27
D24H	60	10.7 ± 0.3	1.58 ± 0.17	506 ± 23
E24	8	8.8 ± 0.3	1.80 ± 0.21	526 ± 34
E24H	60	9.0 ± 0.3	1.67 ± 0.14	540 ± 17
J24	8	8.0 ± 0.4	1.82 ± 0.21	525 ± 32
J24H	60	9.3 ± 0.4	1.88 ± 0.16	591 ± 24

3.3.2 Compressive testing

Due to the more complex nature of the compressive test compared to that of the tensile test, tensile recoil tests were only performed on samples G21 and H21, in order to assess the differences in compressive strength between that pair of samples of contrasting drawdown ratios. Figure 23 presents snapshots from the video of a specimen with failure of top and bottom. Figure 24 presents those of a specimen with failure of top and survival of bottom, whereas Figure 25 presents those of a specimen with survival of top and bottom. In all figures, the snapshot to the left shows the moment before the arc strike, the one in the middle shows the moment of the strike, and the one to the right shows the moment after the arc strike.

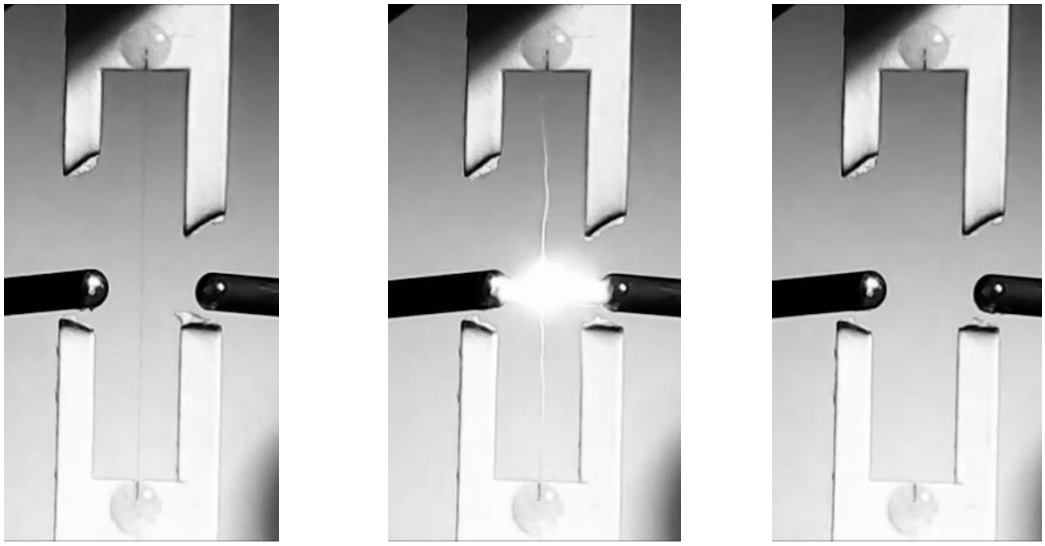

Figure 23. Snapshots of specimen under tensile recoil test. Sample H21, stress ~ 890 MPa, top and bottom fail.

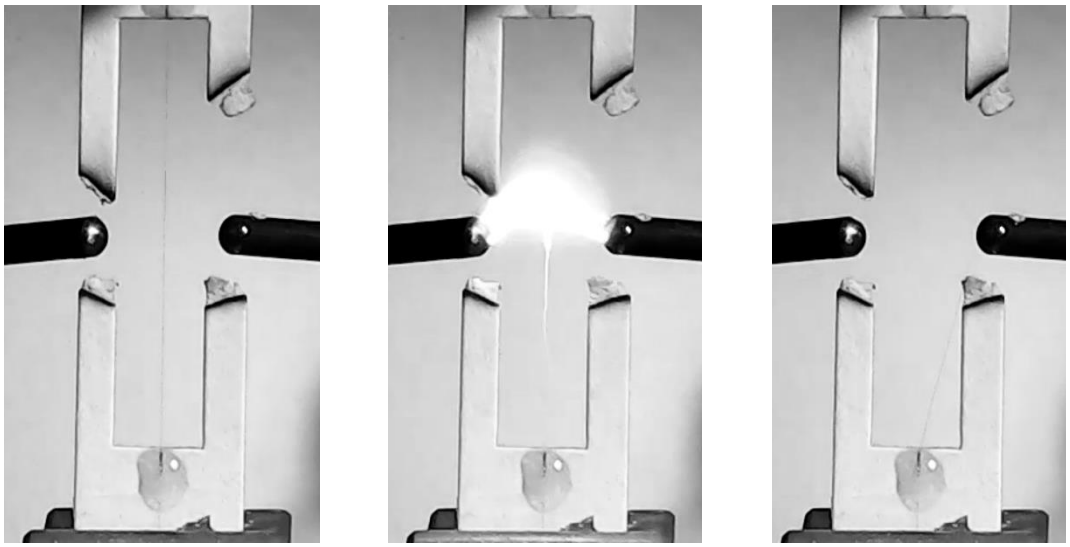

Figure 24. Snapshots of specimen under tensile recoil test. Sample H21, stress ~ 950 MPa, top fail and bottom survival.

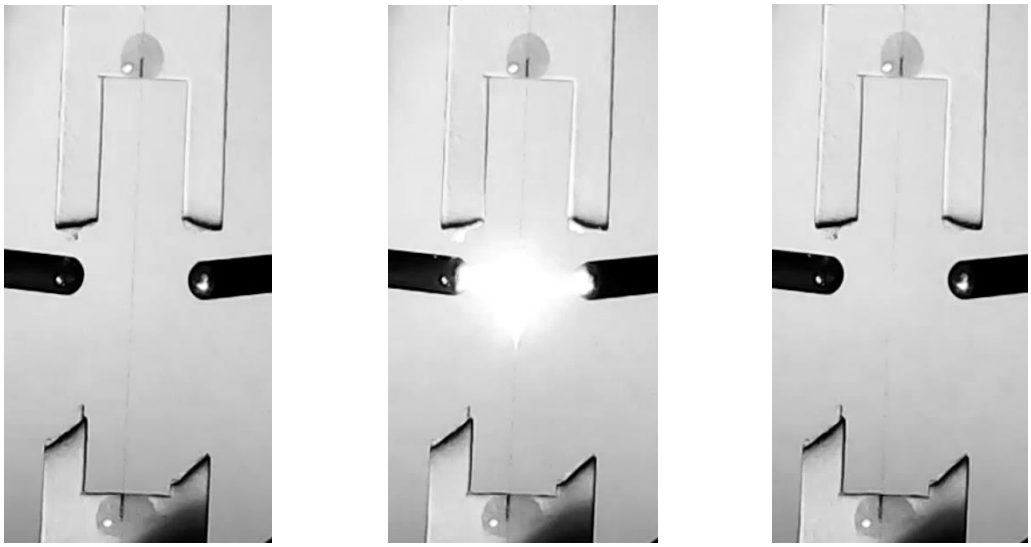

Figure 25. Snapshots of specimen under tensile recoil test. Sample H21, stress ~ 850 MPa, top and bottom survival.

The tensile recoil was performed on samples G21 and H21 over a range of values of compressive stress upon recoil (σ_R) of about 600 to 1000 MPa. The analysis of the binary response data was divided in two bins of values of σ_R, ~ 600-800 MPa, and ~ 800-1000 MPa. In each case, the survival percentage was calculated for both top and bottom. Table 13 and Table 14 present the binary response data of sample G21, and Table 15 and Table 16 present that of sample H21. For the range ~ 600-800 MPa of compressive stress, the average survival was 65% for sample G21 and 67% for sample H21. For the range ~ 800-1000 MPa of compressive stress, the average survival was only 35% for both samples. In other words, the percentage of filament half survival upon tensile recoil shows little difference between samples G21 and H21. This means that there are no significant differences in the compressive strength between the two carbon fiber samples of equivalent

d_{cf} and HTT, yet contrasting DDR. Overall, this means that lower DDR had a significant positive effect on tensile strength, without being detrimental for compressive strength.

Table 13. Binary response data from tensile recoil test of sample G21, range ~ 600-800 MPa of compressive stress at recoil.

Specimen	σ_R, MPa	Top	Bottom
1	600	1	1
2	600	1	1
3	658	1	1
4	709	1	1
5	718	0	1
6	723	1	1
7	727	1	1
8	743	1	1
9	746	1	1
10	751	0	0
11	754	0	0
12	754	0	0
13	756	0	1
14	757	0	0
15	766	0	0
16	771	1	1
17	778	1	1
18	787	1	1
19	787	1	1
20	803	0	0
Survival %		60	70

Table 14. Binary response data from tensile recoil test of sample G21, range ~ 800-1000 MPa of compressive stress at recoil.

Specimen	σ_R, MPa	Top	Bottom
1	804	0	0
2	804	0	0
3	804	0	0
4	805	1	1
5	817	0	0
6	824	0	0
7	826	1	1
8	829	1	1
9	830	0	0
10	842	0	0
11	844	1	1
12	855	0	0
13	856	1	1
14	902	0	0
15	907	0	1
16	909	1	1
17	909	0	0
18	953	0	1
19	956	0	0
20	1006	0	0
Survival %		30	40

Table 15. Binary response data from tensile recoil test of sample H21, range ~ 600-800 MPa of compressive stress at recoil.

Specimen	σ_R, MPa	Top	Bottom
1	583	1	1
2	605	1	1
3	609	1	1
4	670	1	1
5	692	1	1
6	714	1	1
7	724	1	1
8	744	0	0
9	747	1	1
10	749	0	0
11	749	0	0
12	751	1	0
13	753	1	1
14	755	0	0
15	769	1	1
16	778	1	1
17	779	0	1
18	781	1	0
19	793	0	0
20	800	1	1
21	804	1	1
22	805	0	0
23	805	1	1
Survival %		70	65

Table 16. Binary response data from tensile recoil test of sample H21, range ~ 800-1000 MPa of compressive stress at recoil.

Specimen	σ_R, MPa	Top	Bottom
1	806	1	1
2	807	1	0
3	814	1	1
4	829	1	1
5	830	1	1
6	833	0	0
7	847	0	1
8	849	0	0
9	849	0	0
10	851	1	1
11	853	0	0
12	855	0	0
13	856	1	0
14	859	0	0
15	869	0	0
16	890	0	0
17	894	0	0
18	896	0	0
19	903	0	0
20	907	1	1
21	922	0	0
22	951	0	1
23	1008	0	0
Survival %		35	35

3.4 Conclusions

Tensile and compressive properties between mesophase pitch-based carbon fibers of different spinning drawdown ratios yet equivalent fiber diameters, heat treatment conditions and transverse microstructures were compared. The results of this study have revealed that a defect-limited property such as tensile strength is favored by a decreasing drawdown ratio, thus, MPCF tensile strength was observed to increase with decreasing drawdown ratio when other parameters were held constant (carbon fiber diameter and heat treatment temperature). For instance, tensile strength increased from 1.42 ± 0.19 to 2.31 ± 0.28 GPa for a drop in DDR from 189 ± 29 to 14 ± 2, for constant fiber diameter about 8 μm and HTT of 2100 °C. This behavior represents an anomaly with respect to the typical one observed in PAN-based carbon fibers, for which an increased spinning DDR leads to improved mechanical strength, due to the enhanced molecular orientation along fiber axis. For MPCFs, we believe that an increased DDR can lead to enhanced graphitic layer plane alignment in the intra-crystalline region, but also leads to more defects in the inter-crystalline regions leading to more significant weak links that decrease fiber strength. Also, the results of this study have revealed that compressive strength is not significantly influenced by spinning drawdown ratio between carbon fiber samples of equivalent fiber diameter and heat treatment temperature. The results of the tensile recoil test performed on two carbon fiber samples of ~ 8 μm diameter, heat-treated to 2100 °C and with different drawdown ratios (189 ± 29 vs. 14 ± 2) showed a similar filament half survival percentage (35%) in the range 800-1000 MPa of compressive stress.

CHAPTER 4

EFFECT OF MESOPHASE DRAWDOWN RATIO ON CARBON FIBER TRANSPORT PROPERTIES

4.1 Introduction

Chapters 2 and 3 presented the microstructure and mechanical properties of carbon fibers resulting from controlled spinning conditions. The main goal of this chapter is to report the effect of drawdown ratio during pitch fiber spinning on the transport properties of resulting MPCFs, namely electrical and thermal conductivities. To avoid the confounding of variables, the study was conducted for carbon fiber samples of equivalent fiber diameter and heat treatment conditions, the same way it was done in the previous chapter.

4.2 Experimental

4.2.1 Materials and processing

The materials and processing methods used in this part of the study were the same described in Chapters 2 and 3. Carbon fiber samples in Table 6 heat-treated via a low heating rate of ~ 8 °C/min were used to study the effect of drawdown ratio on electrical resistivity and correlated thermal conductivity. The effect of heating rate on electrical

resistivity was studied the same way it was done for tensile strength in Chapter 3. Subsets of oxidized samples B, D, E and J in Table 5 were heat-treated to 2400 °C using two heating rates, ~ 8 and ~ 60 °C/min.

For the measurement of thermal conductivity using the LFA technique, one additional as-spun fiber sample was used, labeled as K, obtained from ARMP mesophase pitch, using the same experimental procedure detailed in section 2.2.2 for fiber processing. As-spun samples D, J and K, were heat-treated to 2400 °C using the high heating rate program also described in section 2.2.2.

4.2.2 Fiber characterization

Electrical resistivity

Electrical resistivity (ρ) of single carbon fiber filaments was measured by a two-probe method. The two-probe method is a simple method for resistivity measurement and is adequate when sample resistance is much larger than the contact resistance. For all present measurements, the resistance of an individual carbon fiber was of the order of 1 kΩ, whereas the contact resistance was only about 1 Ω (i.e., 0.1% of fiber resistance). A schematic of the method is shown in Figure 26, adapted from Singh [80], where I is the current flowing thorough the specimen, V is the voltage drop across the specimen, L is the length of the specimen, and A is the cross-sectional area of the specimen. The resistivity ρ is calculated as

$$\rho = \frac{V}{I}\frac{A}{L} = R\frac{A}{L} \tag{17}$$

where R is the resistance across the sample.

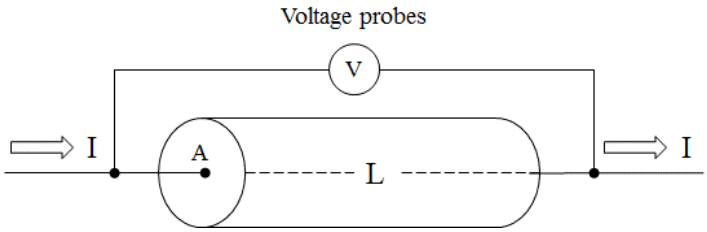

Figure 26. Schematic of two probe method used for electrical resistivity measurement.

Test specimens were prepared following a procedure similar to that used to mount single filaments for tensile testing. The only difference was the use of a quick-curing adhesive to bond the filament to the centerline of the cardboard tab, such as acrylate glue or adhesive tape. No epoxy resin was required because the electrical resistivity measurement does not subject the filament to any stress. A tab carrying a test specimen, with a gage length of ~ 15 mm, was laid between two cooper wires, and the contact resistance between the fiber and the wires was reduced by applying flash dry silver paint (SPI Supplies, West Chester, PA). The resistance across the sample was measured with an ohmmeter and the resistivity was calculated using equation 17, with A being the cross-sectional area of the fiber and L being the length of the fiber between the two copper wires, which was set to 10 mm. The cross-sectional area was determined from the diameter of the fiber, measured by laser diffraction or light microscopy, assuming a circular cross-section.

Thermal conductivity (κ) was estimated from the electrical resistivity measurements using the Issi-Lavin correlation, equation 1, which is valid for mesophase pitch-based carbon fibers at 300 K [32]:

$$\kappa = 440000/(\rho+258) - 295 \quad (1)$$

Analysis of thermal conductivity

A laser/light flash analysis (LFA) technique was used to estimate the thermal conductivity of carbon fibers. Rather than directly measuring the thermal conductivity of single filaments or fiber bundles, the LFA technique measures the thermal diffusivity of a composite of continuous fibers, and the thermal conductivity of the fiber sample of interest is estimated from the former using rule of mixtures for a composite of known composition. Details of the calculation are presented in section 4.3.2. The standard sample size of the composites used in the LFA technique are up to 25.4 mm diameter, or 8 x 10 x 12.7 mm square, and up to 3 mm thick.

The measurement of the thermal diffusivity is realized by quickly heating up the bottom side of the composite with either a laser or xenon light flashes, and measuring the time that it takes for the heat to be conducted through the sample and cause a temperature rise on the top side, with the rate of rise being inversely proportional to thermal conductivity. The measurements were performed in a NETZSCH LFA 447, which can use two configurations: through the plane of the composite (measurement in vertical direction), where fibers are perpendicular to the plane of the composite; and in the plane of the

composite (measurement in horizontal direction), where fibers are parallel to the plane of the composite. In the present study, in-plane measurements were carried out because the preparation of the composite is simpler and requires less amount of sample.

For the in-plane measurements, the sample was mounted in a sample holder plate, as shown in Figure 27 (a), and covered with a mask like the one shown in Figure 27 (b). The holder plate and mask are designed so that the energy input on the bottom of the sample and the energy output on the top of the sample are located at different lateral points, therefore the temperature rise from one side of the sample to other is a reflection of thermal diffusivity in the plane of the composite, as shown in Figure 27 (d). The mask has four holes arranged in a cross pattern from which the temperature rise is detected, as seen in Figure 27 (b). Since unidirectional fiber composites were used in this study, only two holes along the direction of the fiber were used, and the other two were disabled by covering them with electrical tape, as shown in Figure 27 (c)

The heat pulse on the one side (typically bottom) of the composite sample is produced by a xenon lamp, purposely placed in a parabolic mirror to focus large part of the radiation on the sample and illuminate the entire sample homogenously. The measurement of the temperature rise on the other side (typically top) of the sample is realized by an Indium-Antimonide infrared detector, which is cooled with liquid nitrogen.

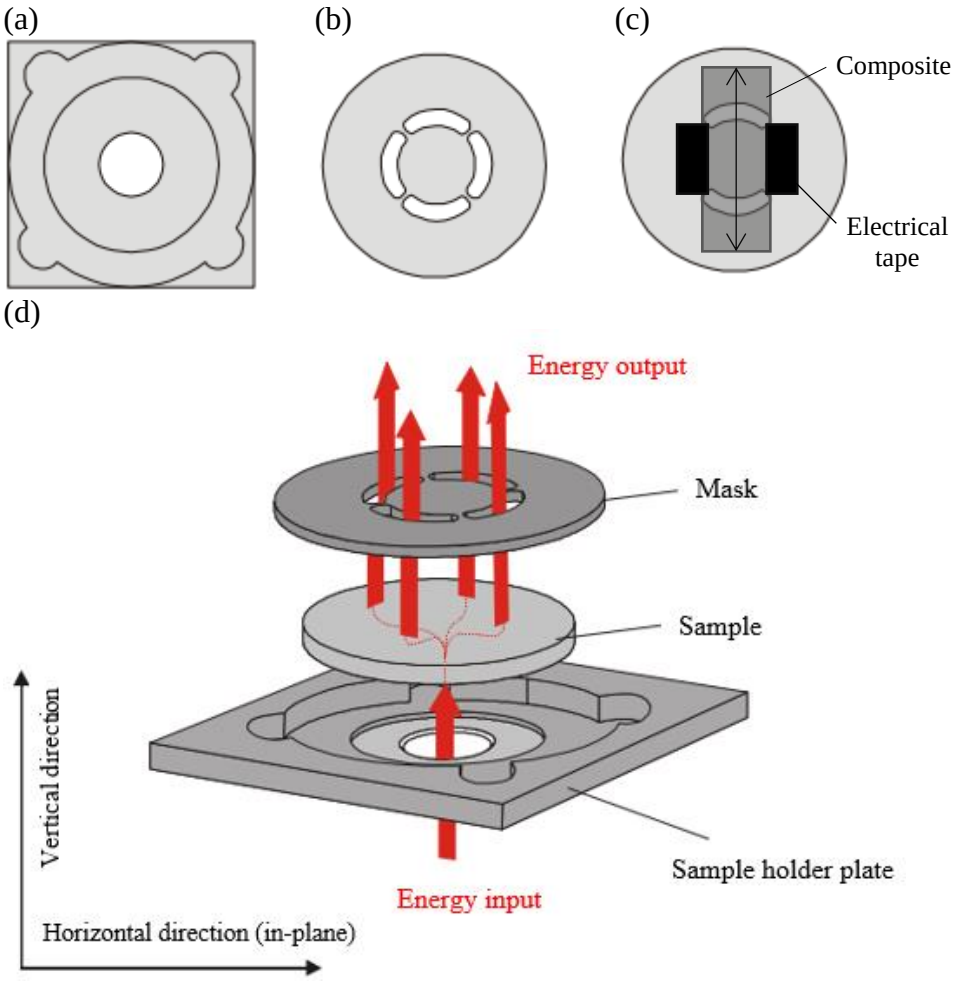

Figure 27. In-plane measurement of thermal diffusivity in a NETZSCH analyzer: (a) sample holder plate, (b) mask, (c) schematic of mask with two holes covered and composite below mask showing direction of fibers, (d) heat flow through sample.

The composites for the LFA technique were consolidated using an epoxy resin as polymer matrix (Devcon 2-Ton, ITW Performance Polymers). The composites were made into slats of ~ 0.4 mm thickness, 24 mm length and 10 mm width by covering the bottom of a silicone mold with a layer of fibers, with the fibers laid in the plane of the slat, along its length. Uncured epoxy resin was then poured on top of the fibers and spread thoroughly with a spatula to impregnate the fibers, taking care to avoid damaging the fibers with the

spatula. The complete impregnation of the fibers with the epoxy resin was confirmed by the epoxy resin flowing down to the bottom of the mold to the point of slightly covering the fiber layer. The excess epoxy resin was then removed from the top of the fiber layer, leaving just the surface of the fibers wet with epoxy resin. The epoxy resin was allowed to cure for a minimum of 12 hours, after which the composite was extracted from the mold and carefully polished with sandpaper to reduce its thickness.

Each composite was sputter-coated with a thin layer (~ 50 nm) of silver on both sides. The sputtering was carried out in a SPI-Module Sputter Coater 11430-AB under argon atmosphere, using a plasma current of 18 mA for 90 seconds. The purpose of the silver coating was to minimize the radiation heat transfer through the sample, since the polymer matrix can be transparent to the wavelengths of the laser/light.

Next, the composite was sprayed on both sides with a layer of graphite (SEG Aerosol Super Enhanced Graphite, ZYP Coating), using the holder and mask shown in Figure 27 (a) and (b) as frames, so that the graphite was applied preferentially on the points where energy is to enter and exit to composite, as shown in Figure 27 (d). The graphite coating was used to enhance the absorption of energy on one side of the sample, and the emission of infrared energy to the detector from the other side. Figure 28 (a) shows a schematic of the composite and Figure 28 (b) shows a representative silver-coated composite used in the LFA technique.

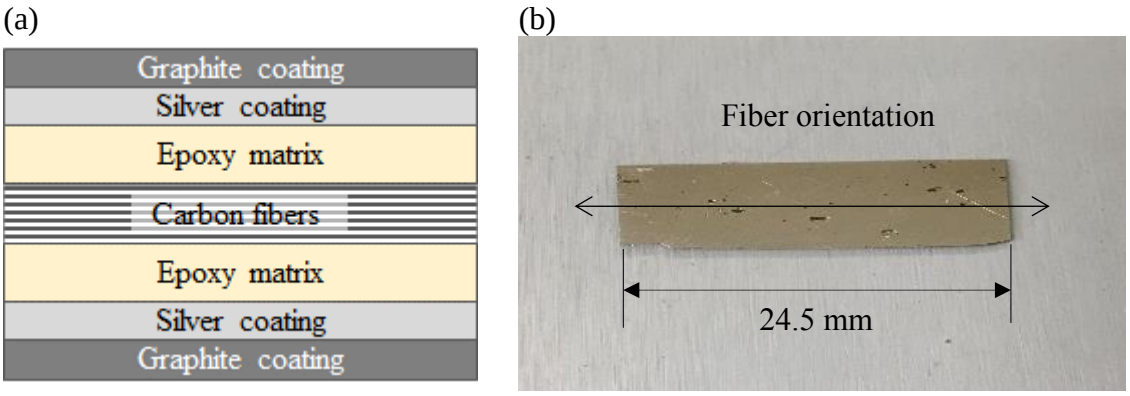

Figure 28. (a) schematic of a carbon fiber/epoxy resin composite; (b) silver coated composite for LFA technique, showing the orientation of the fibers in the composite.

4.3 Results and discussion

4.3.1. Electrical resistivity

Table 17 presents the electrical resistivity, ρ, and correlated thermal conductivity, κ, for the experimental carbon fiber samples heat-treated to 2100 °C. For pairs C21-D21 and G21-H21, low DDR results in lower electrical resistivity, which translates into higher electrical conductivity and correlated thermal conductivity, while the opposite is true for pairs A21-B21 and E21-F21; however, only for pair A21-B21 is the difference significant.

Table 17. Electrical resistivity and correlated thermal conductivity of experimental carbon fiber samples heat-treated to 2100 °C.

Sample	d_{cf}, µm	ρ, µΩ·m	Estimated* κ, W/m·K	DDR
A21	12.9 ± 0.5	5.9 ± 0.7	235 ± 49	117 ± 28
B21	12.3 ± 0.5	6.5 ± 0.2	188 ± 11	17 ± 3
C21	10.4 ± 0.6	7.0 ± 0.5	168 ± 26	58 ± 10
D21	10.5 ± 0.2	6.6 ± 0.3	186 ± 13	32 ± 3
E21	8.9 ± 0.4	6.2 ± 0.5	215 ± 30	44 ± 5
F21	8.9 ± 0.3	6.1 ± 0.2	213 ± 13	19 ± 3
G21	8.3 ± 0.4	6.1 ± 0.1	209 ± 5	189 ± 29
H21	8.5 ± 0.9	5.6 ± 0.7	260 ± 62	14 ± 2

* Issi-Lavin correlation

Figure 29 presents the plots of electrical resistivity (from Table 17) vs. crystallite coherence length (from Table 7) for the experimental carbon fiber samples heat-treated to 2100 °C, showing a moderate inverse relationship (Pearson coefficient = -0.369 with p-value = 0.369). This behavior is expected and it has been reported in previous studies [19,81], showing that larger graphitic crystallites result in increased electrical conductivity (i.e., decreased electrical resistivity).

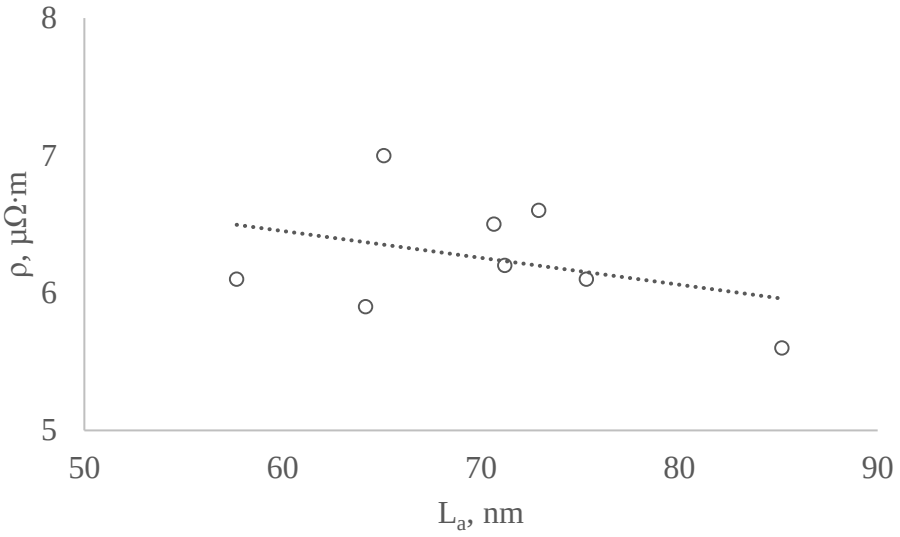

Figure 29. Electrical resistivity vs. crystallite coherence length for experimental carbon fiber samples heat-treated to 2100 °C.

The correlated thermal conductivity ranged from ~ 165 to 260 W/m·K, with an average of 210 W/m·K, for the carbon fiber samples heat-treated to 2100 °C. The values above are lower than those from previous studies on carbon fibers based on AR-type mesophase pitches, with some authors reporting a correlated thermal conductivity of ~ 550 W/m·K for carbon fibers heat-treated to 2600 °C [58]. K1100 carbon fibers were used as a control sample with measured $\rho = 1.3 \pm 0.3$ μΩ·m and estimated $\kappa = 857 \pm 83$ W/m·K; such values are consistent with the ones reported in the literature [33].

Finally, Table 18 presents the electrical resistivity and correlated thermal conductivity of carbon fiber samples heat-treated to 2400 °C at two heating rates: ~ 8 and ~ 60 °C/min. Four pairs of carbon fiber samples were compared and the samples in each pair had the same spinning conditions. Average electrical resistivity across samples of

heating rate ~ 60 °C/min is 3.4 μΩ·m, which is 44% smaller than the one reported for petroleum-derived, mesophase pitch-based carbon fibers of high sulfur content, heat-treated at the same rate and final temperature [79]. For all pairs, the samples of high heating rate showed a lower electrical resistivity, which is consistent with the behavior reported for the petroleum-derived, mesophase pitch-based carbon fibers aforementioned. In the case of those carbon fibers, it was believed that an increased heating rate reduced the fiber damage caused by sulfur removal from 1600 to 2000 °C, which in turn lessened the misorientation of graphite basal planes, therefore improving lattice-dependent properties such as tensile modulus (as mentioned in section 3.3.1) and electrical resistivity. In the present study, the mesophase pitch used for fiber processing is assumed to be sulfur-free due to its synthetic origin, therefore the origin of the relationship between transport properties and heating rate remains unclear. It was observed, however, that for the same high temperature treatment conditions (heating rate and final temperature), the electrical resistivity of ARMP-based carbon fibers was lower than that of the petroleum-based, mesophase pitch-based carbon fibers of high sulfur content. One evident reason for this is the smaller proportion of heteroelements (N, S, O) in the synthetic mesophase pitch, compared to petroleum-based or coal tar-based mesophase pitches. Elemental analysis of a synthetic, naphthalene-derived AR-type pitch revealed an oxygen content < 0.30% and no nitrogen or sulfur were reported [82], while the sulfur in petroleum-derived pitches can be as high as 5% [79].

Table 18. Electrical resistivity and correlated thermal conductivity of experimental carbon fiber samples heat-treated to 2400 °C at two heating rates.

Sample pair	Rate, °C/min	d_{cf}, μm	ρ, μΩ·m	Estimated κ, W/m·K
B24	8	15.5 ± 0.8	3.6 ± 0.2	418 ± 27
B24H	60	14.8 ± 0.7	2.8 ± 0.1	519 ± 21
D24	8	10.7 ± 0.1	3.9 ± 0.1	388 ± 15
D24H	60	10.7 ± 0.3	3.3 ± 0.2	453 ± 21
E24	8	8.8 ± 0.3	4.6 ± 0.4	328 ± 29
E24H	60	9.0 ± 0.3	4.1 ± 0.4	377 ± 56
J24	8	8.0 ± 0.4	4.3 ± 0.2	348 ± 20
J24H	60	9.3 ± 0.4	3.5 ± 0.3	435 ± 40

4.3.2. Thermal conductivity

Direct thermal conductivity measurements using a single carbon fiber have been performed by Piraux et al. [83], but such measurements were extremely difficult. Subsequently, those measurements were carefully correlated to the electrical resistivity measurements that led to the Issi-Lavin correlation. As another approach, the axial thermal conductivity of carbon fibers has also been back-calculated from measured composite conductivity of fibers aligned in the thickness direction of a disk and using the LFA transient method [84]. End effects complicated the measurements and fiber conductivity values estimated from composite samples deviated 20 to 50% from those obtained directly from fibers or as specified by fiber manufacturers.

Therefore, a simpler approach was attempted here using the fixture developed by NETZSCH, shown in Figure 27. This fixture provides a longitudinal component to heat conduction path, leading to measuring a combination of axial and through-thickness conductivity of the composite. Heat conducts from the core of the sample towards the

periphery, and the transient temperature increase is used to calculate the lateral (longitudinal) composite conductivity. Then, calculation of the carbon fiber thermal conductivity for each sample was done as follows. The composite (identified by the subscript c) was made up of a polymer matrix (identified by the subscript m) and a continuous carbon fiber of unknown thermal conductivity (identified by the subscript f). The mass fractions, volume fractions and densities of the matrix and the fiber are m_m, v_m and ρ_m, and m_f, v_f, and ρ_f, respectively.

The density of the composite, ρ_c, was calculated as

$$\rho_c = \rho_m v_m + \rho_f v_f \tag{18}$$

The heat capacity of the composite, C_c, was calculated as

$$C_c = C_m m_m + C_f m_f \tag{19}$$

From the thermal diffusivity of the composite measured by the LFA technique, the thermal conductivity of the composite was calculated as

$$k_c = \alpha_c \rho_c C_c \tag{20}$$

where k_c is the thermal conductivity of the composite, α_c is the thermal diffusivity of the composite, ρ_c is the density of the composite, and C_c is the heat capacity of the composite. The thermal conductivity of the carbon fiber, k_f, was then calculated as

$$k_f = \frac{k_c - k_m v_m}{v_f} \tag{21}$$

where k_m is the thermal conductivity of the matrix.

The parameters used in equations 18 through 21 are presented in Table 19. The density of the fiber, ρ_f, the density of the polymer matrix, ρ_m, and the heat capacity of the fiber, C_f, were taken from the literature.

The heat capacity of the polymer matrix, C_m, was determined as the average of four modulated-DSC replicates, carried out in a TA Instruments DSC Q1000 under helium atmosphere. The program used for this modulated measurements was (i) equilibrating at 25.0 °C, (ii) modulating ± 1.0 °C every 60 s, and (iii) isothermal for 15 min.

The thermal conductivity of the polymer matrix, κ_m, was determined by LFA analysis performed to a sample of the cured epoxy resin that resulted in a value of thermal diffusivity of 0.129 mm^2/s. The thermal conductivity of the polymer matrix was then calculated as

$$k_m = 0.129\ \frac{mm^2}{s} \times 1.75\ \frac{J}{g \cdot K} \times 1.15\ \frac{g}{cm^3} = 0.26\ \frac{W}{m \cdot K}$$

Table 19. Parameters used for the calculation of carbon fiber thermal conductivity

Parameter	Value	Reference
ρ_f	2.00 g/cm^3	[31,85]
ρ_m	1.15 g/cm^3	[86]
C_f	0.71 J/g·K	[84]
C_m	1.75 J/g·K	Determined by DSC
k_m	0.26 W/m·K	Determined by LFA

Table 20 presents the fiber volume fraction v_f and the thickness of the composites used in the LFA technique.

Table 20. Characteristics of the composites used in the LFA measurement.

Sample	v_f	Thickness, mm
D24H	0.08	0.4
J24H	0.10	0.3
K24H	0.11	0.5
K1100	0.18	0.3
T650	0.33	0.4

The conditions used for the measurement of thermal diffusivity that were common for all tested samples were the following:

- Number of shots: 3
- Filter %: 100
- Lamp voltage: 270 V
- Pulse width: 0.31 ms
- Number of points: 2000

Different durations were used for the various samples: sample K1100, 500 ms; samples D24H, J24H and K24H, 750 ms; sample T650, 2000 ms; and the polymer matrix sample, 3000 ms.

Figure 30 presents representative LFA curves of samples K1100 and T650, and Figure 31 presents those of the experimental carbon fiber samples. Sample K1100 shows a signal that increases rapidly before levelling at about 150 ms, while sample T650 shows a signal that starts to level after 1400 ms. Also, the signal of sample K1100 levels to a more intense signal, ~ 0.5 V, while that of sample T650 levels to ~ 0.3 V. Among the

experimental carbon fiber samples, the signal of sample J24H increases rapidly and levels at about 400 ms, while samples D24H and K24H level after 500 ms to a less intense signal. The representative LFA curve of a polymer matrix is presented in Figure 32, tested as a control sample to show the absence of signal whatsoever.

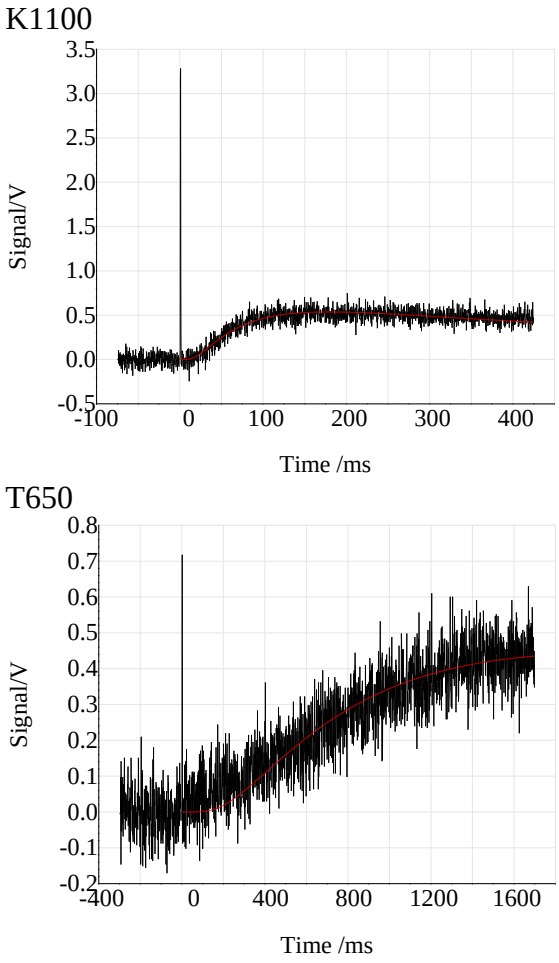

Figure 30. Representative LFA curves of commercial carbon fibers K1100 and T650.

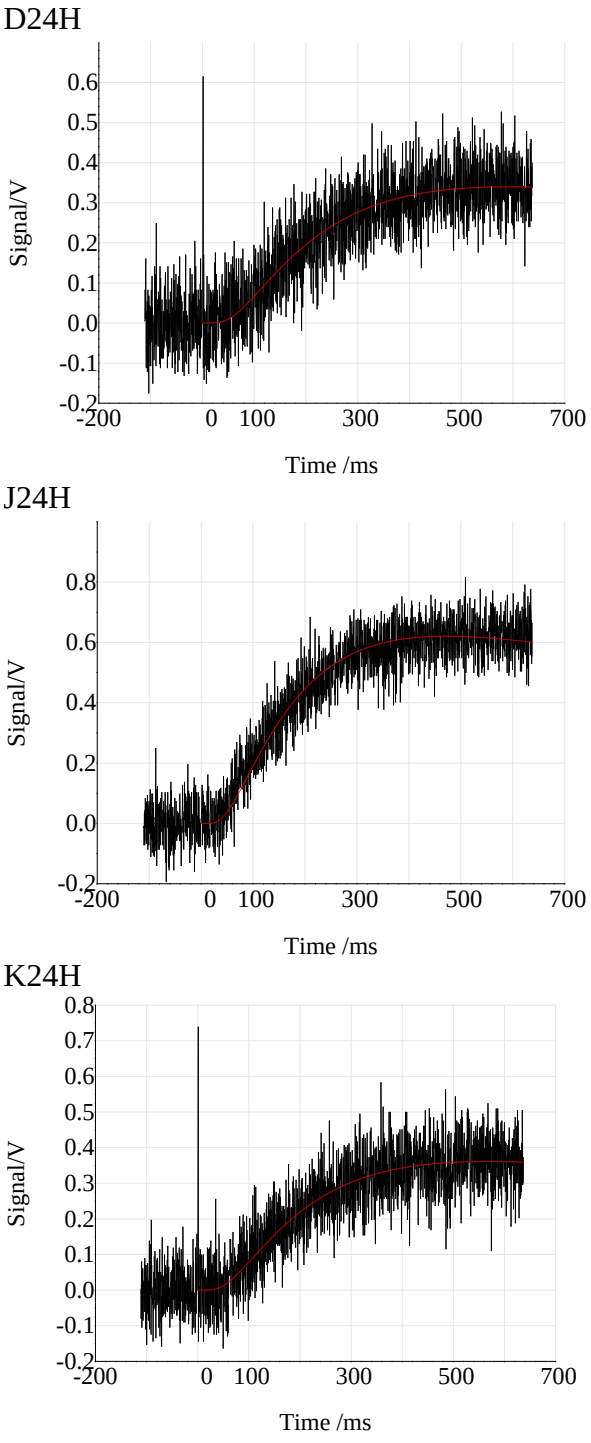

Figure 31. Representative LFA curves of experimental carbon fiber samples D24H, J24H and K24H.

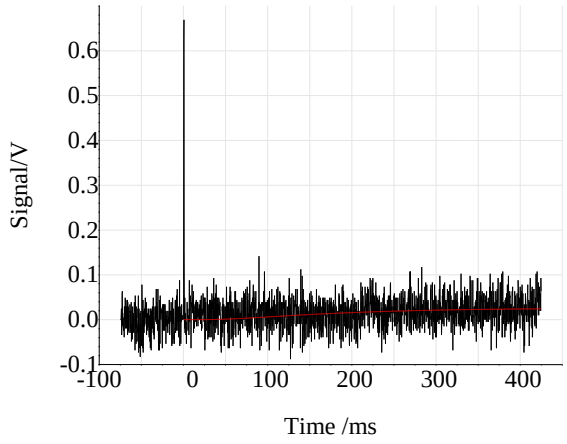

Figure 32. Representative LFA curve of polymer matrix.

Figure 33 presents the thermal conductivity, measured by LFA and correlated from electrical resistivity measurements, of commercial and experimental carbon fiber samples. The commercially-available carbon fibers tested were K1100 (MP-based) and T650 (PAN-based). K1100 represents a sample of high thermal conductivity (the highest thermal conductivity among carbon fibers) and T650 one of low thermal conductivity. Correlated thermal conductivity was not calculated for T650 because the Lavin et al. correlation is only appropriate for mesophase pitch-based carbon fibers, i.e., the value of the measured electrical resistivity, 17.0 ± 1.1 μΩ·m, was beyond the applicable range of equation 1.

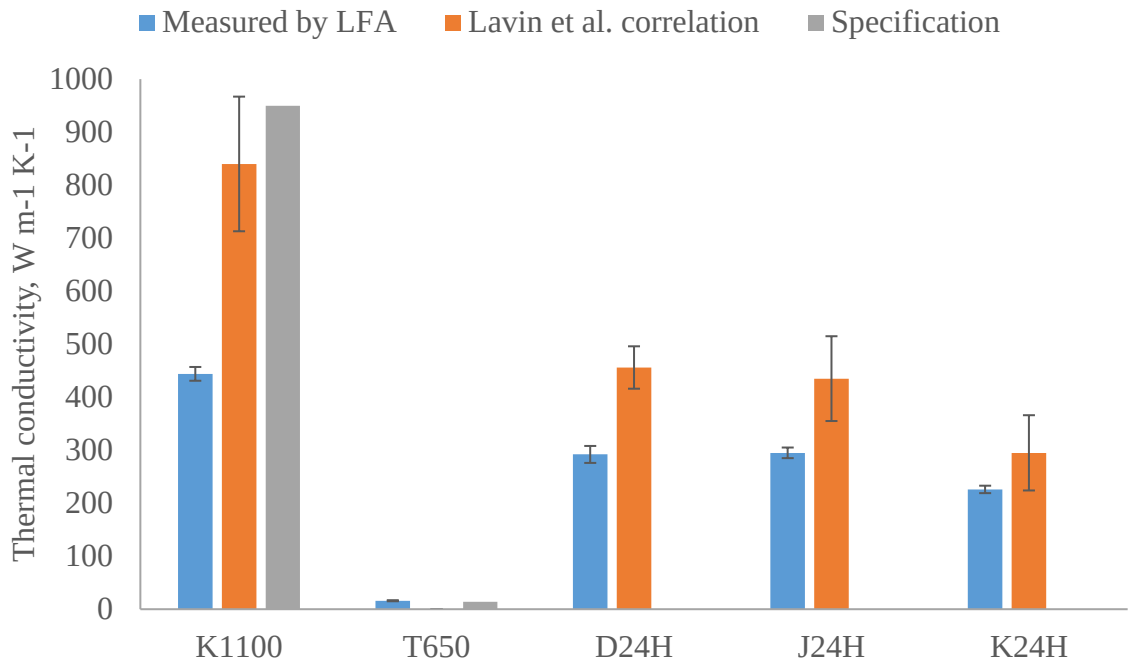

Figure 33. Thermal conductivity of commercial and experimental carbon fiber samples.

Values of thermal conductivity estimated by LFA method are about 60 to 80% of those obtained from the Issi-Lavin correlation or product specification sheet. The ratios of thermal conductivity obtained by LFA to thermal conductivity obtained by Issi-Lavin correlation were D24H, 0.6; J24H, 0.7; K24H, 0.8. The smallest difference was observed for sample T650, the one with the lowest thermal conductivity among the tested samples, while the greatest difference was observed for sample K1100, the one with the highest thermal conductivity.

The reason behind this differences is that the path through which the heat is conducted from the bottom to the top of the composite consists of more than just conduction along the carbon fiber axis; conduction through the plane of the composite also

takes place. The latter involves both conduction across the transverse section of the carbon fiber and the polymer matrix. Using the analogy of thermal resistance for heat conduction, a circuit of resistances (in series) to the heat flow from the bottom to the top of the composite can be simplified as the sum of resistances along two main paths: longitudinal, along the fiber axis; and transverse, across the cross-section of the fiber and the polymer matrix.

As a simplifying assumption, the resistance to conduction for any path is assumed to scale as L/κ, where L is the length of the conduction path and k is the thermal conductivity, then the total resistance is given by $R_l+R_t= L_l/\kappa_l + L_t/\kappa_t$. Here the subscripts *l* and t identify the longitudinal and transverse paths described above. For this analysis, κ_l will be approximated by the fiber volume fraction times the correlated thermal conductivity (or the specification value in case of sample T650). L_l is the difference in the lateral positions between the energy input on the bottom of the sample and the energy output on the top of the sample, which for the sample holder and mask shown in Figure 27, is about 5 mm. L_t is given by the thickness of the composite, and κ_t is the transverse thermal conductivity of the composite, which is assumed to be of the order of 0.5 W/m·K, for composites with a $v_f < 0.5$, based on the work by Rolfes and Hammerschmidt [87].

The ratio of thermal resistances of the two paths were calculated: K1100, 20; T650, 1; D24H, 6; J24H, 5; K24H, 7. In other words, the thermal resistance in the transverse path of heat conduction is much larger than the one found in the longitudinal path of heat conduction, except for sample T650, for which the resistance is equivalent in both paths. This explains the good match between the LFA-measured and specification values of

thermal conductivity for sample T650, and the larger differences observed in the other samples. Because of the lower value of κ_t compared to that of κ_l, the transverse path is the limiting step in the conduction of heat from the bottom to the top of the composite. This, is turn, is caused by the anisotropy of the carbon fiber, with the radial thermal conductivity being a fraction of the axial thermal conductivity, coupled with the low thermal conductivity of the polymer matrix itself.

It should be noted, however, that the values of R_t / R_l were determined as a rough approximation. The approach of thermal resistances detailed above used an assumption of heat transfer in steady state, whereas the heat transfer is time-dependent in LFA technique. Also, even a minor out-of-plane misorientation of carbon fibers can significantly change the conduction path. Therefore, the method was used here for relative comparisons. In contrast, a previous study by Alway-Cooper et al. [84] on the LFA technique used unidirectional composites with the fiber direction parallel to the overall heat flow direction during the LFA test (as opposed to the present work, where the fiber direction was perpendicular to the overall heat flow direction). The measured value was 544 ± 190 W/m·K for the axial thermal conductivity of K1100 carbon fiber, which is about 50% of the literature value. In other words, the value of 444 ± 13 W/m·K obtained in this study for K1100 compares well with the value obtained earlier, considering that current composite/technique required significantly less amount of fiber and time for preparation.

Table 21. Carbon fiber diameter and spinning conditions of experimental carbon fiber samples used for the measurement of thermal conductivity.

Sample	d_{cf}, µm	d_0, µm	DDR	LFA-based κ, W/m·K	Estimated κ, W/m·K
D24H	10.7 ± 0.3	75	32 ± 3	292 ± 16	456 ± 40
J24H	9.3 ± 0.4	75	43 ± 5	295 ± 10	435 ± 80
K24H	14.8 ± 0.4	150	69 ± 8	226 ± 7	295 ± 71

For the experimental samples, the LFA-based thermal conductivity shows a good correlation with values obtained from Issi-Lavin correlation (i.e., inverse electrical resistivity with a Pearson coefficient = 0.987 with p-value = 0.101). Samples D24H and J24H, which have equivalent transverse microstructure and heat treatment temperature, have a similar measured thermal conductivity of under 300 W/m·K, given similar fiber diameters and drawdown ratios. For K24H fibers, the estimated conductivity was slightly smaller than that of the other two samples, although not statistically significant. It is noted, however, these fibers had a much larger diameter and would be expected to have a higher conductivity (thicker carbon fibers are known to show slightly higher conductivity). Because that was not case, there is an indication (although weak) of the inverse effect DDR on thermal conductivity. It should be emphasized that producing composite samples requires a significant quantity of carbon fibers (as compared with individual filament tests), which were not available towards the latter part of this dissertation. Nonetheless, the LFA approach used here illustrates a method for comparative study of thermal conductivity. Although it involves many approximations, the measured values of thermal conductivity from lateral measurements were comparable to those obtained by the more complex

transverse measurements in which the fibers are perpendicular to the plane of the composite.

4.4 Conclusions

Electrical conductivity and estimated thermal conductivity of mesophase pitch-based carbon fibers produced from different spinning drawdown ratios were compared. The results of this study indicate that the transport properties of MPCFs were not significantly influenced by the drawdown ratio used during melt spinning of precursor pitch fibers. In other words, while a low DDR was found to be favorable for tensile strength, it did not enhance electrical/thermal conductivities. However, the lower drawdown ratio did not prove detrimental to these transport properties either.

CHAPTER 5

CONCLUSIONS AND RECOMMENDATIONS

5.1 Conclusions

The improvement of mechanical properties of mesophase pitch-based carbon fibers will enable their use in a wider range of structural applications as fiber reinforcement in composites, taking full advantage of a precursor that has the potential to outdo polyacrylonitrile in terms of cost and carbon yield. This improvement, coupled with the retention of their superior modulus and electrical/thermal conductivity, could be of immense societal benefit in terms of a high-strength, lightweight material suitable for automotive applications with enhanced fuel efficiency. Therefore, as discussed earlier, the approach used in this dissertation was to experimentally study the effect of precursor fiber spinning conditions, particularly drawdown ratio (DDR), which has not been systematically investigated in prior studies. This study addressed the role of DDR on the fiber microstructure and the resulting properties of carbon fibers so produced.

The experimental methodology included the processing of precursor fibers from a synthetic mesophase pitch, using capillary diameters as small as 50 μm, which combined with the sensitive temperature dependence of pitch viscosity make the melt spinning of pitch a complex process. Thus, pitch fibers, as thin as 10 μm, were successfully spun in this study. Carbonization was conducted primarily at 2100 °C (limited samples at 2400 °C)

to attain carbon fibers diameters as small as 8 μm, smaller than the typical ones for this type of fibers.

A line-origin, radial (similar to spokes of a wheel) texture was obtained in all the carbon fiber samples. Although custom-built spinneret of different capillary sizes were used, the overall flow characteristics were held uniform to retain this transverse microstructure across all samples produced. The graphitic morphology of carbon fibers was assessed by wide-angle x-ray diffraction technique and found to be consistent with prior results in the literature. The two-theta peaks associated with (002) sets of planes were observed at 26.0°, corresponding to d_{002} of 0.342 nm. Because of instrumental limitations, subtle differences in crystalline development could not be detected as a function of DDR.

The use of Raman spectroscopy enabled the characterization of the carbon crystallite features and their defect density, which led to the identification of an inverse relationship between drawdown ratio and crystallite size along the fiber axis. This observation established a link with the outcome of tensile testing, where an increase in tensile strength was demonstrated with decreasing DDR, while holding carbon fiber diameter constant. The sample of low DDR displayed a larger crystallite coherence length (L_a) and distance between defects (L_D). For a given fiber length, a longer average crystallite size would translate into a smaller size of the defective inter-crystalline regions and would result in enhanced tensile strength because strength is a defect-dominated property.

Importantly, the observed gain in tensile strength with decreasing pitch spinning DDR did not adversely impact other carbon fiber properties. Compressive strength and

transport properties of these carbon fibers with reduced DDR did not decrease, but were found to display no measurable differences.

In summary, decreasing drawdown ratio was observed to have a positive effect on tensile strength when fiber diameter and carbonization temperature were held constant, without having a detrimental effect on compressive strength or transport properties. The findings of this dissertation could aid in the better understanding and control of the spinning conditions of mesophase pitches, leading to MPCFs with enhanced mechanical properties while retaining superior electrical and thermal conductivities.

5.2 Recommendations for future work

Recommendations for future work stemming from the present research can be broadly classified into four categories based on (i) precursor pitch, (ii) spinning/process, (iii) other transverse microtextures, and (iv) analytical methods.

First, in future studies, petroleum-derived mesophase pitches should be investigated as precursor for fiber processing. Such approach would extend the findings of the present work with a carbon fiber precursor of significant economic potential and societal benefit to produce high-performance, light-weight carbon fibers. The synthetic AR-type pitches used in this study are no longer in production by Mitsubishi Gas Chemical Company. On the other hand, petroleum mesophase pitches could be produced at a low cost, with recent technological developments projecting a cost under US $1.50/lb [48].

As explained in section 2.2.1, although synthetic pitches are ideal for technical studies given the consistency in properties, both synthetic and petroleum-based mesophase pitches have similar molecular architectures. Evidence for this are the molecular weight distributions obtained by matrix-assisted laser desorption/ionization (MALDI) spectroscopy from literature studies, shown in Figure 34. AR-type pitches exhibit a molecular weight distribution with a peak at ~ 500 Da, and petroleum-derived mesophase pitches display a comparable distribution with a large peak at ~ 500 Da and a smaller one at ~ 750 Da, corresponding to some oligomer. In contrast, MALDI of an isotropic pitch shows an oligomeric nature with a peak at ~ 300 Da corresponding to monomer, and smaller peaks at ~ 500, ~ 750 and ~ 1000 Da likely corresponding to the equivalent of dimer, trimer and tetramers.

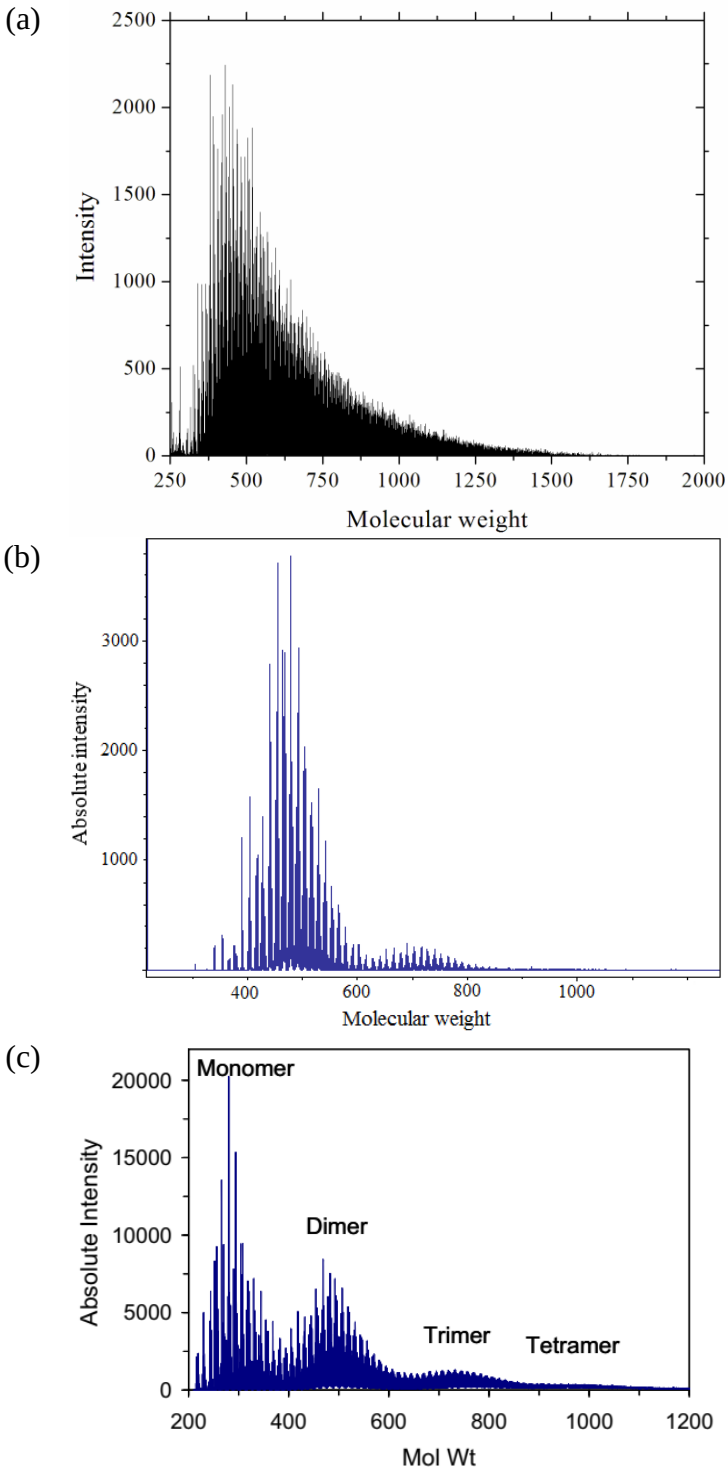

Figure 34. MALDI spectra of (a) AR synthetic mesophase pitch [88], (b) petroleum-based 100% mesophase pitch [5], and (c) M-50 isotropic petroleum pitch [89].

A sufficient amount of pitch precursor, potentially obtained from cost-competitive petroleum, would allow the use of a continuous extruder for the processing of precursor pitch fibers, as opposed to the current batch unit. A continuous process helps improve spinning yield and stability. Further, the introduction of other modifications in spinning, such as deformation of pitch flow before extrusion, could lead to the development of alternative transverse cross-sections in the resulting carbon fibers. For instance, random or onion-skin textures, are known to have a different range of mechanical and transport properties.

Finally, to improve the measurements of crystalline structure by wide-angle x-ray diffraction, future tests can be carried out using an instrument with higher resolution, specifically designed for fiber diffraction. Then, subtle changes in crystallinity arising in samples of different spinning conditions can be detected. Also, the measurements of thermal conductivity by LFA could be improved by reducing the thickness of the composites, either by further grinding and polishing of composites consolidated by the technique applied in this study, or by using another technique such as vacuum bagging, which allows the conformation of thinner composites with a smaller volume fraction of polymer matrix.

APPENDIX

A1. Indicated compliance, C, vs gage length by cross-sectional area, L/A, for sample D21

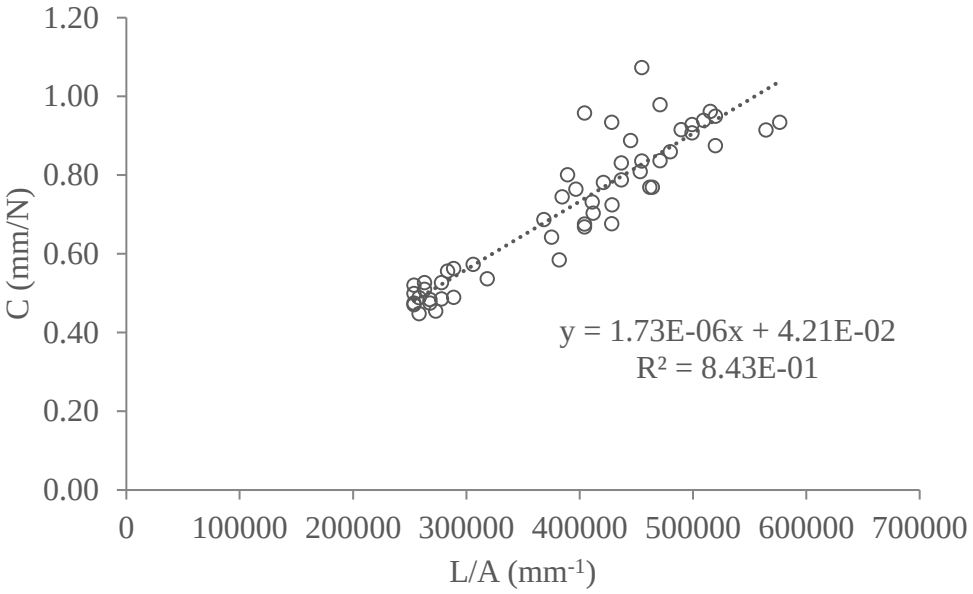

The inverse of the slope of the regression equation gives the corrected tensile modulus, E_c, in MPa:

$$E_c = \frac{1}{1.73\times10^{-6}} = 578035 \text{ MPa} = 578 \text{ GPa}$$

LITERATURE CITED

[1] Frank E, Steudle LM, Ingildeev D, Spoerl JM, Buchmeiser MR. Carbon fibers: precursor systems, processing, structure, and properties. Angewandte Chemie International Edition 2014;53:5262-98.

[2] Stewart R. Carbon fibre market poised for expansion. Reinforced Plastics 2011;55:26-31.

[3] Sloan J. Carbon fiber has designs on production wheels. Composites World 2018;4:30-3.

[4] Bahl O, Shen Z, Lavin JG, Ross RA. Manufacture of carbon fibers. Carbon fibers 1998;3:1.

[5] Bermudez V, Lukubira S, Ogale AA. 1.3 Pitch Precursor-Based Carbon Fibers. In: Beaumont PWR, Zweben CH, editors. Comprehensive Composite Materials II, Oxford: Elsevier; 2018, p. 41-65.

[6] Newcomb BA. Processing, structure, and properties of carbon fibers. Composites Part A: Applied Science and Manufacturing 2016;91:262-82.

[7] Kim J, Lee B, Peck D, Yoon S, Jung D. Pitch-based carbon fibers from coal tar or petroleum residue under the same processing condition. Carbon letters 2016;19:72-8.

[8] Prauchner M, Pasa V, Otani S, Otani C. Biopitch-based general purpose carbon fibers: Processing and properties. Carbon 2005;43:591-7.

[9] Brooks J, Taylor G. The formation of graphitizing carbons from the liquid phase. Carbon 1965;3:185-93.

[10] White J, Guthrie G, Gardner J. Mesophase microstructures in carbonized coal-tar pitch. Carbon 1967;5:517-IN8.

[11] Lewis IC, McHenry ER, Singer LS. Process for producing carbon fibers from mesophase pitch 1976.

[12] Maeda T, Zeng SM, Tokumitsu K, Mochida I. Preparation of isotropic pitch precursors for general purpose carbon fibers (GPCF) by air blowing—I. Preparation of spinnable isotropic pitch precursor from coal tar by air blowing. Carbon 1993;31:407-12.

[13] Edie DD, McHugh JJ. High Performance Carbon Fibers. In: Burchell TD, editor. Carbon Materials for Advanced Technologies, Oxford: Elsevier Science Ltd; 1999, p. 119-138.

[14] Mora E, Blanco C, Prada V, Santamarıa R, Granda M, Menendez R. A study of pitch-based precursors for general purpose carbon fibres. Carbon 2002;40:2719-25.

[15] Eser S, Andresen J. Properties of fuels, petroleum pitch, petroleum coke, and carbon materials. ASTM MANUAL SERIES MNL 2004:757-86.

[16] Park S, Heo G. Precursors and Manufacturing of Carbon Fibers. In: Park S, editor. Carbon Fibers, Dordrecht: Springer Netherlands; 2015, p. 31-66.

[17] Kandiyoti R, Herod A, Bartle KD, Morgan TJ. Solid fuels and heavy hydrocarbon liquids: thermal characterization and analysis. : Elsevier, 2016.

[18] Diefendorf RJ. Pitch Precursor Carbon Fibers. In: Kelly A, Zweben C, editors. Comprehensive Composite Materials, Oxford: Pergamon; 2000, p. 35-83.

[19] Huson M. High-performance pitch-based carbon fibers. In: Anonymous Structure and Properties of High-Performance Fibers: Elsevier; 2017, p. 31-78.

[20] Mochida I, Shimizu K, Korai Y, Otsuka H, Fujiyama S. Structure and carbonization properties of pitches produced catalytically from aromatic hydrocarbons with HFBF3. Carbon 1988;26:843-52.

[21] Mochida I, Yoon S, Korai Y. Mesoscopic structure and properties of liquid crystalline mesophase pitch and its transformation into carbon fiber. The Chemical Record 2002;2:81-101.

[22] Kundu S. Investigation of flow and microstructure in rheometric and processing flow conditions for liquid crystalline pitch. 2006.

[23] Edie D, Dunham M. Melt spinning pitch-based carbon fibers. Carbon 1989;27:647-55.

[24] Ziabicki A. Fundamentals of fibre formation: the science of fibre spinning and drawing. : Wiley New York, 1976.

[25] Oberlin A. Carbonization and graphitization. Carbon 1984;22:521-41.

[26] Buckley JD, Edie DD. Carbon-carbon materials and composites. : William Andrew, 1993.

[27] Peebles LH. Carbon fibers: formation, structure, and properties. : CRC Press, 2018.

[28] Ōtani S, Ōya A. Progress of Pitch-Based Carbon Fiber in Japan. In: Anonymous Petroleum-Derived Carbons: American Chemical Society; 1986, p. 323-334.

[29] De Bont P, Scholte P, Hottenhuis M, Van Kempen G, Kerssemakers J, Tuinstra F. Atomic structure of longitudinal sections of a pitch-based carbon fiber studied by STM. Appl Surf Sci 1994;74:73-80.

[30] Emmerich FG. Young's modulus, thermal conductivity, electrical resistivity and coefficient of thermal expansion of mesophase pitch-based carbon fibers. Carbon 2014;79:274-93.

[31] Morgan P. Carbon Fibers and Their Composites. Boca Raton, FL: CRC Press, 2005.

[32] Lavin J, Boyington D, Lahijani J, Nysten B, Issi J. The Correlation of Thermal-conductivity With Electrical-resistivity in Mesophase Pitch-based Carbon-fiber. Carbon 1993;31:1001-2.

[33] Jeon Y, Alway-Cooper R, Morales M, Ogale AA. Chapter 2.8 - Carbon Fibers. In: Somiya S, editor. Handbook of Advanced Ceramics (Second Edition), Oxford: Academic Press; 2013, p. 143-154.

[34] Callister WD, Rethwisch DG. Fundamentals of materials science and engineering. : Wiley London, UK:, 2000.

[35] Qin X, Lu Y, Xiao H, Wen Y, Yu T. A comparison of the effect of graphitization on microstructures and properties of polyacrylonitrile and mesophase pitch-based carbon fibers. Carbon 2012;50:4459-69.

[36] Kim B, Kotegawa T, Eom Y, An J, Hong I, Kato O et al. Enhancing the tensile strength of isotropic pitch-based carbon fibers by improving the stabilization and carbonization properties of precursor pitch. Carbon 2016;99:649-57.

[37] Park M, Jung M, Lee Y. Significant reduction in stabilization temperature and improved mechanical/electrical properties of pitch-based carbon fibers by electron beam irradiation. Journal of Industrial and Engineering Chemistry 2016;37:277-87.

[38] Greene M, Schwartz RW, Treleaven J. Short residence time graphitization of mesophase pitch-based carbon fibers. Carbon 2002;40:1217-26.

[39] Edie D. The effect of processing on the structure and properties of carbon fibers. Carbon 1998;36:345-62.

[40] Hamada T, Nishida T, Sajiki Y, Matsumoto M, Endo M. Structures and physical properties of carbon fibers from coal tar mesophase pitch. J Mater Res 1987;2:850-7.

[41] Kundu S, Ogale AA. Rheostructural studies on a synthetic mesophase pitch during transient shear flow. Carbon 2006;44:2224-35.

[42] Matsumoto M, Iwashita T, Arai Y, Tomioka T. Effect of spinning conditions on structures of pitch-based carbon fiber. Carbon 1993;31:715-20.

[43] Yan J, Rey A. Theory and simulation of texture formation in mesophase carbon fibers. Carbon 2002;40:2647-60.

[44] Grecov D, Rey AD. Computational rheology of carbonaceous mesophases. Carbon 2004;42:1257-61.

[45] Wang Y, Wang C, Bai Y, Bo Z. Effect of the drawing process on the wet spinning of polyacrylonitrile fibers in a system of dimethyl sulfoxide and water. J Appl Polym Sci 2007;104:1026-37.

[46] Kirsten M, Meinl J, Schönfeld K, Michaelis A, Cherif C. Characteristics of wet-spun and thermally treated poly acrylonitrile fibers. J Appl Polym Sci 2016;133:43698.

[47] Braga CP, de Castro Dutra, Carlos Henrique Monteiro, de Castro LD, de Andrade CT. Influence of heat and pressure treatment on the rheological behavior of petroleum pitches. Fuel 2009;88:853-60.

[48] Sloan J. Coming to carbon fiber: Low-cost mesophase pitch precursor. Composites World Weekly 2016;May 10th.

[49] Mitsubishi Gas Chemical Company. AR Resin. http://www.aromaticchemicals.com/other/ar.html. ;2015:2.

[50] Alger M. Polymer science dictionary. : Springer Science & Business Media, 1996.

[51] Chhabra RP, Richardson JF. Non-Newtonian flow in the process industries: fundamentals and engineering applications. : Butterworth-Heinemann, 1999.

[52] Perry A, Ineichen B, Eliasson B. Fibre diameter measurement by laser diffraction. J Mater Sci 1974;9:1376-8.

[53] Tuinstra F, Koenig Já. Characterization of graphite fiber surfaces with Raman spectroscopy. J Composite Mater 1970;4:492-9.

[54] Tuinstra F, Koenig JL. Raman spectrum of graphite. J Chem Phys 1970;53:1126-30.

[55] Cançado L, Takai K, Enoki T, Endo M, Kim Y, Mizusaki H et al. General equation for the determination of the crystallite size L a of nanographite by Raman spectroscopy. Appl Phys Lett 2006;88:163106.

[56] Cançado LG, Jorio A, Ferreira EM, Stavale F, Achete C, Capaz R et al. Quantifying defects in graphene via Raman spectroscopy at different excitation energies. Nano letters 2011;11:3190-6.

[57] Iwashita N, Park CR, Fujimoto H, Shiraishi M, Inagaki M. Specification for a standard procedure of X-ray diffraction measurements on carbon materials. Carbon 2004;42:701-14.

[58] Alway-Cooper RM, Anderson DP, Ogale AA. Carbon black modification of mesophase pitch-based carbon fibers. Carbon 2013;59:40-8.

[59] Yoon S, Korai Y, Mochida I, Yokogawa K, Fukuyama S, Yoshimura M. Axial nano-scale microstructures in graphitized fibers inherited from liquid crystal mesophase pitch. Carbon 1996;34:83-8.

[60] Korai Y, Hong S, Mochida I. Development of longitudinal mesoscopic textures in mesophase pitch-based carbon fibers through heat treatment. Carbon 1999;37:203-11.

[61] Lu S, Blanco C, Rand B. Large diameter carbon fibres from mesophase pitch. Carbon 2002;40:2109-16.

[62] Rogers DK. A study of the stabilization, carbonization, and graphitization of mesophase pitch-based carbon fibers. 1993.

[63] Ogale A, Lin C, Anderson D, Kearns K. Orientation and dimensional changes in mesophase pitch-based carbon fibers. Carbon 2002;40:1309-19.

[64] Wood K. Wind turbine blades: Glass vs. carbon fiber. CW Composites World 2012.

[65] LeGault M. Drones: Composite UAVs take flight. CW Composites World 2018;4:36-44.

[66] ASTM. D3379-75. Standard Test Method for Tensile Strength and Young's Modulus for High-Modulus Single-Filament Materials. 1989.

[67] Allen SR. Tensile recoil measurement of compressive strength for polymeric high performance fibres. J Mater Sci 1987;22:853-9.

[68] Edie D, Fox N, Barnett B, Fain C. Melt-spun non-circular carbon fibers. Carbon 1986;24:477-82.

[69] Minus M, Kumar S. The processing, properties, and structure of carbon fibers. JOM 2005;57:52-8.

[70] Zhang Y, Wang X, Pan N, Postle R. Weibull analysis of the tensile behavior of fibers with geometrical irregularities. J Mater Sci 2002;37:1401-6.

[71] Wang F, Shao J. Modified Weibull distribution for analyzing the tensile strength of bamboo fibers. Polymers 2014;6:3005-18.

[72] Ticoalu A, Aravinthan T, Cardona F. A study into the characteristics of gomuti (Arenga pinnata) fibre for usage as natural fibre composites. J Reinf Plast Compos 2014;33:179-92.

[73] Naito K. Tensile properties and weibull modulus of some high-performance polymeric fibers. J Appl Polym Sci 2013;128:1185-92.

[74] El Asloun M, Donnet J, Guilpain G, Nardin M, Schultz J. On the estimation of the tensile strength of carbon fibres at short lengths. J Mater Sci 1989;24:3504-10.

[75] Naito K, Yang J, Tanaka Y, Kagawa Y. The effect of gauge length on tensile strength and Weibull modulus of polyacrylonitrile (PAN)-and pitch-based carbon fibers. J Mater Sci 2012;47:632-42.

[76] Tagawa T, Miyata T. Size effect on tensile strength of carbon fibers. Materials Science and Engineering: A 1997;238:336-42.

[77] Huang X. Fabrication and properties of carbon fibers. Materials 2009;2:2369-403.

[78] Kim M, Jang D, Tejima S, Cruz-Silva R, Joh H, Kim HC et al. Strengthened PAN-based carbon fibers obtained by slow heating rate carbonization. Scientific reports 2016;6:22988.

[79] Rogers D, Jones S, Fain C, Edie D. Graphitization of a high-sulfur mesophase pitch-based fiber. Carbon 1993;31:303-13.

[80] Singh Y. Electrical resistivity measurements: a review. 2013;22:745-56.

[81] Issi J, Nysten B. Electrical and thermal transport in carbon fibers. In: Donnet J, Wang TK, Rebouillat S, Peng JCM, editors.
Carbon Fibers, New York: Marcel Dekker; 1998, p. 371-462.

[82] Dumont M, Dourges M, Bourrat X, Pailler R, Naslain R, Babot O et al. Carbonization behaviour of modified synthetic mesophase pitches. Carbon 2005;43:2277-84.

[83] Piraux L, Issi J, Coopmans P. Apparatus for thermal conductivity measurements on thin fibres. Measurement 1987;5:2-5.

[84] Alway-Cooper RM, Theodore M, Anderson DP, Ogale AA. Transient heat flow in unidirectional fiber–polymer composites during laser flash analysis: Experimental measurements and finite element modeling. J Composite Mater 2013;47:2399-411.

[85] Peebles LH, Yanovsky YG, Sirota A. Mechanical properties of carbon fibers. In: Donnet J, Wang TK, Rebouillat S, Peng JCM, editors. Carbon Fibers: Marcel Dekker; 1998, p. 311-369.

[86] ITW Performance Polymers. Technical Data Sheet – 2 Ton Epoxy. https://itwperformancepolymers.com/media/10869/tds-2-ton-epoxy.pdf. 2018;2019:2.

[87] Rolfes R, Hammerschmidt U. Transverse thermal conductivity of CFRP laminates: a numerical and experimental validation of approximation formulae. Composites Sci Technol 1995;54:45-54.

[88] Kundu S, Naskar AK, Ogale AA, Anderson DP, Arnold JR. Observations on a low-angle X-ray diffraction peak for AR-HP mesophase pitch. Carbon 2008;46:1166-9.

[89] Cristadoro A, Kulkarni SU, Burgess WA, Cervo EG, Räder HJ, Müllen K et al. Structural characterization of the oligomeric constituents of petroleum pitches. Carbon 2009;47:2358-70.